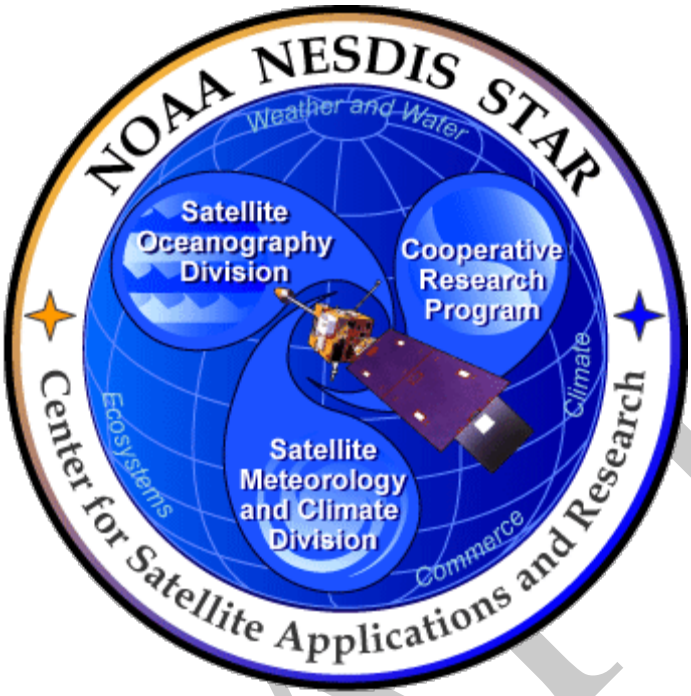

NOAA NESDIS
CENTER for SATELLITE APPLICATIONS and RESEARCH

Enterprise Algorithm Theoretical Basis Document For Cloud Type and Cloud Phase

Michael Pavolonis, NOAA/NESDIS/STAR
Corey Calvert, University of Wisconsin - CIMSS

Version 3.0
June 1, 2020

TABLE OF CONTENTS

1 INTRODUCTION 13
1.1 Purpose of This Document 13
1.2 Who Should Use This Document 13
1.3 Inside Each Section 13
1.4 Related Documents 14
1.5 Revision History 14
2 OBSERVING SYSTEM OVERVIEW 15
2.1 Products Generated 15
2.1.1 Product Requirements 15
2.2 Instrument Characteristics 18
3 ALGORITHM DESCRIPTION 21
3.1 Algorithm Overview 21
3.2 Processing Outline 22
3.3 Algorithm Input 24
3.3.1 Primary Sensor Data 24
3.3.2 Derived Data 24
3.3.3 Ancillary Data 24
3.3.4 Radiative Transfer Models 25
3.4 Theoretical Description 26
3.4.1 Physics of the Problem 26
3.4.2 Mathematical Description 31
3.4.3 Algorithm Output 74
3.5 GOES-17 Loop Heat Pipe Anomaly Mitigation 78
3.5.1 GOES-17 Mitigated Cloud Type/Phase Determination Logic 79
3.5.2 GOES-17 Mitigated Cloud Phase Comparison to GOES-16 90
4 TEST DATA SETS AND OUTPUTS 94
4.1 Simulated/Proxy Input Data Sets 94
4.1.1 SEVIRI and VIIRS Data 94
4.2 Output from Simulated/Proxy Inputs Data Sets 97
4.2.1 Precisions and Accuracy Estimates 99
4.2.2 Error Budget 100
4.2.3 Validation Summary 106
5 PRACTICAL CONSIDERATIONS 107
5.1 Numerical Computation Considerations 107
5.2 Programming and Procedural Considerations 107
5.3 Quality Assessment and Diagnostics 108
5.4 Exception Handling 108
5.5 Algorithm Validation 108
6 ASSUMPTIONS AND LIMITATIONS 108
6.1 Performance 109
6.2 Assumed Sensor Performance 109
6.3 Pre-Planned Product Improvements 110
6.3.1 Incorporation of solar channels 110
6.3.2 Use of 10.4-μm channel 110

6.3.3 Use of additional water vapor channels 110
7 REFERENCES 111

LIST OF FIGURES

Figure 1: High Level Flowchart of the ACT illustrating the main processing sections. The tail of the pixel loop arrows indicates the start of a loop over all pixels in current scan line segment. The head of the arrow indicates the end of the loop. The first loop "yes" condition is that the pixel is earth geolocated and has valid spectral data (according to the L1b calibration quality flags). The "yes" condition for the second loop is that the pixel is earth geolocated, has valid spectral data, and is cloudy. The third loop is over all pixels. 23
Figure 2: The imaginary index of refraction for liquid water (red) and ice (blue) is shown as a function of wavelength. 27
Figure 3: The 8.5/11 μm scaled extinction ratio (β(8.5/11μm)) is shown as a function of the effective particle radius for liquid water spheres (red) and ice plates (blue). These β-ratios were derived from the single scatter properties. 30
Figure 4: The 12/11 μm scaled extinction ratio (β(12/11μm)) is shown as a function of the effective particle radius for liquid water spheres (red) and ice plates (blue). These β-ratios were derived from the single scatter properties. 31
Figure 5: The impact of the gradient filter is shown for the scene depicted by the false color Red-Green-Blue (RGB) image (top panel). The β_{tropo}(8.5/11μm) at each pixel is shown in the bottom, left panel and the bottom, right panel is the same as the bottom left, except the β_{tropo}(8.5/11μm) for the LRC of each pixel is shown. Notice how anomalous values near cloud edges are absent from the LRC image. 40
Figure 6: Peirce-Hanssen-Kuipers skill score metrics are shown as a function of the $\beta_{sopaque}$(12/11μm) threshold used to distinguish between clouds with a 11-μm cloud optical depth of less than and greater than 2.0. The probability of false alarm (POF) is shown in blue, the probability of detection (POD) is shown in red, and the skill score is depicted by the black solid line. The $\beta_{sopaque}$(12/11μm) threshold that maximizes the skill score is depicted by the dashed black line. This analysis is based on over 8000 SEVIRI/CALIOP match-ups. 43
Figure 7: Peirce-Hanssen-Kuipers skill score metrics are shown as a function of the absolute difference in the 7.4 μm – 11 μm opaque cloud temperature (T_{opaque}(diff)) threshold used to distinguish between clouds with a 11-μm cloud optical depth of less than and greater than 2.0. The probability of false alarm (POF) is shown in blue, the probability of detection (POD) is shown in red, and the skill score is depicted by the black solid line. The T_{opaque}(diff) threshold that maximizes the skill score is depicted by the dashed black line. This analysis is based on over 8000 SEVIRI/CALIOP match-ups. 45
Figure 8: The normalized distribution of β_{mtropo}(7.4/11μm) is shown for single layer (black) and multilayered (red) definite ice clouds. CALIOP was used to identify single layer clouds with a cloud top temperature of 233 K or less and multilayered cloud systems where the cloud top temperature of the highest cloud layer is 233 K or less. The threshold used to distinguish between single and multilayered ice cloud systems is shown in blue. 48
Figure 9: The cumulative distribution function (CDF) of $\beta_{sopaque}$(8.5/11μm) for 5 CALIOP-derived cloud top temperature bins is shown for 5 different bins of 7.4 μm

opaque cloud temperature (T_{opaque}(7.4μm)). In panel A, 233 K < T_{opaque}(7.4μm) < 243 K. In panel B, 243 K < T_{opaque}(7.4μm) < 253 K. In panel C, 253 K < T_{opaque}(7.4μm) < 263 K. In panel D, T_{opaque}(7.4μm) > 263 K. Finally in panel E, T_{opaque}(7.4μm) is undefined because the cloud is well below the peak of the 7.4 μm weighting function or the cloud is too optically thin to be differentiated from the 7.4 μm clear sky signal. 55
Figure 10: The cumulative distribution function (CDF) of β_{stropo}(8.5/11μm) for 5 CALIOP-derived cloud top temperature bins is shown for 3 different bins of 7.4 μm opaque cloud temperature (T_{opaque}(7.4μm)). In panel A, 233 K < T_{opaque}(7.4μm) < 243 K. In panel B, 243 K < T_{opaque}(7.4μm) < 253 K. In panel C, 253 K < T_{opaque}(7.4μm) < 263 K. 62
Figure 11: The cumulative distribution function (CDF) of $\beta_{sopaque}$(8.5/11μm) for 5 CALIOP-derived cloud top temperature bins is shown for 4 different bins of 11 μm opaque cloud temperature (T_{opaque}(11μm)). In panel A, 233 K < T_{opaque}(11μm) < 243 K. In panel B, 243 K < T_{opaque}(11μm) < 253 K. In panel C, 253 K < T_{opaque}(11μm) < 263 K. In panel D, 263 K < T_{opaque}(11μm) < 273 K. 67
Figure 12: A flow chart of the decision tree used to determine cloud type using the results of several logical tests described in Section 3.4.2.6.1 through Section 3.4.2.6.16 is shown. 71
Figure 13: The impacts of the median filter are shown. Unfiltered cloud type output is shown on the top and filtered cloud type output on the bottom. Note how the median filter removes artifacts near the edge of the different cloud categories indicated by different colors. 73
Figure 14 - False color images for GOES-17 on October 17, 2019 at 8:00/12:00 UTC (top left/right respectively) and the corresponding GOES-17 cloud phase products (bottom left/right respectively). The GOES-17 data was not impacted by the LHP anomaly at 8:00 UTC, but severely impacted at 12:00 UTC. 79
Figure 15 – Time series of the ACT cloud phase fraction from GOES-16 full-disk data from June 1, 2017 – November 24, 2017. The red data points represent the fraction of ice clouds 82
Figure 16 - Distribution of the 10.3 μm (left) and 11.2 μm (right) single layer tropopause emissivity for liquid and ice pixels determined by a manually-labeled GOES-16 training data set. 83
Figure 17 - Distribution of the 3.9 μm pseudo-emissivity calculated using the 10.3 μm (left) and 11.2 μm (right) BT for liquid and ice pixels determined by a manually-labeled GOES-16 training data set. 84
Figure 18 - Distribution of the 10.3/11.2 μm Beta ratios calculated using the single-layer tropopause (top left), multi-layer tropopause (top right), single-layer opaque (bottom left) and multi-layer opaque (bottom right) assumptions for liquid and ice pixels determined by a manually-labeled GOES-16 training data set. 85
Figure 19 – Ratio of the ice/liquid conditional probabilities pertaining to the [εstropo10μm, εpseudo3.9,10μm] (left) and [εstropo11μm, εpseudo3.9,11μm] (right) LUTs for pixels over water. All bins contain ratio values greater than 0.0 with bin values less than 1.0 shaded gray. 86
Figure 20 - Ratio of the ice/liquid conditional probabilities pertaining to the [εstropo10μm, βstropo10/11μm] (top left), [εstropo10μm, βmtropo10/11μm] (top

right), [εstropo10μm**,** βsopaque10/11μm**] (bottom left) and [**εstropo10μm**,** βmopaque10/11μm**] (bottom right) LUTs for pixels over water. All bins contain ratio values greater than 0.0 with bin values less than 1.0 shaded gray.** 87
Figure 21 – False color image (left) and Bayesian ice cloud probability (right) for the GOES-17 CONUS domain on August 29, 2019 at 10:01 UTC..... 88
Figure 22: A flow chart of the decision tree used to determine cloud type during the GOES-17 FPT mitigation period using the calculated Bayesian ice probability..... 89
Figure 23 - False color image (top left), Bayesian ice cloud probability (top right), cloud type (bottom left) and cloud phase (bottom right) for the GOES-17 CONUS domain on August 29, 2019 at 10:01 UTC. The cloud type and cloud phase products were both generated using the Bayesian ice cloud probability..... 90
Figure 24 – False color images for GOES-17 (left) and GOES-16 (right) on October 17, 2019 at 12:00 UTC where the full-disk domains overlap and satellite viewing angles are less than 50º. The GOES-17 image is severely degraded due to the LHP anomaly..... 91
Figure 25 - False color image for GOES-17 (top left), GOES-16 cloud phase (top right), GOES-17 cloud phase produced without mitigation logic (bottom left) and GOES-17 cloud phase produced with mitigation logic (bottom right) on October 17, 2019 at 12:00 UTC where the full-disk domains overlap and satellite viewing angles are less than 50º. 92
Figure 26: SEVIRI RGB image from 12 UTC on November 24, 2006. 95
Figure 27: Illustration of the CALIPSO data used in this study. Top image shows a 2d backscatter profile. Bottom image shows the detected cloud layers overlaid onto the backscatter image. Cloud layers are color magenta..... 96
Figure 28: Example results (using SEVIRI) from the ACT algorithm for November 25, 2005. The top, left panel is a RGB false color image and the top, right and bottom, left panels show the cloud type and cloud phase results, respectively..... 97
Figure 29: A more detailed look at the cloud type results shown in Figure 28 for a small region near the Ivory Coast of Africa. 98
Figure 30: Example cloud top phase and cloud type output are shown for a VIIRS granule over Asia on November 10, 2012 at 03:39 UTC. False color images are shown in the top two panels and the cloud phase (left) and type (right) are shown in the bottom two panels. The CALIPSO ground track is overlaid on each panel..... 99
Figure 31: The total cloud phase error as a function of the assumed error in classifying potentially mixed phase clouds is shown when the minimum cloud optical depth qualifier is *ignored* (top) and when it *is* applied (bottom) with the solid black line. The dashed red line is the allowed error from the F&PS. The dashed blue line is the actual accuracy achieved without including potentially mixed phase clouds in the validation analysis. 102
Figure 32: Same as Figure 31, except for cloud type. 105

LIST OF TABLES

Table 1: GOES-R cloud top phase product requirements. The Geographic Coverage definitions are: M=Mesoscale, C=CONUS, and FD=Full Disk. 16
Table 2: GOES-R cloud type product requirements. The Geographic Coverage definitions are: M=Mesoscale, C=CONUS, and FD=Full Disk. 17
Table 3: JPSS Risk Reduction cloud top phase product requirements. 18
Table 4: JPSS Risk Reduction cloud type product requirements. 18
Table 5: Channel numbers and wavelengths for the ABI. 19
Table 6: Channel numbers and wavelengths for the NPP VIIRS. 19
Table 7: Inputs used in calculation of Local Radiative Center (LRC). The gradient filter function used in the calculation is described in the AIADD document. 39
Table 8: The thresholds used by the Low Surface Emissivity (LSE) Test as a function of sensor. 41
Table 9: The thresholds used by the β(12/11μm) Opaque Cloud (BOC) Test as a function of sensor. 43
Table 10: The thresholds used by the Opaque Cloud Temperature Difference (OCTD) Test as a function of sensor. 45
Table 11: The thresholds used by the Water Vapor Multilayered Detection (WVMD) Test as a function of sensor 49
Table 12: The thresholds used by the Infrared Window Multilayered Detection (IWMD) Test as a function of sensor. 50
Table 13: "BOWVIC_Thresh1" threshold values used in the $\beta_{sopaque}$(8.5/11μm) and Water Vapor Ice Cloud (BOWVIC) Test as a function of sensor and 7.4 μm opaque cloud temperature (T_{opaque}(7.4μm)) 55
Table 14: "BOWVIC_Thresh2" threshold values used in the $\beta_{sopaque}$(8.5/11μm) and Water Vapor Ice Cloud (BOWVIC) Test as a function of sensor and 7.4 μm opaque cloud temperature (T_{opaque}(7.4μm)) 56
Table 15: "BOWVIC_Thresh3" threshold values used in the $\beta_{sopaque}$(8.5/11μm) and Water Vapor Ice Cloud (BOWVIC) Test as a function of sensor and 7.4 μm opaque cloud temperature (T_{opaque}(7.4μm)) 56
Table 16: "BOWVIC_Thresh4" threshold values used in the $\beta_{sopaque}$(8.5/11μm) and Water Vapor Ice Cloud (BOWVIC) Test as a function of sensor and 7.4 μm opaque cloud temperature (T_{opaque}(7.4μm)) 56
Table 17: "BOWVIC_Thresh5" threshold values used in the $\beta_{sopaque}$(8.5/11μm) and Water Vapor Ice Cloud (BOWVIC) Test as a function of sensor and 7.4 μm opaque cloud temperature (T_{opaque}(7.4μm)) 57
Table 18: "BOWVIC_Thresh6" threshold values used in the $\beta_{sopaque}$(8.5/11μm) and Water Vapor Ice Cloud (BOWVIC) Test as a function of sensor and 7.4 μm opaque cloud temperature (T_{opaque}(7.4μm)) 57
Table 19: The third and fourth thresholds used by the $\beta_{sopaque}$(8.5/11μm) and Water Vapor Ice Cloud LRC-only (BOWVIC-LRC) Test as a function of sensor. 58
Table 20: The thresholds used by the $\beta_{sopaque}$(8.5/11μm) Opaque Ice Cloud (BOIC) Test as a function of sensor 60

Table 21: "BTWVIC_Thresh1" threshold values used in the $\beta_{stropo}(8.5/11\mu m)$ and Water Vapor Ice Cloud (BTWVIC) Test as a function of sensor and 7.4 μm opaque cloud temperature ($T_{opaque}(7.4\mu m)$)..... 63
Table 22: "BTWVIC_Thresh2" threshold values used in the $\beta_{stropo}(8.5/11\mu m)$ and Water Vapor Ice Cloud (BTWVIC) Test as a function of sensor and 7.4 μm opaque cloud temperature ($T_{opaque}(7.4\mu m)$)..... 63
Table 23: The "BTWVIC_Thresh3" and " BTWVIC_Thresh4" thresholds used by the $\beta_{stropo}(8.5/11\mu m)$ Water Vapor Ice Cloud (BTWVIC) Test as a function of sensor..... 63
Table 24: The thresholds used by the Sub-classify Ice Cloud (SCIC) Test as a function of sensor. 65
Table 25: "MP_Thresh1" threshold values used in the Mixed Phase (MP) Test as a function of sensor and 11 μm opaque cloud temperature ($T_{opaque}(11\mu m)$). 67
Table 26: "MP_Thresh2" threshold values used in the Mixed Phase (MP) Test as a function of sensor and 11 μm opaque cloud temperature ($T_{opaque}(11\mu m)$). 68
Table 27: "MP_Thresh3" threshold values used in the Mixed Phase (MP) Test as a function of sensor and 11 μm opaque cloud temperature ($T_{opaque}(11\mu m)$). 68
Table 28: "MP_Thresh4" threshold values used in the Mixed Phase (MP) Test as a function of sensor and 11 μm opaque cloud temperature ($T_{opaque}(11\mu m)$). 69
Table 29: Correspondence between cloud phase and cloud type categories. 73
Table 30: A description of the cloud type output. 74
Table 31: A description of the cloud phase output. 74
Table 32: A complete description of the cloud type/phase quality flag output is shown. 75
Table 33: A complete description of the cloud type/phase Product Quality Information (PQI) output is shown. 76
Table 34: A complete description of the cloud type/phase metadata output is shown. 78
Table 35: The GOES-17 IR channel focal plane temperature thresholds used for the ACT algorithm. 80
Table 36 - Collocated GOES-16, GOES-17 (unmitigated) and GOES-17 (mitigated) cloud phase product categories compared to "truth" data composed of manually-labeled ice/liquid cloud pixels from October 17, 2019 between 0-9 UTC and 18-23 UTC, when the GOES-17 data is not impacted by the LHP anomaly..... 93
Table 37 – Collocated GOES-16, GOES-17 (unmitigated) and GOES-17 (mitigated) cloud phase product categories compared to "truth" data composed of manually-labeled ice/liquid cloud pixels from October 17, 2019 between 9-18 UTC when the GOES-17 data is degraded by the LHP anomaly. 93
Table 38: The SEVIRI bands used to test the ACT algorithm is shown relative to the corresponding ABI bands. 94
Table 39: The VIIRS bands used to test the JRRCT algorithm. 95
Table 40: ABI cloud phase validation statistics *without* invoking minimum cloud optical depth qualifier are shown. The liquid water and supercooled water categories are combined since differences between the two categories are solely a function of the measured 11-μm brightness temperature. Potentially mixed phase clouds ($268\ K < T_{cld} < 238\ K$) are counted in the total statistics. 101
Table 41: Same as Table 40, except the minimum cloud optical depth qualifier *is* invoked..... 101

Table 42: The accuracy of the JRRCT cloud phase product is shown as a function the minimum CALIOP cloud optical depth considered and the geographic region. The numbers in parenthesis indicates the number of data points where the JRRCT and CALIOP agree compared to the total number of VIIRS/CALIOP matchups..... 103
Table 43: ABI cloud type validation statistics *without* invoking minimum cloud optical depth qualifier are shown. The liquid water and supercooled water categories are combined since differences between the two categories are solely a function of the measured 11-μm brightness temperature. Potentially mixed phase clouds (268 K < T_{cld} < 238 K) are counted in the total statistics..... 104
Table 44: Same as Table 43, except the minimum cloud optical depth qualifier *is* invoked..... 104
Table 45: The accuracy of the JRRCT cloud type product is shown as a function the minimum CALIOP cloud optical depth considered and the geographic region. The numbers in parenthesis indicates the number of data points where the JRRCT and CALIOP agree compared to the total number of VIIRS/CALIOP matchups..... 106

LIST OF ACRONYMS

ABI – Advanced Baseline Imager
AC – Above Cloud
ACT – ABI Cloud Type/Phase
AIADD – Algorithm Interface and Ancillary Data Description
ARM – Atmospheric Radiation Measurement
ATBD – Algorithm Theoretical Basis Document
AVHRR – Advanced Very High Resolution Radiometer
BOC – β (12/11μm) Opaque Cloud
BOIC – $\beta_{sopaque}$(8.5/11μm) Opaque Ice Cloud
BOWVIC – $\beta_{sopaque}$(8.5/11μm) and Water Vapor Ice Cloud
BOWVIC-LRC – $\beta_{sopaque}$(8.5/11μm) and Water Vapor Ice Cloud LRC-only
BTWVIC – β_{stropo}(8.5/11μm) and Water Vapor Ice Cloud
CALIOP – Cloud-Aerosol Lidar with Orthogonal Polarization
CALIPSO – Cloud-Aerosol Lidar and Infrared Pathfinder Satellite Observation
CDF – Cumulative Distribution Function
CIMSS – Cooperative Institute for Meteorological Satellite Studies
CONUS – Continental United States
ECMWF – European Centre for Medium-Range Weather Forecasts
EOS – Earth Observing System
ESA – European Space Agency
F&PS – Functional & Performance Specification
FPT – Focal Plane Temperature
GFS – Global Forecast System
GOES – Geostationary Operational Environmental Satellite
HF – Homogeneous Freezing
IWMD – Infrared Window Multilayered Detection
JPSS – Joint Polar Satellite System
JRRCT – JPSS Risk Reduction Cloud Type/Phase
LHP – Loop Heat Pipe
LRC – Local Radiative Center
LSE – Low Surface Emissivity
LUT – Look-up Table
MODIS – Moderate Resolution Imaging Spectroradiometer
MP – Mixed Phase
NASA – National Aeronautics and Space Agency
NESDIS – National Environmental Satellite, Data, and Information Service
NOAA – National Oceanic and Atmospheric Administration
NPP – National Polar-orbiting Partnership
NWP – Numerical Weather Prediction
OCTD – Opaque Cloud Temperature Difference
OIC – Overall Ice Cloud
OMC – Overall Multilayered Cloud
OOC – Overall Opaque Cloud
POD – Probability of Detection

POES – Polar Operational Environmental Satellite
POF – Probability of False Alarm
RGB – Red-Green-Blue
RRPS – Risk Reduction Product System
RTM – Radiative Transfer Model
SCIC – Sub-Classify Ice Cloud
SEVIRI – Spinning Enhanced Visible and Infrared Imager
SLW – Supercooled Liquid Water
SSEC – Space Science and Engineering Center
STAR – Center for Satellite Applications and Research
TOA – Top of Atmosphere
TRR – Test Readiness Review
UTC – Coordinated Universal Time
VIIRS – Visible Infrared Imaging Radiometer Suite
WVMD – Water Vapor Multilayered Detection

ABSTRACT

This document provides a high level description of the physical basis for the determination of cloud type and cloud phase information, of each cloudy pixel within images taken by the Advanced Baseline Imager (ABI) flown on the GOES-R series of NOAA geostationary meteorological satellites and by the Suomi National Polar-orbiting Partnership (NPP) Visible Infrared Imaging Radiometer Suite (VIIRS) meteorological satellite. The cloud phase is determined from the cloud type information within the same algorithm module. Thus, the cloud type and cloud phase are described in the same Algorithm Theoretical Basis Document (ATBD). The cloud phase and type categories are based on heritage NOAA cloud phase and type products.

The ABI cloud type/phase (ACT) algorithm and the Joint Polar Satellite System (JPSS) Risk Reduction cloud type/phase (JRRCT) algorithm utilizes a series of spectral and spatial tests to determine the cloud type (liquid water, supercooled water, mixed phase, optically thin ice, optically thick ice, and multilayered ice). The ACT algorithm utilizes ABI channels 10 (7.4 μm), 11 (8.5 μm), 14 (11 μm), and 15 (12 μm), while the JRRCT algorithm utilizes VIIRS channels M14 (8.5 μm), M15 (10.8 μm) and M16 (12 μm), which are all infrared channels. In lieu of brightness temperature differences, effective absorption optical depth ratios are used in the spectral tests. Effective absorption optical depth ratios, allow for improved sensitivity to cloud microphysics, especially for optically thin clouds. The validation analysis indicates that the algorithm with comfortably meet the accuracy requirements.

1 INTRODUCTION

1.1 Purpose of This Document

The cloud type Algorithm Theoretical Basis Document (ATBD) provides a high level description of the physical basis for the determination of cloud type and cloud phase information, of each cloudy pixel within images taken by the Advanced Baseline Imager (ABI) flown on the GOES-R series of NOAA geostationary meteorological satellites and by the Suomi National Polar-orbiting Partnership (NPP) Visible Infrared Imaging Radiometer Suite (VIIRS) meteorological satellite. The cloud phase is determined from the cloud type information within the same algorithm module. Thus, the cloud type and cloud phase are described in the same ATBD. Output from the cloud type and cloud phase algorithms are made available to all subsequent algorithms that require knowledge of the cloud type or phase of cloudy pixels. The cloud type and phase algorithm only operates on cloudy pixels and, hence, depends on the ABI or VIIRS cloud mask.

1.2 Who Should Use This Document

The intended users of this document are those interested in understanding the physical basis of the algorithms and how to use the output of this algorithm to optimize the cloud phase and type for a particular application. This document also provides information useful to anyone maintaining or modifying the original algorithm.

1.3 Inside Each Section

This document is broken down into the following main sections.

- **System Overview**: Provides relevant details of the ABI and the VIIRS and provides a brief description of the products generated by the algorithm.

- **Algorithm Description**: Provides all the detailed description of the algorithm including its physical basis, its input and its output.

- **Test Data Sets and Outputs:** Provides a detailed description of the data sets used to develop and test the GOES-R ABI cloud type/phase (ACT) algorithm and the Joint Polar Satellite System (JPSS) Risk Reduction cloud type/phase (JRRCT) algorithm and describes the algorithm output.

- **Practical Considerations:** Provides a description of algorithm programming and quality control considerations.

- **Assumptions and Limitations**: Provides an overview of the current limitations of the approach and gives the plan for overcoming these limitations with further algorithm development.

1.4 Related Documents

- GOES-R Functional & Performance Specification Document (F&PS)
- GOES-R ABI Cloud Product Validation Plan Document
- Algorithm Interface and Ancillary Data Description (AIADD) Document

1.5 Revision History

- 9/30/2008 - Version 0.1 of this document was created by Michael J Pavolonis (NOAA/NESDIS/STAR). Version 0.1 represents the first draft of this document.

- 6/30/2009 – Version 1.0 of this document was created by Michael J Pavolonis (NOAA/NESDIS/STAR). In this revision, Version 1.0 was revised to meet 80% delivery standards.

- 6/30/2010 – Version 2.0 of this document was created by Michael J Pavolonis (NOAA/NESDIS/STAR). In this revision, Version 2.0 was revised to meet 100% delivery standards.

- 9/15/2010 – Version 2.0 of this document was revised by Michael J Pavolonis (NOAA/NESDIS/STAR). In this revision, Version 2.0 was revised further to meet 100% delivery standards.

- 12/9/2015 – Version 2.0 of this document was revised by Michael J Pavolonis (NOAA/NESDIS/STAR). In this revision, Version 2.0 was revised further to incorporate in VIIRS for JRRCT algorithm.

2 OBSERVING SYSTEM OVERVIEW

This section will describe the products generated by the ACT Algorithm and the JRRCT Algorithm and the requirements it places on the sensor.

2.1 Products Generated

The cloud type product consists of 6 cloud classifications. In addition, the cloud phase product consists of 4 cloud classifications. The cloud type categories are: warm liquid water cloud, supercooled liquid water, mixed phase, opaque ice, cirrus (e.g. semi-transparent ice clouds), and multilayered cloud (with semi-transparent upper-layer). The cloud phase categories are: warm liquid water phase, supercooled liquid water phase, mixed phase, and ice phase. The cloud phase is directly derived from the cloud type categories. The cloud type product contains information on multilayered clouds and cirrus that is useful to higher-level algorithms such as the cloud top height retrieval. The cloud phase and type categories are consistent with heritage products such as those from Moderate Resolution Imaging Spectroradiometer (MODIS) and Advanced Very High Resolution Radiometer (AVHRR).

Downstream cloud algorithms, such as the cloud height, the cloud optical properties algorithms, the fog detection/fog depth algorithm, and the cloud-icing algorithm, require the cloud type and phase products. The cloud type and phase information can also be used in advanced ABI and VIIRS applications such as severe weather prediction and tropical cyclone intensity estimation.

2.1.1 Product Requirements

The F&PS spatial, temporal, and accuracy requirements for the GOES-R cloud top phase and cloud type are shown below in Table 1 and Table 2, respectively.

Table 1: GOES-R cloud top phase product requirements. The Geographic Coverage definitions are: M=Mesoscale, C=CONUS, and FD=Full Disk.

Name	User & Priority	Geographic Coverage	Vertical Res.	Horiz. Res.	Mapping Accuracy	Msmnt. Rang	Msmnt. Accuracy	Refresh Rate/Coverage Time Option (Mode 3)	Refresh Rate Option (Mode 4)	Data Latency	Long-Term	Product Measurement Precision
Cloud Top Phase	GOES-R	C	Cloud Top	2 km	1 km	Liquid/ solid/ supercooled/ mixed	80% Correct Classification	5 min	5 min	266 sec	TBD	1.5 categories ***(requested change to NA)***
Cloud Top Phase	GOES-R	FD	Cloud Top	2 km	1 km	Liquid/ solid/ supercooled/ mixed	80% Correct Classification	15 min	15 min	806 sec	TBD	1.5 categories ***(requested change to NA)***
Cloud Top Phase	GOES-R	M	Cloud Top	2 km	1 km	Liquid/ solid/ supercooled/ mixed	80% Correct Classification	5 min	NA	266 sec	TBD	1.5 categories ***(requested change to NA)***

Name	User & Priority	Geographic Coverage	Temporal Coverage Qualifiers	Product Extend Qualifiers	Cloud Cover Conditions Qualifiers	Product Statistics Qualifier
Cloud Top Phase	GOES-R	C	Day and night	Quantitative out to at least 65 degrees LZA and qualitative beyond	In presence of clouds with optical depth >1. Clear conditions down to cloud top associated with threshold accuracy	Over specified geographic area
Cloud Top Phase	GOES-R	FD	Day and night	Quantitative out to at least 65 degrees LZA and qualitative beyond	In presence of clouds with optical depth >1. Clear conditions down to cloud top associated with threshold accuracy	Over specified geographic area
Cloud Top Phase	GOES-R	M	Day and night	Quantitative out to at least 65 degrees LZA and qualitative beyond	In presence of clouds with optical depth >1. Clear conditions down to cloud top associated with threshold accuracy	Over specified geographic area

Table 2: GOES-R cloud type product requirements. The Geographic Coverage definitions are: M=Mesoscale, C=CONUS, and FD=Full Disk.

Name	User & Priority	Geographic Coverage	Vertical Res.	Horiz. Res.	Mapping Accuracy	Msmnt. Rang	Msmnt. Accuracy	Refresh Rate/Coverage Time Option (Mode 3)	Refresh Rate Option (Mode 4)	Data Latency	Long-Term	Product Measurement Precision
Cloud Type	GOES-R	C	NA	10 km	5 km	7 Types	60% correct classification	15 min	5 min	536 sec	TBD	2.5 categories ***(requested change to NA)***
Cloud Type	GOES-R	FD	NA	2 km	1 km	7 Types	60% correct classification	15 min	5 min	159 sec	TBD	2.5 categories ***(requested change to NA)***
Cloud Type	GOES-R	M	NA	2 km	1 km	7 Types	60% correct classification	15 min	NA	266 sec	TBD	2.5 categories ***(requested change to NA)***

Name	User & Priority	Geographic Coverage	Tempral Coverage Qualifiers	Product Extend Qualifiers	Cloud Cover Conditions Qualifiers	Product Statistics Qualifier
Cloud Type	GOES-R	C	Day and night	Quantitative out to at least 65 degrees LZA and qualitative beyond	In presence of clouds with optical depth >1. Clear conditions down to cloud top associated with threshold accuracy	Over specified geographic area
Cloud Type	GOES-R	C	Day and night	Quantitative out to at least 65 degrees LZA and qualitative beyond	In presence of clouds with optical depth >1. Clear conditions down to cloud top associated with threshold accuracy	Over specified geographic area
Cloud Type	GOES-R	C	Day and night	Quantitative out to at least 65 degrees LZA and qualitative beyond	In presence of clouds with optical depth >1. Clear conditions down to cloud top associated with threshold accuracy	Over specified geographic area

The JPSS Risk Reduction Product System (RRPS) requirements for the JRRCT algorithm for cloud top phase and cloud type are shown below in Table 3 and Table 4, respectively.

Table 3: JPSS Risk Reduction cloud top phase product requirements.

Name	Cloud Top Phase
User & Priority	JPSS
Geographic Coverage	Global
Vertical Res.	Cloud Top
Horizontal Res.	0.75 km
Msmnt Range	Liquid/solid/supercooled/mixed (6 categories)
Msmnt Accuracy	80% correct classification
Refresh Rate	90 minutes
Data Latency	30 minutes after granule is available
Timeliness	≤ 3 hours
Temporal Coverage Qualifiers	Day and night
Product Extend Qualifiers	Quantitative out to at least 65 degrees LZA and qualitative beyond
Cloud Cover Conditions Qualifiers	In presence of clouds with optical depth > 1. Clear conditions down to cloud top associated with threshold accuracy
Product Statistics Qualifier	Over specified geographic area

Table 4: JPSS Risk Reduction cloud type product requirements.

Name	Cloud Type
User & Priority	JPSS
Geographic Coverage	Global
Vertical Res.	Cloud Top
Horizontal Res.	0.75 km
Msmnt Range	7 categories
Msmnt Accuracy	60% correct classification
Refresh Rate	90 minutes
Data Latency	30 minutes after granule is available
Timeliness	≤ 3 hours
Temporal Coverage Qualifiers	Day and night
Product Extend Qualifiers	Quantitative out to at least 65 degrees LZA and qualitative beyond
Cloud Cover Conditions Qualifiers	In presence of clouds with optical depth > 1. Clear conditions down to cloud top associated with threshold accuracy
Product Statistics Qualifier	Over specified geographic area

2.2 Instrument Characteristics

The cloud type and phase algorithm will be applied to each cloudy ABI or VIIRS pixel. Table 5 summarizes the channels used by the ACT while Table 6 summarizes the

channels used by the JRRCT. Recall that the cloud phase product is produced from the cloud type product.

Table 5: Channel numbers and wavelengths for the ABI.

Channel Number	*Wavelength (μm)*	*Used in ACT*
1	0.47	
2	0.64	
3	0.86	
4	1.38	
5	1.61	
6	2.26	
7	3.9	
8	6.15	
9	7.0	
10	7.4	✓
11	8.5	✓
12	9.7	
13	10.35	
14	11.2	✓
15	12.3	✓
16	13.3	

Table 6: Channel numbers and wavelengths for the NPP VIIRS.

Channel Number	*Wavelength (μm)*	*Used in JRRCT*
M1	0.412	
M2	0.445	
M3	0.488	
M4	0.555	
M5	0.672	
M6	0.746	
M7	0.865	
M8	1.240	
M9	1.378	
M10	1.61	
M11	2.25	
M12	3.7	
M13	4.05	
M14	8.55	✓
M15	10.763	✓
M16	12.013	✓

The ACT and JRRCT relies on infrared radiances to avoid day/night/terminator discontinuities. The algorithm relies on spectral and spatial tests, as well as the ABI or

VIIRS cloud mask, respectively. The performance of the cloud type algorithm is therefore sensitive to any imagery artifacts or instrument noise as well as the correct identification of cloudy pixels. Calibrated observations are also critical because the cloud type compares the observed values to those from a forward radiative transfer model. The channel specifications are given in the F&PS section 3.4.2.1.4.0 and in JPSS RRPS Requirement 1.2.7. We are assuming the performance outlined in the F&PS and JPSS RRPS requirements during our development efforts.

3 ALGORITHM DESCRIPTION

Below is a complete description of the final algorithm.

3.1 Algorithm Overview

The cloud type and phase products serve a critical role in the cloud property component of the GOES-R ABI and VIIRS processing system. Cloud top phase is a fundamental cloud property that is required by downstream cloud algorithms such as the cloud top height algorithm, the cloud optical property algorithm, the fog detection/fog depth algorithm, and the cloud-icing algorithm.

The GOES-R and JRRCT cloud type categories are based on the heritage Geostationary Operational Environmental Satellite (GOES) and Polar Operational Environmental Satellite (POES) Advanced Very High Resolution Radiometer (AVHRR) cloud type categories adopted by National Environmental Satellite, Data, and Information Service (NESDIS)/Center for Satellite Applications and Research (STAR). These categories were chosen on the basis that they could be derived from the measured radiances at all times during the day, unlike morphological cloud categories (e.g. stratus, stratocumulus, altocumulus, etc…), which can only be derived reliably when daylight is present. The chosen categories are also useful to downstream algorithms like cloud top height and cloud optical properties. The cloud type categories for cloudy pixels are:

- **Warm liquid water** (liquid water cloud with an opaque cloud temperature greater than 273 K)
- **Supercooled liquid water** (liquid water topped cloud with an opaque cloud temperature less than 273 K)
- **Mixed phase clouds** (high probability of containing both liquid water and ice near cloud top)
- **Optically thin ice clouds** (ice clouds which have an infrared optical depth of about 2.0 or less)
- **Optically thick ice clouds** (high emissivity ice topped clouds, infrared optical depths greater than 2.0)
- **Multilayered clouds** (optically thin ice cloud overlapping a lower optically thick cloud layer)

The cloud phase categories for cloudy pixels are:

- **Warm liquid water** (liquid water cloud with an opaque cloud temperature greater than 273 K)
- **Supercooled liquid water** (liquid water topped cloud with an opaque cloud temperature less than 273 K)
- **Mixed phase clouds** (high probability of containing both liquid water and ice near cloud top)
- **Ice phase clouds** (all ice topped clouds)

The cloud phase product is derived from the cloud type product. One can simply think of the cloud phase product as a slightly less descriptive version of the cloud type output. As Table 5 and Table 6 show, the ACT and JRRCT algorithm does not use solar-contaminated channels. A satellite-measured reflectance is a function of cloud microphysics, surface type, viewing and illumination geometry, and other factors. Due to the complex nature of scattering in the visible and near-infrared, and our inability to quickly simulate satellite reflectance values, we have chosen to avoid using sunlight contaminated channels at this time. One advantage of using infrared-only approach is that the algorithm performance is spectrally day/night independent (e.g. the same procedure is applied at all times).

The ACT and JRRCT derive the following ABI and VIIRS cloud products listed in the F&PS and JPSS RRPS requirements, respectively.

- Cloud type (6 cloud categories)
- Cloud phase (4 cloud categories)

Both of these products are derived at the pixel level for all cloudy pixels.

In addition, the ACT and JRRCT derive the following products that are not included in the F&PS and JPSS RRPS requirements, respectively.

- Quality Flags (defined in Section 3.4.3)
- Product Quality Information (defined in Section 3.4.3)
- Metadata (defined in Section 3.4.3)

3.2 Processing Outline

As described earlier, the cloud type algorithm requires *a priori* knowledge of which pixels are cloudy. Thus, prior to calling the cloud type algorithm, the ABI or VIIRS cloud mask algorithm must be applied. Given this requirement, the algorithm processing precedence is as follows: ABI (or VIIRS) cloud mask --> cloud type/phase routine. The ACT or JRRCT requires multiple scan lines of ABI or VIIRS data, respectively, due to the spatial analysis that is utilized in the algorithm. Complete scan line segments should consist of at least the minimum number of scan lines required by the Gradient Filter, which is described in detail in the AIADD. While overlap between adjacent scan line segments is beneficial, scan line overlap was not used in the development and validation of this algorithm. The processing outline of the ACT is summarized in Figure 1. The same process applies for the JRRCT except that the M14, M15 and M16 VIIRS channels are needed instead of ABI channels 10, 11, 14 and 15.

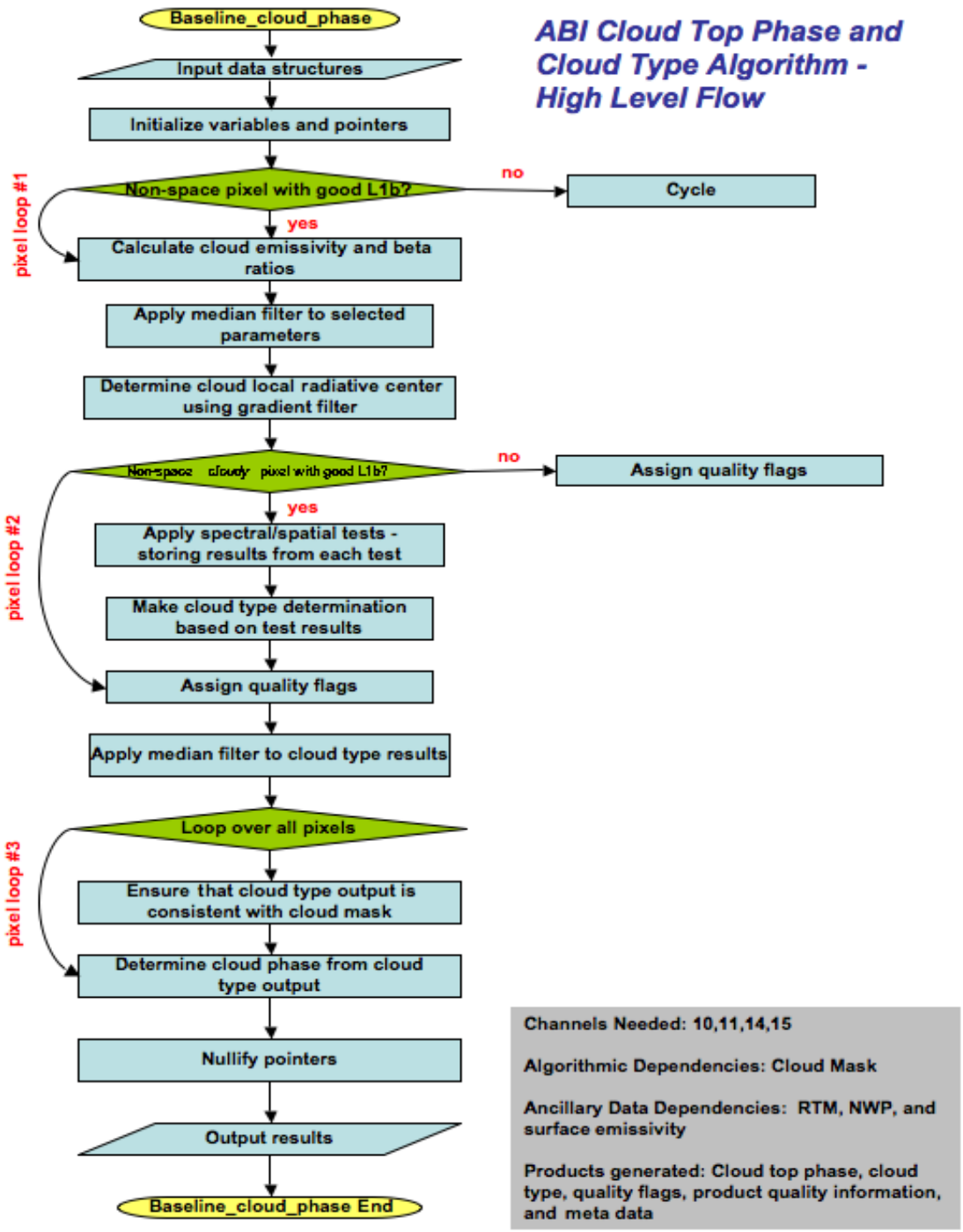

Figure 1: High Level Flowchart of the ACT illustrating the main processing sections. The tail of the pixel loop arrows indicates the start of a loop over all pixels in current scan line segment. The head of the arrow indicates the end of the loop. The first loop "yes" condition is that the pixel is earth geolocated and has valid spectral data (according to the L1b calibration quality flags). The "yes" condition for the second loop is that the pixel is earth geolocated, has valid spectral data, and is cloudy. The third loop is over all pixels.

3.3 Algorithm Input

This section describes the input needed to process the ACT and JRRCT. While the ACT and JRRCT operates on a pixel-by-pixel basis, surrounding pixels are needed for spatial analysis. Therefore, the ACT and JRRCT must have access to a group of pixels. In its current configuration, we run the ACT and JRRCT on segments comprised of 200 scan-lines. The minimum scan line segment size required to implement the ACT and JRRCT is driven by the minimum number of scan lines required to fully utilize the gradient filter routine (see AIADD Document for more details). The following sections describe the actual input needed to run the ACT and JRRCT.

3.3.1 Primary Sensor Data

The list below contains the primary sensor data currently used by the ACT and JRRCT. By primary sensor data, we mean information that is derived solely from the ABI and VIIRS observations and geolocation information.

- Calibrated radiances for ABI channels 10 (7.4 μm), 11 (8.5 μm), 14 (11 μm), and 15 (12 μm) or for VIIRS channels M14 (8.5 μm), M15 (10.8 μm), and M16 (12 μm)
- Calibrated brightness temperature for ABI channel 14 (11 μm) or VIIRS channel M15 (10.8 μm)
- Sensor viewing zenith angle
- L1b quality information from calibration for ABI channels 10, 11, 14, and 15 or for VIIRS channels M14, M15 and M16
- Space mask (is the pixel geolocated on the surface of the Earth?)
- ABI or VIIRS cloud mask output (product developed by cloud team)

3.3.2 Derived Data

The following upstream ABI or VIIRS derived products are needed by the ACT or JRRCT, respectively.

- ABI (or VIIRS) cloud mask output – the ACT (or JRRCT) requires the ABI (or VIIRS) cloud mask described in the cloud mask ATBD. The cloud mask is used to identify cloudy pixels. The cloud phase is not determined for clear pixels.

3.3.3 Ancillary Data

The following data lists and briefly describes the ancillary data requited to run the ACT and JRRCT. By ancillary data, we mean data that requires information not included in the ABI and VIIRS observations or geolocation data.

- **Surface emissivity of ABI channel 11 (8.5 μm) or VIIRS channel M14 (8.5 μm)**
  A global database of monthly mean infrared land surface emissivity is required for ABI channel 11 or VIIRS channel M14. The ACT and JRRCT utilizes surface emissivity derived using the Moderate Resolution Imaging Spectroradiometer (MODIS). Emissivity is available globally at ten generic wavelengths (3.6, 4.3, 5.0, 5.8, 7.6, 8.3, 9.3, 10.8, 12.1, and 14.3 microns) with 0.05 degree spatial resolution (Seemann et al. 2008). The ten wavelengths serve as anchor points in the linear interpolation to any wavelength between 3.6 and 14.3 microns. The monthly emissivities have been integrated over the ABI and VIIRS spectral response functions to match the ABI and VIIRS channels. This data set and the procedure for spectrally and spatially mapping it to the ABI and VIIRS are described in detail in Seemann et al. (2008) and the AIADD Document.

- **Profiles of pressure and temperature**
  The calculation of cloud emissivity requires profiles of pressure and temperature from a global Numerical Weather Prediction (NWP) model. In addition, knowledge of the location of the surface and tropopause levels is required. While six-hour forecasts were used in the development of the ACT and JRRCT, and, as such, are recommended, any forecast in the 0 to 24 hour range is acceptable. Details concerning the NWP data can be found in the AIADD Document.

3.3.4 Radiative Transfer Models

The following lists and briefly describes the data that must be calculated by a radiative transfer model and derived prior to running the ACT and JRRCT algorithm. See the AIADD Document for a more detailed description.

- **Black cloud radiance profiles for ABI channels 10, 11, 14, and 15 and VIIRS channels M14, M15, and M16**
  The ACT and JRRCT requires the radiance emitted upward by a black body surface and transmitted through a non-cloudy atmosphere, with gaseous absorption, to the top of the atmosphere as a function of the atmospheric level of the black surface. The black cloud radiance is computed as a function of NWP grid cells and viewing angle (it is not computed at the pixel resolution), as described in detail in the AIADD Document.

- **Top-of-atmosphere clear-sky radiance estimates for ABI channels 10, 11, 14, and 15 and VIIRS channels M14, M15, M16**
  The ACT and JRRCT require knowledge of the top-of-atmosphere radiance ABI or VIIRS would sense under clear-sky conditions at each pixel.

3.4 Theoretical Description

The methodology described in this section is based on the physical concepts described in Pavolonis (2010a and 2010b).

3.4.1 Physics of the Problem

The cloud type algorithm utilizes ABI Channels 10, 11, 14, and 15 or VIIRS channels M14, M15, and M16. These channels have an approximate central wavelength of 7.4, 8.5, 11, and 12 μm for ABI and 8.5, 11, and 12 μm for VIIRS, respectively. These central wavelengths will be referred to rather than the ABI or VIIRS channel numbers throughout the "Theoretical Description."

The spectral sensitivity to cloud composition is perhaps best understood by examining the imaginary index of refraction for liquid and ice, m_i, as a function of wavelength. The imaginary index of refraction is often directly proportional to absorption/emission strength for a given particle composition, in that larger values are indicative of stronger absorption of radiation at a particular wavelength. However, absorption due to photon tunneling, which is proportional to the real index of refraction, can also contribute to the observed spectral absorption under certain circumstances (Mitchell, 2000). For simplicity, only absorption by the geometrical cross section, which is captured by the imaginary index of refraction, is discussed here. Figure 2 shows m_i for liquid water (Downing and Williams, 1975) and ice (Warren and Brandt, 2008). The m_i can be interpreted as follows. In Figure 2, one sees that around 8.5 - 10 μm liquid water and ice absorb approximately equally, while near 11 – 13.5 μm ice absorbs more strongly than water. Thus, all else being equal, the difference in measured radiation (or brightness temperature) between an 8.5 μm channel and an 11 μm channel (or 12 μm or 13.3 μm channel) will be larger for an ice cloud compared to a liquid water cloud. The previous statement is only accurate if the liquid water and ice cloud have the same particle concentrations at the same vertical levels in the same atmosphere, and have the same particle size and shape distribution. That is what is meant by "all else being equal." While Figure 2 is insightful, it can also be deceiving if not interpreted correctly. For example, it is possible that a liquid water cloud in a certain vertical layer with a certain particle distribution will look identical (in measurement space) to an ice cloud at the same vertical layer (in the same atmosphere), but with a different particle distribution. As another example, a scene with a liquid water cloud in one type of atmosphere (e.g. maritime tropical) may exhibit the same measured spectral radiance as a scene with an ice cloud in another type of atmosphere (e.g. continental mid-latitude).

In order to maximize the sensitivity to cloud phase/type, the information contained in Figure 2 must be extracted from the measured radiances as best as possible. One way of doing this is to account for the background conditions (e.g. surface temperature, surface emissivity, atmospheric temperature, and atmospheric water vapor) of a given scene in an effort to isolate the cloud microphysical signal. This is difficult to accomplish with

traditional brightness temperatures and brightness temperature differences. In the following section, we derive a data space that accounts for the background conditions.

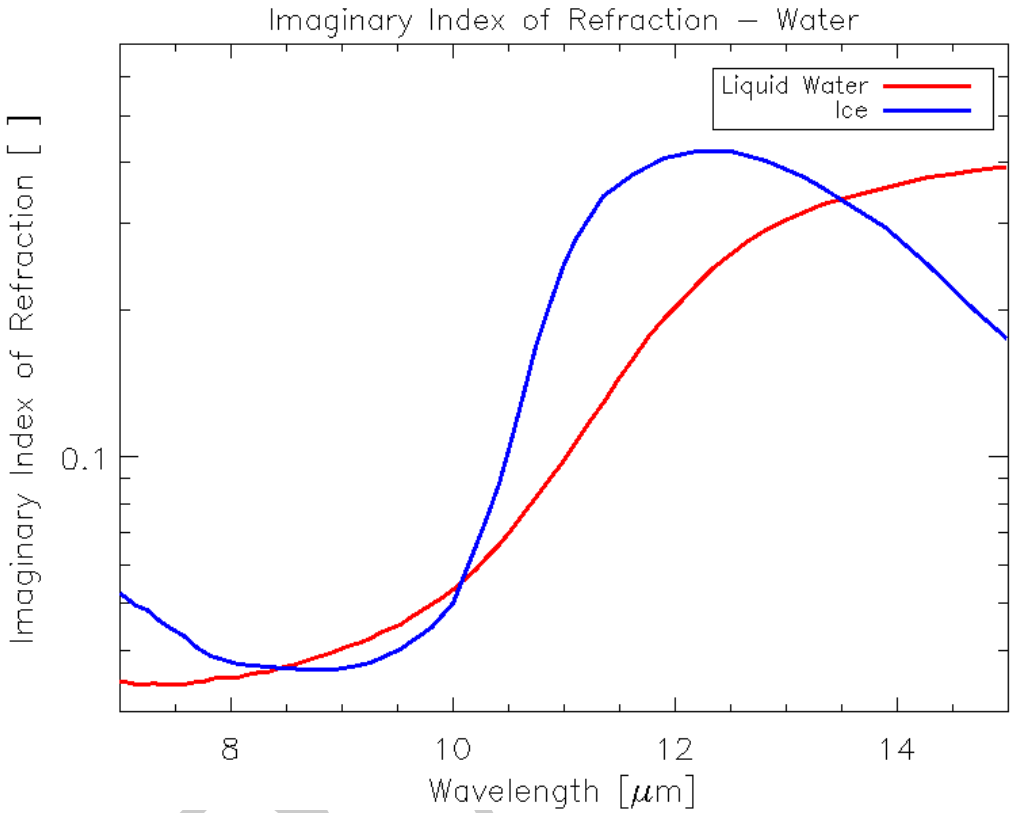

Figure 2: The imaginary index of refraction for liquid water (red) and ice (blue) is shown as a function of wavelength.

3.4.1.1 Infrared Radiative Transfer

Assuming a satellite viewing perspective (e.g. upwelling radiation), a fully cloudy field of view, a non-scattering atmosphere (no molecular scattering), and a negligible contribution from downwelling cloud emission or molecular emission that is reflected by the surface and transmitted to the top of troposphere (Zhang and Menzel (2002) showed that this term is very small at infrared wavelengths), the cloudy radiative transfer equation for a given infrared channel or wavelength can be written as in Equation 1 (e.g. Heidinger and Pavolonis, 2009; Pavolonis, 2010a).

$$R_{obs}(\lambda) = \varepsilon(\lambda)R_{ac}(\lambda) + t_{ac}(\lambda)\varepsilon(\lambda)B(\lambda,T_{eff}) + R_{clr}(\lambda)(1-\varepsilon(\lambda)) \quad \text{(Eq. 1)}$$

In Equation 1, λ is wavelength, R_{obs} is the observed top-of-atmosphere (TOA) radiance, R_{clr} is the TOA clear sky radiance. R_{ac} and t_{ac} are the above cloud to TOA upwelling atmospheric radiance and transmittance, respectively. B is the Planck Function, and T_{eff} is the effective cloud temperature. The effective cloud emissivity (Cox, 1976) is given by ε. To avoid using additional symbols, the angular dependence is simply implied.

Equation 1, while commonly used, is derived step by step in Pavolonis (2010a), if interested.

Equation 1 can readily be solved for the effective cloud emissivity as follows:

$$\varepsilon(\lambda) = \frac{R_{obs}(\lambda) - R_{clr}(\lambda)}{[B(\lambda, T_{eff}) t_{ac}(\lambda) + R_{ac}(\lambda)] - R_{clr}(\lambda)} \quad \text{(Eq. 2)}$$

In Equation 2, the term in brackets in the denominator is the blackbody cloud radiance that is transmitted to the TOA plus the above cloud (ac) atmospheric radiance. This term is dependent upon the effective cloud vertical location. The cloud vertical location dependence will be discussed in detail in later sections. Other than $R_{obs}(\lambda)$, the information needed to evaluate this expression is provided by the output from the clear sky radiative transfer model described in the AIADD Document.

The cloud microphysical signature cannot be captured with the effective cloud emissivity alone for a single spectral channel or wavelength. It is the spectral variation of the effective cloud emissivity that holds the cloud microphysical information. To harness this information, the effective cloud emissivity is used to calculate effective absorption optical depth ratios; otherwise known as β-ratios (see Inoue 1987; Parol et al., 1991; Giraud et al., 1997; and Heidinger and Pavolonis, 2009). For a given pair of spectral emissivities ($\varepsilon(\lambda_1)$ and $\varepsilon(\lambda_2)$):

$$\beta_{obs} = \frac{\ln[1 - \varepsilon(\lambda_1)]}{\ln[1 - \varepsilon(\lambda_2)]} = \frac{\tau_{abs}(\lambda_1)}{\tau_{abs}(\lambda_2)} \quad \text{(Eq. 3)}$$

Notice that Equation 3 can simply be interpreted as the ratio of effective absorption optical depth (τ) at two different wavelengths. The word "effective" is used since the cloud emissivity depends upon the effective cloud temperature. The effective cloud temperature is most often different from the thermodynamic cloud top temperature since the cloud emission originates from a layer in the cloud. The depth of this layer depends upon the cloud transmission profile, which is generally unknown. One must also consider that the effects of cloud scattering are implicit in the cloud emissivity calculation since the actual observed radiance will be influenced by cloud scattering to some degree. In other words, no attempt is made to separate the effects and absorption and scattering. At wavelengths in the 10 to 13 μm range, the effects of cloud scattering for upwelling radiation are quite small and usually negligible. But at infrared wavelengths in the 8 – 10 μm range, the cloud reflectance can make a 1 – 3% contribution to the top of atmosphere radiance (Turner, 2005). Thus, it is best to think of satellite-derived effective cloud emissivity as a radiometric parameter, which, in most cases, is proportional to the fraction of radiation incident on the cloud base that is absorbed by the cloud. See Cox (1976) for an in depth explanation of effective cloud emissivity.

An appealing quality of β_{obs}, is that it can be interpreted in terms of the single scatter properties, which can be computed for a given cloud composition and particle

distribution. Following Van de Hulst (1980) and Parol et al. (1991), a spectral ratio of scaled extinction coefficients can be calculated from the single scatter properties (single scatter albedo, asymmetry parameter, and extinction cross section), as follows.

$$\beta_{theo} = \frac{[1.0 - \omega(\lambda_1)g(\lambda_1)]\sigma_{ext}(\lambda_1)}{[1.0 - \omega(\lambda_2)g(\lambda_2)]\sigma_{ext}(\lambda_2)} \quad \text{(Eq. 4)}$$

In Equation 4, β_{theo} is the spectral ratio of scaled extinction coefficients, ω is the single scatter albedo, g is the asymmetry parameter, and σ_{ext} is the extinction cross section for an assumed particle distribution. At wavelengths in the 8 – 15 μm range, where multiple scattering effects are small, β_{theo}, captures the essence of the cloudy radiative transfer such that,

$$\beta_{obs} \approx \beta_{theo} \quad \text{(Eq. 5)}$$

Equation 4, which was first shown to be accurate for observation in the 10 – 12 μm "window" by Parol et al. (1991), only depends upon the single scatter properties. It does not depend upon the observed radiances, cloud height, or cloud optical depth. By using β-ratios as opposed to brightness temperature differences, we are not only accounting for the non-cloud contribution to the radiances, we are also providing a means to tie the observations back to theoretical size distributions. This framework clearly has practical and theoretical advantages over traditional brightness temperature differences. Parol et al. (1991) first showed that Equation 5 is a good approximation. Pavolonis (2010a) also showed that Equation 5 is a good approximation throughout the 10 - 13 μm window. Faster computers and improvements in the efficiency and accuracy of clear sky radiative transfer modeling have allowed for more detailed exploration of the β data space and computation of β-ratios on a global scale. As such, Pavolonis (2010a) and Pavolonis (2010b) showed that β-ratios offer improved sensitivity to cloud phase relative to brightness temperature differences for the same channel pair.

3.4.1.2 Cloud Phase Differences in β-Space

The 8.5, 11 μm channel pair (ABI Channels 11 and 14, VIIRS channels M14 and M15) contains the most direct information on cloud phase. From this channel pair, a β-ratio was constructed such that the 11 μm channel is placed in the denominator of Equations 3 and 4. Hereafter, this β is referred to as β(8.5/11μm). The single scatter property relationship (Equation 4) can be used to establish a theoretical relationship for β(8.5/11μm) as a function of cloud phase and cloud particle size. Figure 3 shows the β(8.5/11μm), given by the single scatter properties (see Equation 4), for liquid water and ice as a function of the effective particle radius. The single scatter properties of liquid water spheres were calculated using Mie theory. The ice single scatter properties were taken from the Yang et al. (2005) database, assuming a plate habit. Our analysis of the Yang et al. (2005) database indicates that the sensitivity to particle habit is small compared to the sensitivity to composition and particle size, so only a single ice habit is

shown for the sake of clarity. From this figure, one can see that liquid water and ice clouds can be distinguished over most of the effective particle radius range. Unlike brightness temperature differences, these β relationships are only a function of the cloud microphysical properties.

An analogous β-ratio can be constructed from the 11, 12 μm (ABI Channels 14 and 15, VIIRS channels M15 and M16) single scatter properties. This β-ratio, hereafter β(12/11μm), is shown as a function of the effective particle radius in Figure 4. Clearly, this β-ratio contains little to no information on cloud phase. β(12/11μm), however, is sensitive to particle size. This sensitivity will be exploited in the ACT and JRRCT algorithm to identify opaque clouds. For opaque clouds, the 11-μm brightness temperature is generally a good proxy for the thermodynamic cloud top temperature, which is useful information when inferring cloud phase. For instance, clouds with a cloud top temperature greater than 273 K, the melting point of water at typical atmospheric pressures, cannot contain ice at cloud top. The methodology used to identify opaque clouds from β(12/11μm) will be explained in detail in a later section.

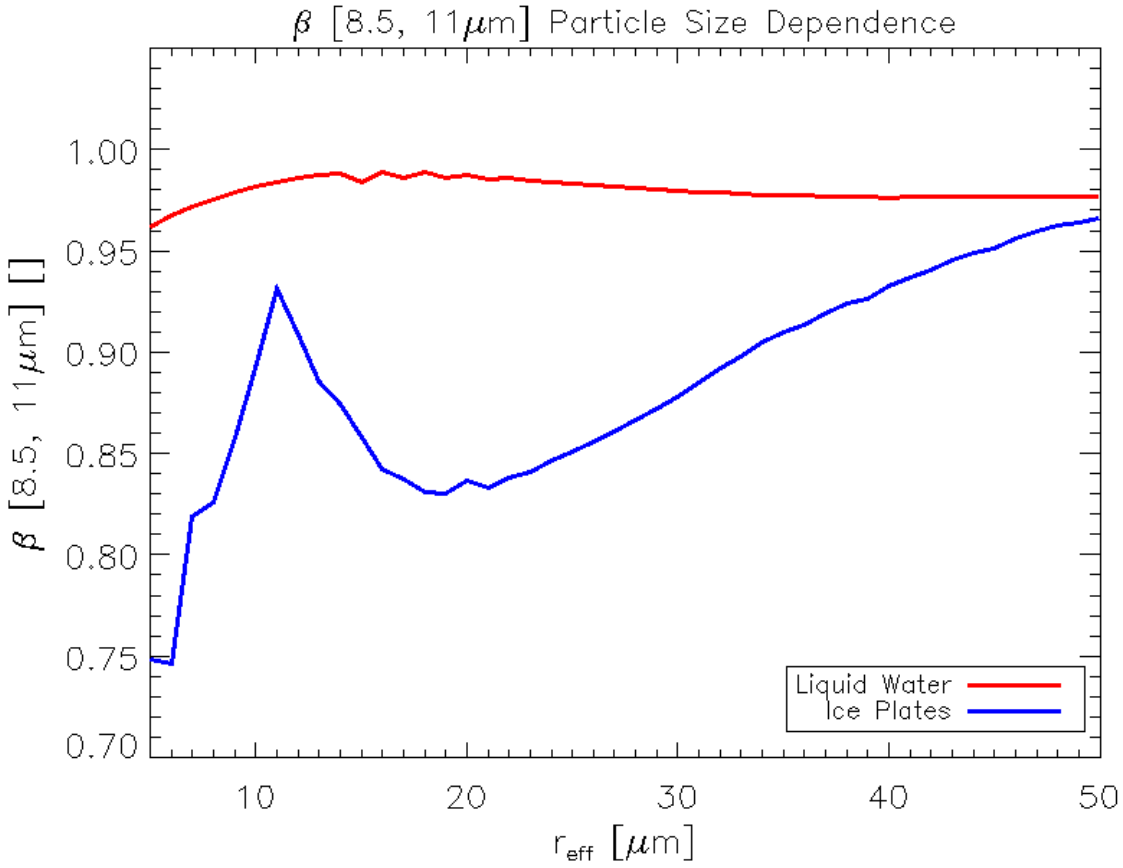

Figure 3: The 8.5/11 μm scaled extinction ratio (β(8.5/11μm)) is shown as a function of the effective particle radius for liquid water spheres (red) and ice plates (blue). These β-ratios were derived from the single scatter properties.

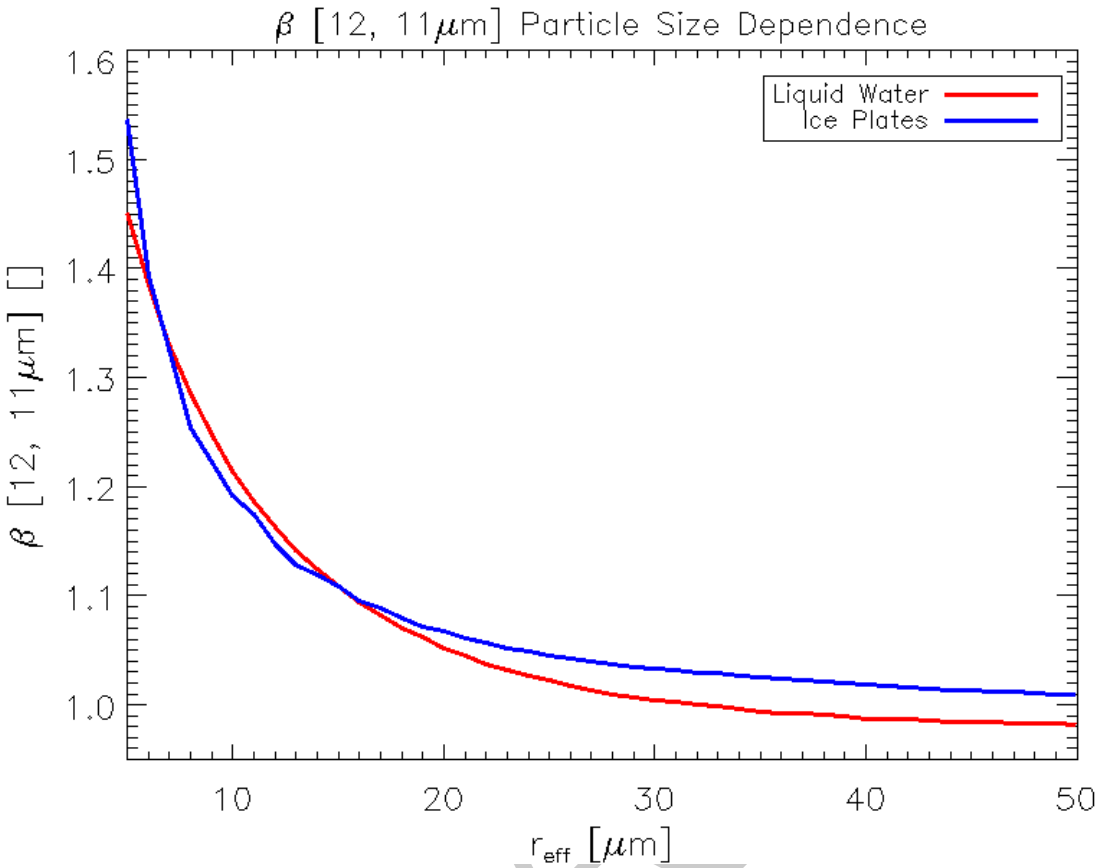

Figure 4: The 12/11 μm scaled extinction ratio (β(12/11μm)) is shown as a function of the effective particle radius for liquid water spheres (red) and ice plates (blue). These β-ratios were derived from the single scatter properties.

3.4.2 Mathematical Description

These subsections describe in detail how the ACT and JRRCT algorithm is implemented. Firstly, a description of how measured radiances are converted to an emissivity based data space is given. The use of spatial information is explained next, followed by a detailed description of recipe (based on the spectral and spatial "ingredients") used to determine cloud type and phase.

3.4.2.1 Converting the Measured Radiances to Emissivities and β-Ratios

As shown in Section 3.4.1.1, effective cloud emissivity is dependent on the position of the cloud within the vertical column (see Equation 2).

Given the measured radiances at 7.4, 8.5, 11, and 12 μm (ABI channels 10, 11, 14, and 15) or at 8.5, 10.8 and 12 μm (VIIRS channels M14, M15, and M16) and estimates of the clear sky radiance, clear sky transmittance, and the temperature profile, Equations 2 and 3 are used to compute β for the following spectral pairs: (8.5, 11 μm), (12, 11 μm), and (7.4, 11 μm) for ABI and (8.5, 11 μm), (12, 11 μm) for VIIRS. Given these spectral

pairs, the 11 μm emissivity is always placed in the denominator of Equation 3. Hereafter, these β's are referred to as β(8.5/11μm), β(12/11μm), and β(7.4/11μm), respectively. The only missing piece of information is the effective cloud vertical level, which is needed in computing the cloud emissivity. The effective cloud vertical level is the level where the temperature profile is equal to the extinction weighted cloud temperature. As shown in Pavolonis (2010a) and Pavolonis (2010b), the sensitivity of β to the effective cloud vertical level is often small when "window" channel pairs are used. As such, cloud microphysical information can be gleaned even by assuming a constant effective cloud vertical level. The retrieval of the actual effective cloud vertical level is unnecessary for this application and beyond the scope of this algorithm. In addition, the cloud phase must also be known to properly constrain the cloud microphysics in a formal retrieval of the cloud vertical level. That is why the cloud phase/type algorithm must work in the absence of cloud height information (e.g. the cloud height retrieval depends on the cloud phase). To mitigate this limitation in the ACT and JRRCT algorithm, four different cloud vertical level formulations are applied to Equation 2. These assumptions are given the following names.

1. Single layer tropopause assumption
2. Multilayered tropopause assumption
3. Single layer opaque cloud assumption
4. Multilayered opaque cloud assumption

The aim of applying these four assumptions is to probe the β data space for cloud microphysical information such that cloud type can be accurately inferred for non-opaque and opaque clouds, under single and multilayered cloudy conditions.

3.4.2.1.1 Single Layer Tropopause Assumption

The first formulation assumes a constant effective cloud level consistent with the thermodynamic tropopause given by Numerical Weather Prediction (NWP) data (see the AIADD Document for more information). Equations 6a – 6g specifically show how this assumption is applied to Equations 2 and 3 for the channel pairs used in the cloud type algorithm. In these equations, $\varepsilon_{stropo}(\lambda)$ is the spectral cloud emissivity computed using the single layer tropopause assumption, and $\beta_{stropo}(\lambda_1/\lambda_2)$ represents the β calculated from this type of cloud emissivity. T_{tropo} is the temperature of the tropopause. $R_{tropo}(\lambda)$ and $t_{tropo}(\lambda)$ are the clear sky atmospheric radiance and transmittance, vertically integrated from the tropopause to the top of the atmosphere, respectively (the calculation of the clear sky radiance and transmittance are described in detail in the AIADD Document). All other terms were defined previously. This formulation is primarily used to determine the cloud type/phase of single layer optically thin clouds.

$$\varepsilon_{stropo}(7.4\mu m) = \frac{R_{obs}(7.4\mu m) - R_{clr}(7.4\mu m)}{[B(7.4\mu m, T_{tropo})t_{tropo}(7.4\mu m) + R_{tropo}(7.4\mu m)] - R_{clr}(7.4\mu m)} \quad \text{(Eq. 6a)}$$

$$\varepsilon_{stropo}(8.5\mu m) = \frac{R_{obs}(8.5\mu m) - R_{clr}(8.5\mu m)}{[B(8.5\mu m, T_{tropo})t_{tropo}(8.5\mu m) + R_{tropo}(8.5\mu m)] - R_{clr}(8.5\mu m)} \quad \text{(Eq. 6b)}$$

$$\varepsilon_{stropo}(11\mu m) = \frac{R_{obs}(11\mu m) - R_{clr}(11\mu m)}{[B(11\mu m, T_{tropo})t_{tropo}(11\mu m) + R_{tropo}(11\mu m)] - R_{clr}(11\mu m)} \quad \text{(Eq. 6c)}$$

$$\varepsilon_{stropo}(12\mu m) = \frac{R_{obs}(12\mu m) - R_{clr}(12\mu m)}{[B(12\mu m, T_{tropo})t_{tropo}(12\mu m) + R_{tropo}(12\mu m)] - R_{clr}(12\mu m)} \quad \text{(Eq. 6d)}$$

$$\beta_{stropo}(8.5/11\mu m) = \frac{\ln[1-\varepsilon_{tropo}(8.5\mu m)]}{\ln[1-\varepsilon_{tropo}(11\mu m)]} \quad \text{(Eq. 6e)}$$

$$\beta_{stropo}(12/11\mu m) = \frac{\ln[1-\varepsilon_{tropo}(12\mu m)]}{\ln[1-\varepsilon_{tropo}(11\mu m)]} \quad \text{(Eq. 6f)}$$

$$\beta_{stropo}(7.4/11\mu m) = \frac{\ln[1-\varepsilon_{tropo}(7.4\mu m)]}{\ln[1-\varepsilon_{tropo}(11\mu m)]} \quad \text{(Eq. 6g)}$$

3.4.2.1.2 Multilayered Tropopause Assumption

Similar to the first formulation, the second cloud vertical level formulation assumes that the cloud vertical level is the tropopause level (given by NWP). Unlike the first formulation, this one includes an additional twist. In this formulation, the clear sky top-of-atmosphere radiance is replaced by the top-of-atmosphere radiance originating from a black (e.g. emissivity = 1.0 at all wavelengths) elevated surface. The elevated black surface is used to roughly approximate a blackbody cloud in the lower troposphere. The black surface is placed at the 0.8 sigma level in a terrain following coordinate system. The ability to detect multilayered clouds with infrared measurements is predicated on the lower cloud layer being colder than the surface and the upper cloud layer being colder than the lower cloud layer (Pavolonis and Heidinger, 2004). The 0.8 sigma level was chosen as a compromise of these two factors. The pressure level (P_{black}) of this black surface is given by Equation 7. In Equation 7, $\sigma = 0.8$, $P_{surface}$ is the pressure of the surface level in the NWP atmospheric pressure profile, and P_{toa} is the pressure at the highest level in the NWP atmospheric pressure profile. The sigma coordinate system is commonly used in dynamical models. The purpose of this formulation is to help identify multilayered cloud systems and determine the cloud phase of the highest cloud layer in a multilayered cloud system. Equations 8a – 8g specifically show how this assumption is applied to Equations 2 and 3 for the channel pairs used in the cloud phase/type algorithm. In these equations, $\varepsilon_{mtropo}(\lambda)$ is the spectral cloud emissivity computed using this formulation, and β_{mtropo} (λ_1/λ_2) represents the β calculated from this type of cloud emissivity. T_{black} is the temperature at the pressure level, P_{black}. $R_{black}(\lambda)$ and $t_{black}(\lambda)$ are the clear sky atmospheric radiance and transmittance, vertically integrated from the level where the atmospheric pressure is equal to P_{black} to the top of the atmosphere,

respectively. The $R_{black}(\lambda)$ and $t_{black}(\lambda)$ terms are simply pulled from pre-calculated profiles of clear sky atmospheric radiance and transmittance using the profile level returned by a standard generic binary search routine when the atmospheric pressure profile is searched for P_{black} (e.g. no interpolation is performed). The derivation of the pre-calculated clear sky atmospheric radiance and transmittance profiles is described in detail in the AIADD Document. All other terms in Equation 81 – 8g were previously defined.

$$P_{black} = (P_{surface} - P_{toa})\sigma + P_{toa} \quad \text{(Eq. 7)}$$

$$\varepsilon_{mtropo}(7.4\mu m) = \frac{R_{obs}(7.4\mu m) - [B(7.4\mu m, T_{black})t_{black}(7.4\mu m) + R_{black}(7.4\mu m)]}{[B(7.4\mu m, T_{tropo})t_{tropo}(7.4\mu m) + R_{tropo}(7.4\mu m)] - [B(7.4\mu m, T_{black})t_{black}(7.4\mu m) + R_{black}(7.4\mu m)]} \quad \text{(Eq. 8a)}$$

$$\varepsilon_{mtropo}(8.5\mu m) = \frac{R_{obs}(8.5\mu m) - [B(8.5\mu m, T_{black})t_{black}(8.5\mu m) + R_{black}(8.5\mu m)]}{[B(8.5\mu m, T_{tropo})t_{tropo}(8.5\mu m) + R_{tropo}(8.5\mu m)] - [B(8.5\mu m, T_{black})t_{black}(8.5\mu m) + R_{black}(8.5\mu m)]} \quad \text{(Eq. 8b)}$$

$$\varepsilon_{mtropo}(11\mu m) = \frac{R_{obs}(11\mu m) - [B(11\mu m, T_{black})t_{black}(11\mu m) + R_{black}(11\mu m)]}{[B(11\mu m, T_{tropo})t_{tropo}(11\mu m) + R_{tropo}(11\mu m)] - [B(11\mu m, T_{black})t_{black}(11\mu m) + R_{black}(11\mu m)]} \quad \text{(Eq. 8c)}$$

$$\varepsilon_{mtropo}(12\mu m) = \frac{R_{obs}(12\mu m) - [B(12\mu m, T_{black})t_{black}(12\mu m) + R_{black}(12\mu m)]}{[B(12\mu m, T_{tropo})t_{tropo}(12\mu m) + R_{tropo}(12\mu m)] - [B(12\mu m, T_{black})t_{black}(12\mu m) + R_{black}(12\mu m)]} \quad \text{(Eq. 8d)}$$

$$\beta_{mtropo}(8.5/11\mu m) = \frac{\ln[1 - \varepsilon_{tropo}(8.5\mu m)]}{\ln[1 - \varepsilon_{tropo}(11\mu m)]} \quad \text{(Eq. 8e)}$$

$$\beta_{mtropo}(12/11\mu m) = \frac{\ln[1 - \varepsilon_{tropo}(12\mu m)]}{\ln[1 - \varepsilon_{tropo}(11\mu m)]} \quad \text{(Eq. 8f)}$$

$$\beta_{mtropo}(7.4/11\mu m) = \frac{\ln[1 - \varepsilon_{tropo}(7.4\mu m)]}{\ln[1 - \varepsilon_{tropo}(11\mu m)]} \quad \text{(Eq. 8g)}$$

3.4.2.1.3 Single Layer Opaque Assumption

This formulation uses the opaque cloud assumption discussed in Pavolonis (2010a). In this case, the effective cloud vertical level is taken to be the level where either the 8.5, 11, or 12 μm cloud emissivity is equal to 0.98. The 7.4 μm channel is not used in this formulation. This formulation is used to determine the cloud phase of optically thin and thick clouds and infer information on cloud opacity. The process for implementing this formulation is as follows.

1. For a given channel (8.5, 11, and 12 μm), Equation 2 is rearranged to solve for the black cloud radiance term, $R_{cld}(\lambda)$, that is needed to yield a cloud emissivity of 0.98. Equation 9 shows this rearrangement. In this assumption, the cloud emissivity, $\varepsilon(\lambda)$, in Equation 9 is set to 0.98.

$$R_{cld}(\lambda) = \frac{R_{obs}(\lambda) + R_{clr}(\lambda)[\varepsilon(\lambda) - 1]}{\varepsilon(\lambda)} \quad \text{(Eq. 9) where}$$

$$R_{cld}(\lambda) = B(\lambda, T_{eff}) t_{ac}(\lambda) + R_{ac}(\lambda) \quad \text{(Eq. 10)}$$

2. For a given channel, the $R_{cld}(\lambda)$ calculated in Step 1 is compared to a pre-calculated vertical profile of $R_{cld}(\lambda)$ for the same channel (see the AIADD Document). The profile of $R_{cld}(\lambda)$ is used to determine the weight and anchor points needed to linearly interpolate the profile of $R_{cld}(\lambda)$ to the value calculated using Equation 9 with the assumption that $\varepsilon(\lambda) = 0.98$. Equation 11 shows how the interpolation weight, $W(\lambda,0.98)$, is determined.

$$W(\lambda,0.98) = \frac{R_{cld}(\lambda,0.98) - R_{cld}(\lambda,Z_1)}{R_{cld}(\lambda,Z_2) - R_{cld}(\lambda,Z_1)} \quad \text{(Eq. 11)}$$

   In Equation 11, $R_{cld}(\lambda, 0.98)$ is the value calculated using Equation 9 with the assumption that $\varepsilon(\lambda) = 0.98$. $R_{cld}(\lambda,Z_1)$ and $R_{cld}(\lambda,Z_2)$ are the black cloud radiances within the vertical profile that bound $R_{cld}(\lambda,0.98)$, with $R_{cld}(\lambda,Z_1)$ being the black cloud radiance at the highest (e.g. furthest from the ground) bounding level (Z_1). Z_1 and Z_2 are the vertical array indices corresponding to the interpolation anchor points.

3. Steps 1 and 2 are performed for the 8.5, 11, and 12 μm channels. The interpolation weights and anchor points associated with each channel are used to determine which $R_{cld}(\lambda,0.98)$ occurs at the highest (e.g. furthest from the ground) vertical level.

4. Once it is determined for which channel $R_{cld}(\lambda,0.98)$ occurs at the highest vertical level, the interpolation weight and anchor points for that channel are used to interpolate the $R_{cld}(\lambda)$ of the other two channels to that same level. The highest level is chosen to prevent the cloud emissivity in any of the channels from becoming too large (e.g. > 1.0). Thus, the cloud emissivity is fixed at 0.98 for the

channel where an emissivity of 0.98 occurs at the highest vertical level. This channel is referred to as the reference channel. The interpolation of $R_{cld}(\lambda)$ for the non-reference channels is performed according to Equation 12. Note that by interpolating $R_{cld}(\lambda)$, for the non-reference channels, to the level where the $R_{cld}(\lambda)$ of the reference channel gives an emissivity equal to 0.98, allows the emissivty of the non-reference channels to deviate from 0.98. Recall that cloud microphysical information is related to the spectral variation of cloud emissivity. In Equation 12, $R_{cld\_int}(\lambda)$ is the upwelling black cloud radiance interpolated using the reference weight [$W(\lambda_{ref},0.98)$] and reference anchor points [$R_{cld}(\lambda_{ref},Zref_1)$ and $R_{cld}(\lambda_{ref},Zref_2)$] that give a cloud emissivity of 0.98 at the reference channel. $Zref_1$ and $Zref_2$ are the vertical array indices of the reference interpolation anchor points.

$$R_{cld\_int}(\lambda) = R_{cld}(\lambda, Zref_1) + W(\lambda_{ref}, 0.98)[R_{cld}(\lambda, Zref_2) - R_{cld}(\lambda, Zref_1)] \quad \text{(Eq. 12)}$$

5. Finally, the 8.5, 11, and 12 μm channel cloud emissivities are computed using Equations 13a – 13c. $\beta(8.5/11\mu m)$ and $\beta(12/11\mu m)$ are also computed using Equations 13d and 13e. In these equations, $\varepsilon_{sopaque}(\lambda)$ is the spectral cloud emissivity computed using the single layer opaque cloud assumption, and $\beta_{sopaque}(\lambda_1/\lambda_2)$ represents the β calculated from this type of cloud emissivity. If this formulation is implemented correctly, $\varepsilon_{sopaque}(\lambda)$ at the reference channel should be equal to 0.98.

$$\varepsilon_{sopaque}(8.5\mu m) = \frac{R_{obs}(8.5\mu m) - R_{clr}(8.5\mu m)}{R_{cld\_interp}(8.5\mu m) - R_{clr}(8.5\mu m)} \quad \text{(Eq. 13a)}$$

$$\varepsilon_{sopaque}(11\mu m) = \frac{R_{obs}(11\mu m) - R_{clr}(11\mu m)}{R_{cld\_interp}(11\mu m) - R_{clr}(11\mu m)} \quad \text{(Eq. 13b)}$$

$$\varepsilon_{sopaque}(12\mu m) = \frac{R_{obs}(12\mu m) - R_{clr}(12\mu m)}{R_{cld\_interp}(12\mu m) - R_{clr}(12\mu m)} \quad \text{(Eq. 13c)}$$

$$\beta_{sopaque}(8.5/11\mu m) = \frac{\ln[1 - \varepsilon_{sopaque}(8.5\mu m)]}{\ln[1 - \varepsilon_{sopaque}(11\mu m)]} \quad \text{(Eq. 13d)}$$

$$\beta_{sopaque}(12/11\mu m) = \frac{\ln[1 - \varepsilon_{sopaque}(12\mu m)]}{\ln[1 - \varepsilon_{sopaque}(11\mu m)]} \quad \text{(Eq. 13e)}$$

3.4.2.1.4 Multilayered Opaque Cloud Assumption

This assumption is implemented in exactly the same manner as the "Single Layer Opaque Cloud Assumption" except the top-of-atmosphere clear sky radiance is replaced by the top-of-atmosphere radiance originating from a black elevated surface. Just as in the "Multilayered Tropopause Assumption," the black surface is placed at the 0.8 sigma level in a terrain following coordinate system. The black elevated surface is explained in detail in Section 3.4.2.1.2. As explained in a later section, the "Multilayered Opaque Cloud Assumption" is used to detect multilayered cloud systems. In this formulation, the 8.5, 11, and 12 μm channel cloud emissivities are computed using Equations 14a – 14c (the 7.4 μm channel is not used in this formulation). β(8.5/11μm) and β(12/11μm) are also computed using Equations 14d and 14e. In these equations, $\varepsilon_{mopaque}(\lambda)$ is the spectral cloud emissivity computed using the multilayered opaque cloud assumption, and $\beta_{mopaque}(\lambda_1/\lambda_2)$ represents the β calculated from this type of cloud emissivity.

$$\varepsilon_{mopaque}(8.5\mu m) = \frac{R_{obs}(8.5\mu m) - [B(8.5\mu m, T_{black})t_{black}(8.5\mu m) + R_{black}(8.5\mu m)]}{R_{cld\_interp}(8.5\mu m) - [B(8.5\mu m, T_{black})t_{black}(8.5\mu m) + R_{black}(8.5\mu m)]} \quad \text{(Eq. 14a)}$$

$$\varepsilon_{mopaque}(11\mu m) = \frac{R_{obs}(11\mu m) - [B(11\mu m, T_{black})t_{black}(11\mu m) + R_{black}(11\mu m)]}{R_{cld\_interp}(11\mu m) - [B(11\mu m, T_{black})t_{black}(11\mu m) + R_{black}(11\mu m)]} \quad \text{(Eq. 14b)}$$

$$\varepsilon_{mopaque}(12\mu m) = \frac{R_{obs}(12\mu m) - [B(12\mu m, T_{black})t_{black}(12\mu m) + R_{black}(12\mu m)]}{R_{cld\_interp}(12\mu m) - [B(12\mu m, T_{black})t_{black}(12\mu m) + R_{black}(12\mu m)]} \quad \text{(Eq. 14c)}$$

$$\beta_{mopaque}(8.5/11\mu m) = \frac{\ln[1-\varepsilon_{mopaque}(8.5\mu m)]}{\ln[1-\varepsilon_{mopaque}(11\mu m)]} \quad \text{(Eq. 14d)}$$

$$\beta_{mopaque}(12/11\mu m) = \frac{\ln[1-\varepsilon_{mopaque}(12\mu m)]}{\ln[1-\varepsilon_{mopaque}(11\mu m)]} \quad \text{(Eq. 14e)}$$

3.4.2.2 Opaque Cloud Temperature

The opaque cloud temperature is defined as the temperature at the vertical level where the cloud emissivity for a given channel is equal to a near-opaque value (0.98 in this case). The opaque cloud temperature is useful for determining the atmospherically corrected cloud-top temperature of opaque/near-opaque clouds. In addition, the opaque cloud temperature derived from a window channel can be compared to the opaque cloud temperature derived from an absorption channel to infer information about cloud optical depth. The ABI Cloud Type Algorithm computes the opaque cloud temperature for the 7.4 μm (ABI channel 10) and 11 μm (ABI channel 14) channels, while the JRRCT Algorithm computes the opaque cloud temperature for the VIIRS 11 μm channel (M15). The process for calculating the opaque cloud temperature is as follows.

If the clear sky radiance of a given channel is greater than the observed radiance for that same channel, the following procedure is used to determine the opaque cloud

temperature. For a given channel (7.4 and 11 μm), Equation 2 is rearranged to solve for the black cloud radiance term, $R_{cld}(\lambda)$, that is needed to yield a cloud emissivity of 0.98. Equation 9 shows this rearrangement. In this assumption, the cloud emissivity, $\varepsilon(\lambda)$, in Equation 9 is set to 0.98. The vertical level returned by a standard generic binary search routine is used to locate the value of $R_{cld}(\lambda)$, computed using Equation 9, in the pre-computed vertical profile of $R_{cld}(\lambda)$. The vertical array index returned by the binary search routine is used to grab the opaque cloud temperature from the NWP temperature profile (e.g. no interpolation is performed). As described in the AIADD Document, $R_{cld}(\lambda)$ and NWP temperature need to be available at the same vertical levels. This procedure is applied twice for ABI to separately determine the 7.4 μm and 11 μm opaque cloud temperatures, $T_{opaque}(7.4\mu m)$ and $T_{opaque}(11\mu m)$, respectively. If the 11 μm clear sky radiance is less than the observed radiance (e.g. due to errors in the clear radiance or if the cloud is warmer than the surface), then $T_{opaque}(11\mu m)$ is set to the observed 11 μm brightness temperature. If the 7.4 μm clear sky radiance is less than the observed radiance, then $T_{opaque}(7.4\mu m)$ is set to -999.0.

To determine the cloud type, the radiative parameters ("the ingredients") computed from all of the formulations described in Sections 3.4.2.1 and 3.4.2.2 are used in a logical decision tree (the "recipe"). Prior to describing the decision tree, the use of spatial information in the cloud type/phase algorithm must be explained.

3.4.2.3 Median Spatial Filter

The emissivity and β calculations described in Section 3.4.2.1 can, at times, be noisy, especially near cloud edges, in areas of broken clouds, and for very small cloud optical depths. In order to minimize the occurrence of "salt and pepper" noise, a standard 3 x 3 median filter is applied to certain key variables ($\varepsilon_{stropo}(11\mu m)$, $\beta_{stropo}(8.5/11\mu m)$, $\beta_{sopaque}(8.5/11\mu m)$, $\beta_{stropo}(12/11\mu m)$, and $\beta_{sopaque}(12/11\mu m)$). The median filter simply replaces the value at each pixel with the median value of a 3 x 3 pixel array centered on that pixel. The generic median filter procedure is described in the AIADD Document.

3.4.2.4 Identifying a Pixel's Local Radiative Center

In regions where the radiative signal of a cloud is small, like cloud edges, the various β-ratios are difficult to interpret since the cloud fraction, which is assumed to be 1.0, may be less than 1.0, or very small cloud optical depths may produce a signal that cannot be differentiated from noise. With the spectral information limited, a spatial metric is needed to make a spatially and physically consistent cloud type determination for these types of pixels. To address this problem, the gradient filter procedure, which is described in detail in the AIADD Document, is used to determine the Local Radiative Center (LRC) of each valid pixel. A pixel is valid if it has a valid Earth latitude and longitude and has valid spectral data (based on the L1b calibration flags). The $\varepsilon_{stropo}(11\mu m)$ parameter described in Section 3.4.2.1.1 is used to compute the LRC. The gradient filter

inputs (which are described in detail in the AIADD Document) for this application are listed in Table 7.

Table 7: Inputs used in calculation of Local Radiative Center (LRC). The gradient filter function used in the calculation is described in the AIADD document.

Gradient Variable	Minimum Valid Value of Gradient Variable	Maximum Valid Value of Gradient Variable	Gradient Stop Value	Apply Gradient Filter To
$\varepsilon_{Stropo}(11\mu m)$	0.0	1.0	0.7	All pixels with a valid Earth lat/lon and valid spectral data for ABI channels 10, 11, 14, and 15, for VIIRS channels M14, M15, and M16

The gradient filter allows one to consult the spectral information at an interior pixel within the same cloud in order to avoid using the spectral information offered by pixels with a very weak cloud radiative signal or sub-pixel cloudiness associated with cloud edges. Figure 5 shows how this technique eliminates anomalous $\beta_{stropo}(8.5/11\mu m)$ values at cloud edges. Overall, this use of spatial information allows for a more spatially and physically consistent product. This concept is also explained in Pavolonis (2010b).

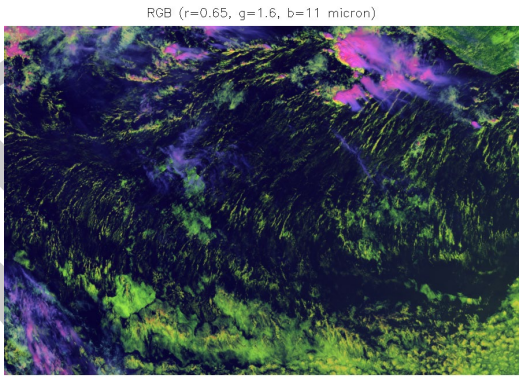

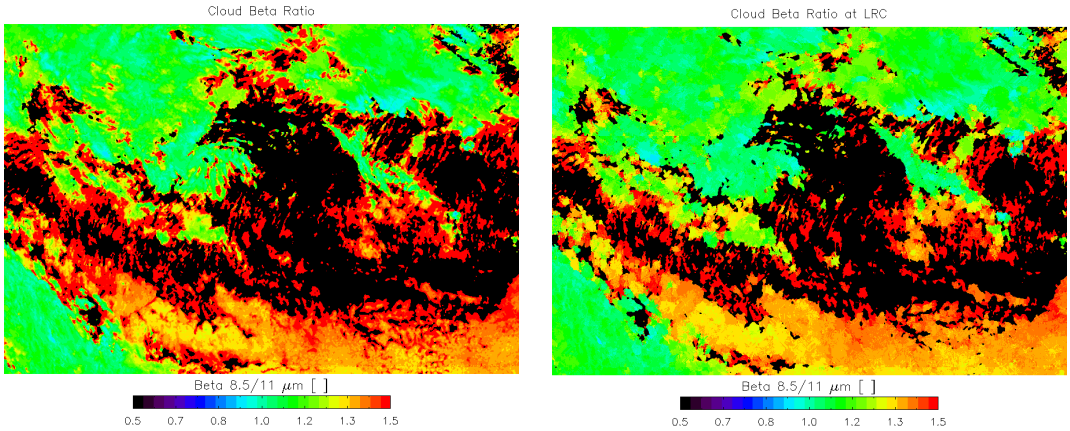

Figure 5: The impact of the gradient filter is shown for the scene depicted by the false color Red-Green-Blue (RGB) image (top panel). The β_{tropo}(8.5/11μm) at each pixel is shown in the bottom, left panel and the bottom, right panel is the same as the bottom left, except the β_{tropo}(8.5/11μm) for the LRC of each pixel is shown. Notice how anomalous values near cloud edges are absent from the LRC image.

3.4.2.5 Use of Spaceborne Lidar and Near-Infrared Reflectance Data to Determine Algorithm Thresholds

The Cloud-Aerosol Lidar with Orthogonal Polarization (CALIOP) on-board the Cloud-Aerosol Lidar and Infrared Pathfinder Satellite Observation (CALIPSO) satellite is a nadir pointing dual wavelength depolarization lidar. CALIPSO is in an afternoon sun-synchronous low earth orbit. Thus, it can be closely co-located in space and time with the Spinning Enhanced Visible and Infrared Imager (SEVIRI) and with Suomi NPP VIIRS at certain times of the day. SEVIRI has 7.4, 8.5, 11, and 12 μm channels that are similar to the ABI and CALIOP is capable of accurately measuring cloud boundaries in the vertical and horizontal. The vertical cloud boundaries can be combined with co-located NWP temperature profiles to provide a good estimate of cloud top temperature, which can be used to infer cloud top phase for certain temperature ranges. The CALIOP cloud phase product was not used at the time of determining algorithm thresholds for the ACT algorithm because that version of the CALIOP cloud phase product was not accurate due to the complexities of multiple scattering and oriented ice crystals (Hu et al., 2009). The next version of the CALIOP cloud phase product should address some of these deficiencies (Hu et al., 2009). The CALIOP cloud boundaries can also be used to calculate a quality estimate of the true cloud emissivity, as in Heidinger and Pavolonis (2009). In developing the ACT, CALIOP and SEVIRI co-locations were used extensively to help define thresholds, verify physical concepts, and validate the algorithm. For the JRRCT algorithm, CALIOP and VIIRS co-locations were used. In addition, near infrared reflectance data (available during the day), which are not used in the cloud type/phase algorithm, were used to adjust thresholds. In the near-infrared, ice is more absorbing than liquid water, thus, ice will generally have a smaller reflectance than liquid water (Pavolonis et al., 2005).

3.4.2.6 Cloud Phase/Type Determination

As stated earlier, the cloud phase is determined from the cloud type output (the cloud phase product is a subset of the more detailed cloud type categories). The cloud type decision tree is composed of several small components (or tests), each aimed at extracting specific information related to cloud type. The algorithm first determines the result of each test and stores that information. Thereafter, the results of the tests are examined in a specific order to determine the cloud type. The following sections will describe each test and the logic used to determine the cloud type from the test results. Please note that all of the inputs needed by the cloud type decision tree (including mathematical symbols) have been defined in previous sections. As a reminder, the overall algorithm processing flow chart is shown in Figure 1.

3.4.2.6.1 Low Surface Emissivity (LSE) Test

Purpose: Determine if certain downstream tests may be negatively impacted by low surface emissivity.

Inputs:

- 8.5 μm (ABI channel 11 or VIIRS channel M14) surface emissivity [$\varepsilon_{sfc}(8.5\mu m)$]
- $\varepsilon_{stropo}(11\mu m)$

Logic:

If ($\varepsilon_{sfc}(8.5\mu m)$ < LSE_Threshold_1 **AND** $\varepsilon_{stropo}(11\mu m)$ < LSE_Threshold_2)

Output = TRUE (a low surface emissivity is present)

Else

Output = FALSE

Thresholds and rational:

Offline radiative transfer model simulations indicate that once the 8.5 μm surface emissivity decreases to about 0.85, the opaque cloud assumption described in Section 3.4.2.1.3 is no longer effective for determining cloud phase or cloud opacity, unless the $\varepsilon_{stropo}(11\mu m)$ exceeds a certain threshold. The thresholds required by the LSE test are listed in Table 8.

Table 8: The thresholds used by the Low Surface Emissivity (LSE) Test as a function of sensor.

Sensor	LSE_Threshold_1	LSE_Threshold_2
NPP VIIRS	0.85	0.50
GOES-R ABI	0.85	0.50
Met-8 SEVIRI	0.85	0.50

Met-9 SEVIRI	0.85	0.50
Terra MODIS	0.85	0.50
Aqua MODIS	0.85	0.50

3.4.2.6.2 β(12/11μm) Opaque Cloud (BOC) Test

Purpose: Determine if a cloud is opaque/nearly opaque using the theory described in Pavolonis (2010a).

Inputs:

- $\varepsilon_{stropo}(11\mu m)$
- $\beta_{sopaque}(12/11\mu m)$

Logic:

If ($\varepsilon_{stropo}(11\mu m)$ > BOC_Threshold_1 **AND** $\beta_{sopaque}(12/11\mu m)$ < BOC_Threshold_2)

Output = TRUE (cloud is nearly opaque)

Else

Output = FALSE

Thresholds and rational:

The cloud type/phase algorithm does not need specific values of the actual cloud optical depth or emissivity. Only a flag indicating if the cloud likely has an 11 μm cloud optical depth greater than about 2.0 (see definition of cloud type categories) is needed. In order to determine if a pixel has a high probability of containing an opaque or near-opaque upper-most cloud layer, $\beta_{sopaque}(12/11\mu m)$ (see Equation 13e) is examined as in Pavolonis (2010a). If the cloud has a large emissivity (at the reference channel), then the $\beta_{sopaque}(12/11\mu m)$ should fall well within the expected theoretical range given by the single scatter properties. If the cloud has an emissivity (at the reference channel) much smaller than 0.98, $\beta_{sopaque}(12/11\mu m)$ should be greatly influenced by the spectral variability in surface emissivity and clear sky gaseous transmittance, and thus, may not fall within the expected theoretical range. This is because the upwelling top-of-atmosphere radiance from an elevated (e.g. above the surface) blackbody surface, and the atmosphere above, converges to the clear sky radiance at a higher (colder) atmospheric level for channels that have a small surface emissivity and/or higher peaking weighting function.

The $\beta_{sopaque}(12/11\mu m)$ threshold was determined objectively using SEVIRI and CALIOP time/space co-locations, where the goal is to identify clouds that have an 11 μm emissivity greater than 0.85 (roughly equivalent to an 11 μm optical depth of 2.0). CALIOP cloud boundaries were used to compute a "true" 11-μm cloud emissivity. In other words, Equation 2 can be evaluated using the CALIOP cloud boundaries and an

NWP temperature profile to estimate the effective cloud level, which is assumed to lie midway between the CALIOP cloud top and cloud bottom (Heidinger and Pavolonis, 2009). Figure 6 shows Peirce-Hanssen-Kuipers skill score metrics as a function of the $\beta_{sopaque}(12/11\mu m)$ threshold used to distinguish between clouds with a 11-µm cloud optical depth of less than and greater than 2.0. A total of about 8000 SEVIRI/CALIOP match-ups were used in this analysis. This objective analysis indicates that a threshold of 1.19 is optimal for SEVIRI and GOES-R (clouds with a $\beta_{sopaque}(12/11\mu m) < 1.19$ are considered to have an 11 µm optical depth greater than 2.0). The thresholds used by the BOC test are listed in Table 9. Overall, these results prove that opaque/near-opaque clouds can be identified with respectable skill using this approach. For the NPP VIIRS threshold, the CALIPSO Hu phase is used and histograms of $\beta_{sopaque}(12/11\mu m)$ for CALIPSO Hu water and ice phases are analyzed and the location of the max CSI value for $\beta_{sopaque}(12/11\mu m)$ is determined for the threshold to use. For NPP VIIRS this threshold value is 1.00.

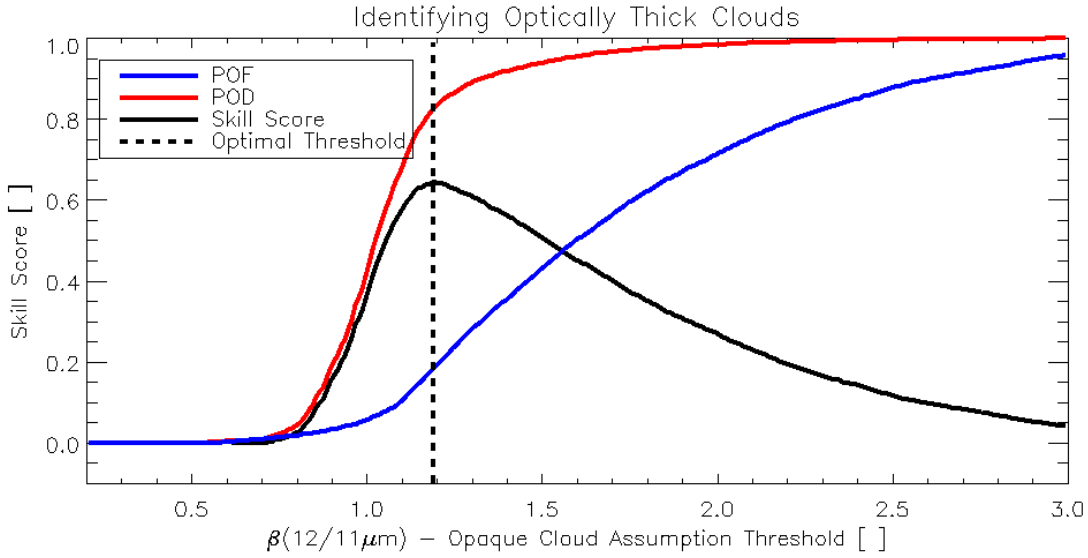

Figure 6: Peirce-Hanssen-Kuipers skill score metrics are shown as a function of the $\beta_{sopaque}(12/11\mu m)$ threshold used to distinguish between clouds with a 11-µm cloud optical depth of less than and greater than 2.0. The probability of false alarm (POF) is shown in blue, the probability of detection (POD) is shown in red, and the skill score is depicted by the black solid line. The $\beta_{sopaque}(12/11\mu m)$ threshold that maximizes the skill score is depicted by the dashed black line. This analysis is based on over 8000 SEVIRI/CALIOP match-ups.

Table 9: The thresholds used by the β(12/11µm) Opaque Cloud (BOC) Test as a function of sensor.

Sensor	BOC_Threshold_1	BOC_Threshold_2
NPP VIIRS	0.05	1.00
GOES-R ABI	0.05	1.19
Met-8 SEVIRI	0.05	1.19
Met-9 SEVIRI	0.05	1.19

Terra MODIS	0.05	1.17
Aqua MODIS	0.05	1.17

3.4.2.6.3 Opaque Cloud Temperature Difference (OCTD) Test

Purpose: Determine if a cloud is opaque/nearly opaque using the difference between $T_{opaque}(7.4\mu m)$ and $T_{opaque}(11\mu m)$, which were described in Section 3.4.2.2.

Inputs:

- $T_{opaque}(7.4\mu m)$
- $T_{opaque}(11\mu m)$
- Absolute value of the $T_{opaque}(7.4\mu m)$ - $T_{opaque}(11\mu m)$ difference [$T_{opaque}(diff)$]

Logic:

If ($T_{opaque}(7.4\mu m)$ > OCTD_Threshold_1 **AND** $T_{opaque}(11\mu m)$ > OCTD_Threshold_2 **AND** $T_{opaque}(diff)$ < OCTD_Threshold_3)

Output = TRUE (cloud is nearly opaque)

Else

Output = FALSE

Thresholds and rational:
This test relies on the 7.4 μm channel, which is not available from VIIRS, so this test is not used in the current JRRCT algorithm and only used in the ABI cloud top phase/type algorithm. Future improvements to the JRRCT algorithm code will remove this dependency and make this test relevant. This test is used to supplement the BOC Test. The physical basis is straightforward. If the absolute difference between the opaque cloud temperature derived from the 7.4 μm channel and the opaque cloud temperature derived from the 11 μm channel is small, the cloud approximates a blackbody and is considered to be opaque/nearly opaque. Given that the 7.4 μm channel has a clear sky weighting function that peaks in the middle troposphere and the clear sky weighting function of the 11 μm channel peaks near the surface, only the presence of an opaque/nearly opaque cloud can cause the absolute difference between the opaque cloud temperatures to be small. Figure 7 shows Peirce-Hanssen-Kuipers skill score metrics as a function of the $T_{opaque}(diff)$ threshold used to distinguish between clouds with a 11-μm cloud optical depth of less than and greater than 2.0. A total of about 8000 SEVIRI/CALIOP match-ups were used in this analysis. This objective analysis indicates that a threshold of 4.5 K is optimal (clouds with a $T_{opaque}(diff)$ < 4.5 K are considered to have an 11 μm optical depth greater than 2.0). The thresholds used by the OCTD test are listed in Table 10.

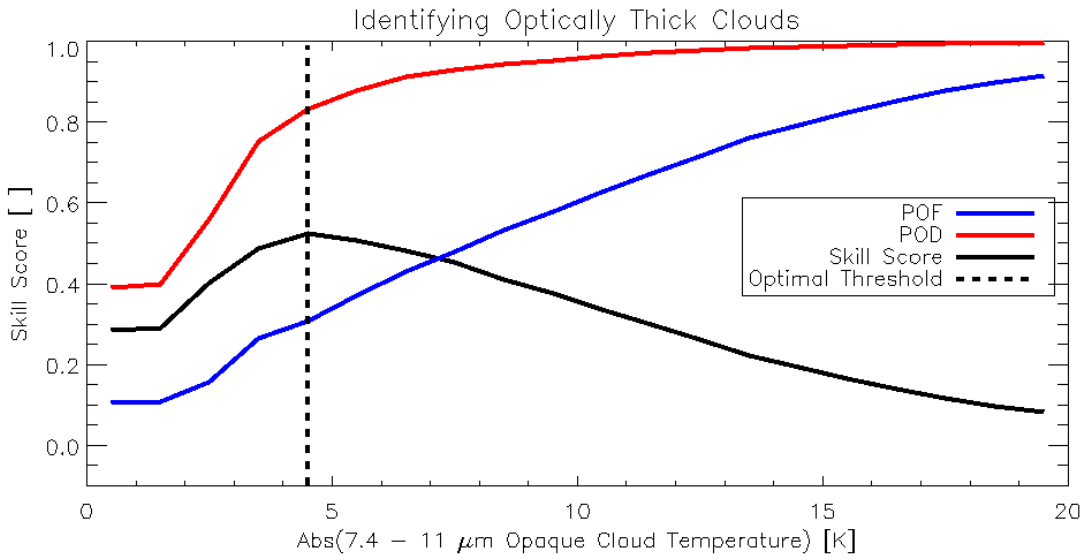

Figure 7: Peirce-Hanssen-Kuipers skill score metrics are shown as a function of the absolute difference in the 7.4 μm – 11 μm opaque cloud temperature (T_{opaque}(diff)) threshold used to distinguish between clouds with a 11-μm cloud optical depth of less than and greater than 2.0. The probability of false alarm (POF) is shown in blue, the probability of detection (POD) is shown in red, and the skill score is depicted by the black solid line. The T_{opaque}(diff) threshold that maximizes the skill score is depicted by the dashed black line. This analysis is based on over 8000 SEVIRI/CALIOP match-ups.

Table 10: The thresholds used by the Opaque Cloud Temperature Difference (OCTD) Test as a function of sensor.

Sensor	OCTD_Threshold_1 [K]	OCTD_Threshold_2 [K]	OCTD_Threshold_3 [K]
NPP VIIRS	N/A	N/A	N/A
GOES-R ABI	170	170	4.5
Met-8 SEVIRI	170	170	4.5
Met-9 SEVIRI	170	170	4.5
Terra MODIS	170	170	4.5
Aqua MODIS	170	170	4.5

3.4.2.6.4 Overall Opaque Cloud (OOC) Test

Purpose: Combine the output from the Low Surface Emissivity Test (LSE), β(12/11μm) Opaque Cloud (BOC) Test, and the Opaque Cloud Temperature Difference (OCTD) Test to determine if a cloud is truly opaque/nearly opaque.

Inputs:

- Result of LSE Test
- Result of BOC Test
- Result of OCTD Test (not used with NPP VIIRS currently)

Logic:

If (LSE Test = TRUE)

Output = OCTD Test (for NPP VIIRS, BOC Test)

Else

Output = BOC Test

Thresholds and rational:
For NPP VIIRS, the BOC test is used even over low emissivity surfaces since there is no 7.4 μm channel on VIIRS, therefore the Opaque Cloud Temperature Difference (OCTD) test cannot be utilized with the JRRCT algorithm. The BOC test is generally more skillful than the OCTD test, except over barren low emissivity surfaces. Thus, the output of the BOC test is used for the ACT algorithm, except over low emissivity surfaces.

3.4.2.6.5 Water Vapor Multilayered Detection (WVMD) Test

Purpose: Detect multilayered cloud systems, where the highest cloud layer is semi-transparent to infrared radiation.

Inputs:
- $\varepsilon_{stropo}(7.4\mu m)$
- $\varepsilon_{mtropo}(11\mu m)$
- $\beta_{mtropo}(7.4/11\mu m)$
- $\beta_{stropo}(12/11\mu m)$
- $\beta_{mtropo}(12/11\mu m)$
- $\beta_{mopaque}(12/11\mu m)$
- $\beta_{sopaque}(8.5/11\mu m)$ at the pixel Local Radiative Center (LRC) [$\beta_{sopaque}(8.5/11\mu m)$_LRC]

Logic:

If ($\varepsilon_{stropo}(7.4\mu m)$ > WVMD_Thresh1 **AND**
$\beta_{mtropo}(7.4/11\mu m)$ > WVMD_Thresh2 **AND**
$\beta_{mtropo}(7.4/11\mu m)$ < WVMD_Thresh3 **AND**
$\beta_{stropo}(12/11\mu m) < \beta_{mtropo}(12/11\mu m)$ **AND**
$\varepsilon_{mtropo}(11\mu m)$ > WVMD_Thresh4 **AND**

$\varepsilon_{mtropo}(11\mu m)$ < WVMD_Thresh5 **AND**
$\beta_{mopaque}(12/11\mu m)$ > WVMD_Thresh6 **AND**
$\beta_{mopaque}(12/11\mu m)$ < WVMD_Thresh7 **AND**
$\beta_{sopaque}(8.5/11\mu m)$_LRC > WVMD_Thresh8 **AND**
$\beta_{sopaque}(8.5/11\mu m)$_LRC < WVMD_Thresh9)

Output = TRUE (multilayered clouds are present)

Else

Output = FALSE

Thresholds and rational:
This test relies on the 7.4 μm channel, which is not available from VIIRS, so this test is not used in the current JRRCT algorithm and only used in the ACT algorithm. Future improvements to the JRRCT algorithm code will remove this dependency and make this test relevant. The multilayered cloud detection methodology is designed to detect semi-transparent upper tropospheric ice clouds that overlap a lower opaque/near-opaque cloud layer. These will be referred to as "multilayered ice clouds" from this point forward. Previous studies (e.g. Heidinger and Pavolonis, 2005) have shown that multilayered ice clouds are a common occurrence. The presence of multiple cloud layers will impact downstream retrievals of cloud macro and microphysical properties, so it is import to identify multilayered cloud systems prior to performing these retrievals. The multilayered cloud detection technique exploits differences in atmospheric weighting functions and microphysical relationships to infer the presence of multilayered clouds. The 7.4-μm channel (ABI Channel 10) atmospheric weighting function generally peaks in the mid to upper troposphere (the exact peak depends on the water vapor profile), while the 11-μm channel (ABI Channel 14) weighting function peaks in the lower troposphere near the surface.

When a semi-transparent high cloud overlaps an opaque/near-opaque lower tropospheric cloud, the 7.4-μm channel will have little sensitivity to the emission from the lower tropopsheric cloud (unless the atmosphere is very dry), while the 11-μm channel will be sensitive to emission from both cloud layers. Thus, the 11-μm cloud emissivity calculated using the "Single Layer Tropopause Assumption" (see Section 3.4.2.1.1) would be much larger than the 7.4-μm emissivity calculated using the same assumptions. If the 7.4-μm and 11-μm cloud emissivities are computed for the same multilayered cloud scenario using the "Multilayered Tropopause Assumption" (see Section 3.4.2.1.2), the following will be result: $\varepsilon_{mtropo}(11\mu m) < \varepsilon_{stropo}(11\mu m)$ and $\varepsilon_{mtropo}(7.4\mu m) \approx \varepsilon_{stropo}(7.4\mu m)$. The sigma level ($\sigma = 0.8$) of the lower opaque cloud layer used in the "Multilayered Tropopause Assumption" was chosen such that it was placed well below the peak of the 7.4-μm channel weighting function. Given this physical basis, $\beta_{mtropo}(7.4/11\mu m)$ is a fairly good indicator of multilayered ice clouds, especially when supplemented with a few additional pieces of information.

Additional spectral information is used to help verify that a multilayered ice cloud is possible. Additional pieces of information are needed because, in reality, the 7.4-μm channel weighting function varies as a function of atmospheric temperature and water vapor and the height and opacity of the lower cloud layer will vary, which leads to ambiguity. Constraints on $\varepsilon_{mtropo}(11\mu m)$ and $\beta_{mopaque}(12/11\mu m)$ are applied in order to be more certain that the uppermost cloud layer is semi-transparent. Further constraints are applied to the value of $\beta_{sopaque}(8.5/11\mu m)$ at the pixel Local Radiative Center (LRC) to help reduce false detects due to certain single layer mid-level clouds. All of the thresholds for the WVMD test are shown in Table 11.

Figure 8 shows the normalized distribution of $\beta_{mtropo}(7.4/11\mu m)$ for single layer and multilayered "definite ice clouds." CALIOP was used to identify single layer clouds with a cloud top temperature of 233 K or less and multilayered cloud systems where the cloud top temperature of the highest cloud layer is 233 K or less. Hence the term "definite ice clouds." A $\beta_{mtropo}(7.4/11\mu m)$ threshold of 0.9 is used to distinguish single layer ice clouds from multilayered ice clouds (multilayered ice clouds have a $0.0 < \beta_{mtropo}(7.4/11\mu m) < 0.9$). Some of the overlap between single layer and multilayered ice clouds shown in Figure 8 is due to errors in the CALIOP vertical feature mask. Further, the saturation optical depth (e.g. optical depth at which transmission approaches zero) of the CALIOP is also slightly smaller than the penetration depth of infrared radiation, which causes additional overlap between the distributions.

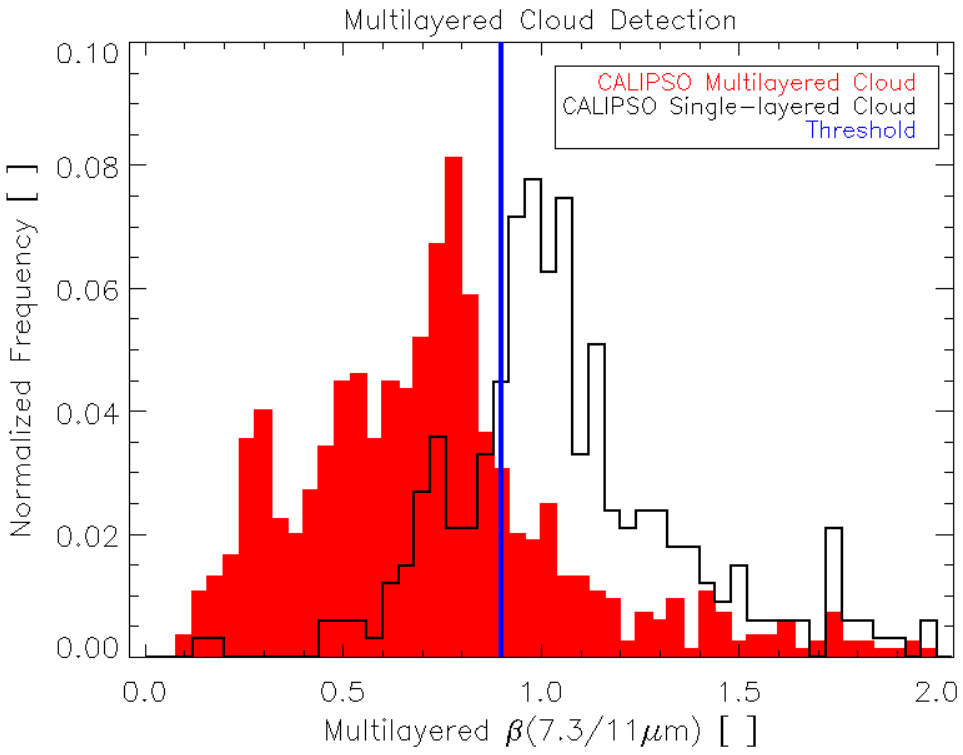

Figure 8: The normalized distribution of $\beta_{mtropo}(7.4/11\mu m)$ is shown for single layer (black) and multilayered (red) definite ice clouds. CALIOP was used to identify single layer clouds with a cloud top temperature of 233 K or less and multilayered

cloud systems where the cloud top temperature of the highest cloud layer is 233 K or less. The threshold used to distinguish between single and multilayered ice cloud systems is shown in blue.

Table 11: The thresholds used by the Water Vapor Multilayered Detection (WVMD) Test as a function of sensor.

Sensor	WVMD_ Thresh1	WVMD_ Thresh2	WVMD_ Thresh3	WVMD_ Thresh4	WVMD_ Thresh5	WVMD_ Thresh6	WVMD_ Thresh7	WVMD_ Thresh8	WVMD Thresh9
NPP VIIRS	N/A	N/A	N/A	N/A	N/A	N/A	N/A	N/A	N/A
GOES-R ABI	0.02	0.10	0.90	0.00	0.60	1.19	2.30	0.40	1.10
Met-8 SEVIRI	0.02	0.10	0.90	0.00	0.60	1.19	2.30	0.40	1.10
Met-9 SEVIRI	0.02	0.10	0.90	0.00	0.60	1.19	2.30	0.40	1.10
Terra MODIS	0.02	0.10	0.90	0.00	0.60	1.19	2.30	0.40	0.95
Aqua MODIS	0.02	0.10	0.90	0.00	0.60	1.19	2.30	0.40	0.95

3.4.2.6.6 Infrared Window Multilayered Detection (IWMD) Test

Purpose: Detect multilayered cloud systems, where the highest cloud layer is semi-transparent to infrared radiation.

Inputs:

- $\varepsilon_{mtropo}(11\mu m)$
- $\beta_{stropo}(12/11\mu m)$
- $\beta_{mtropo}(12/11\mu m)$
- $\beta_{mopaque}(12/11\mu m)$
- $\beta_{stropo}(8.5/11\mu m)$
- $\beta_{mtropo}(8.5/11\mu m)$
- $\beta_{mopaque}(8.5/11\mu m)$
- $\beta_{sopaque}(8.5/11\mu m)$ at the pixel Local Radiative Center (LRC) [$\beta_{sopaque}(8.5/11\mu m)\_LRC$]
- $\beta_{mtropo}(12/11\mu m) - \beta_{stropo}(12/11\mu m)$ [$\beta_{diff}(12/11\mu m)$]

Logic:

PART I (Only 2 different thresholds are used)

If (($\beta_{sopaque}(8.5/11\mu m)\_LRC$ > IWMD_Thresh1 **AND**
$\beta_{sopaque}(8.5/11\mu m)\_LRC$ < IWMD_Thresh2) **OR**
($\beta_{mopaque}(8.5/11\mu m)$ > IWMD_Thresh1 **AND**
$\beta_{mopaque}(8.5/11\mu m)$ < IWMD_Thresh2) **OR**
($\beta_{mtropo}(8.5/11\mu m)$ > IWMD_Thresh1 **AND**

$\beta_{mtropo}(8.5/11\mu m)$ < IWMD_Thresh2))

Ice_signature = TRUE (the highest cloud layer is likely composed of ice)

Else

Ice_signature = FALSE

PART II (depends on results of PART I)

If ($\beta_{stropo}(12/11\mu m)$ > IWMD_Thresh3 **AND**
$\beta_{stropo}(12/11\mu m)$ < IWMD_Thresh4 **AND**
$\varepsilon_{mtropo}(11\mu m)$ > IWMD_Thresh5 **AND**
$\varepsilon_{mtropo}(11\mu m)$ < IWMD_Thresh6 **AND**
$\beta_{diff}(12/11\mu m)$ > IWMD_Thresh7 **AND**
$\beta_{mopaque}(12/11\mu m)$ > IWMD_Thresh8 **AND**
$\beta_{mopaque}(12/11\mu m)$ < IWMD_Thresh9 **AND**
Ice_signature = TRUE)

Output = TRUE (multilayered clouds are present)

Else

Output = FALSE

Thresholds and rational:
The IWMD test is designed to detect multilayered ice clouds that cannot be detected with the WVMD test for GOES-R due to low signal-to-noise in the 7.4 μm channel. However, for NPP VIIRS there is no water vapor channel so the IWMD test is the primary test for multilayered ice cloud detection. When optically thin ice clouds overlap an optically thick lower cloud layer composed of liquid water, the single layer cloud assumptions will often result in values of $\beta_{stropo}(12/11\mu m)$, $\beta_{stropo}(8.5/11\mu m)$, and $\beta_{sopaque}(8.5/11\mu m)$ that are representative of the lower cloud layer. The multilayered assumption will result in values of $\beta_{mtropo}(12/11\mu m)$, $\beta_{mtropo}(8.5/11\mu m)$, and $\beta_{mopaque}(8.5/11\mu m)$ that are representative of the optically thin ice cloud. In contrast, when a single layer cloud is present, both the single layer and multilayered assumptions will be representative of the phase of the single cloud layer. The thresholds for implementing this test can be found in Table 12. These thresholds were derived from a combination of CALIPSO and manual analysis.

Table 12: The thresholds used by the Infrared Window Multilayered Detection (IWMD) Test as a function of sensor.

Sensor	IWMD_ Thresh1	IWMD_ Thresh2	IWMD_ Thresh3	IWMD_ Thresh4	IWMD_ Thresh5	IWMD_ Thresh6	IWMD_ Thresh7	IWMD_ Thresh8	IWMD_ Thresh9
NPP VIIRS	0.10	0.98	0.80	0.98	0.00	0.18	0.03	0.99	2.30

GOES-R ABI	0.40	1.10	0.85	0.98	0.00	0.20	0.03	1.19	2.30
Met-8 SEVIRI	0.40	1.10	0.85	0.98	0.00	0.20	0.03	1.19	2.30
Met-9 SEVIRI	0.40	1.10	0.85	0.98	0.00	0.20	0.03	1.19	2.30
Terra MODIS	0.40	0.95	0.85	0.98	0.00	0.20	0.03	1.19	2.30
Aqua MODIS	0.40	0.95	0.85	0.98	0.00	0.20	0.03	1.19	2.30

3.4.2.6.7 Overall Multilayered Cloud (OMC) Test

Purpose: Combine the results from the WVMD Test and the IWMD Test to determine if a multilayered cloud system is present.

Inputs:

- WVMD Test Result (not used with NPP VIIRS currently)
- IWMD Test Result

Logic:

If (WVMD Test = TRUE **OR** IWMD Test = TRUE)

Output = TRUE (multilayered clouds are present)

Else

Output = FALSE

Thresholds and rational:
The combination of the WVMD and IWMD tests produce a more accurate representation of ice topped multilayered cloud systems. However, the WVMD test is not utilized with NPP VIIRS because no water vapor channel is present. Therefore, the IWMD test is only used for VIIRS to determine if a multilayered cloud system is present.

3.4.2.6.8 Homogeneous Freezing (HF) Test

Purpose: Identify clouds that, based on their 11-μm opaque cloud temperature, very likely have glaciated tops.

Inputs:

- $T_{opaque}(11\mu m)$

Logic:

If ($T_{opaque}(11\mu m)$ > 170.0 K **AND** $T_{opaque}(11\mu m) \leq$ 238.0 K)

Output = TRUE (an ice cloud was detected)

Else

Output = FALSE

Thresholds and rational:
Clouds are assumed to have a glaciated top if the 11-μm brightness temperature is less than or equal to 233 K (-40ºC). This is the typical temperature at which small liquid droplets will freeze spontaneously (Rogers and Yau, 1989). In addition, Korolev et al. (2003) found that for in-cloud temperatures in the 233 – 238 K range, ice is by far the dominant phase, so a threshold of 238 K is used.

3.4.2.6.9 $\beta_{sopaque}(8.5/11\mu m)$ and Water Vapor Ice Cloud (BOWVIC) Test

Purpose: Utilize the cloud phase information offered by β(8.5/11μm) (see Figure 3), with the "opaque cloud assumption" (see Section 3.4.2.1.3) to identify ice clouds of varying optical depth.

Inputs:
- $T_{opaque}(7.4\mu m)$
- $T_{opaque}(7.4\mu m)$ at the pixel Local Radiative Center (LRC) [$T_{opaque}(7.4\mu m)$_LRC]
- $\beta_{sopaque}(8.5/11\mu m)$
- $\beta_{sopaque}(8.5/11\mu m)$ at the pixel LRC [$\beta_{sopaque}(8.5/11\mu m)$_LRC]
- $\beta_{stropo}(12/11\mu m)$

Logic:

It is important to note that the thresholds symbolized in the logic below are a function of $T_{opaque}(7.4\mu m)$ or $T_{opaque}(7.4\mu m)$_LRC.

If ($\beta_{sopaque}(8.5/11\mu m)$ > BOWVIC_Thresh1($T_{opaque}(7.4\mu m)$) **AND**
$\beta_{sopaque}(8.5/11\mu m)$ < BOWVIC_Thresh2($T_{opaque}(7.4\mu m)$) **AND**
$\beta_{sopaque}(8.5/11\mu m)$_LRC > BOWVIC_Thresh3($T_{opaque}(7.4\mu m)$_LRC) **AND**
$\beta_{sopaque}(8.5/11\mu m)$_LRC < BOWVIC_Thresh4($T_{opaque}(7.4\mu m)$_LRC) **AND**
$\beta_{stropo}(12/11\mu m)$ > BOWVIC_Thresh5($T_{opaque}(7.4\mu m)$) **AND**
$\beta_{stropo}(12/11\mu m)$ < BOWVIC_Thresh6($T_{opaque}(7.4\mu m)$)))

Output = TRUE (an ice cloud was detected)

Else

Output = FALSE

Thresholds and rational:
This test relies on the 7.4 μm channel, which is not available from VIIRS, so this test is not used in the current JRRCT algorithm and only used in the ACT algorithm. Future improvements to the JRRCT algorithm code will remove this dependency and make this test relevant. CALIOP vertical cloud boundaries co-located with SEVIRI measurements were used to show the relationship between $\beta_{sopaque}(8.5/11\mu m)$ (see Section 3.4.2.1.3), and cloud top temperature as a function of the 7.4 μm opaque cloud temperature (see Section 3.4.2.2). In this analysis, CALIOP-derived cloud top temperatures (T_{cld}) are divided into five bins or categories. They are:

1. $T_{cld} > 273$ K (warm liquid water)
2. $263\ K < T_{cld} < 273\ K$ (warm mid-level)
3. $243\ K < T_{cld} < 263\ K$ (intermediate mid-level)
4. $233\ K < T_{cld} < 243\ K$ (cold mid-level)
5. $T_{cld} < 233$ K (ice)

The first and fifth bins, defined by the melting and homogeneous freezing points of water, provide fairly unambiguous information on cloud phase. The middle three bins do not provide unambiguous cloud phase information. In-situ observations of mid-level clouds in the mid-latitudes indicate that clouds located above the melting level (273 K) are often composed of both ice and liquid water (e.g. Korolev et al., 2003). Interestingly enough, these mixed phase clouds are almost always composed of liquid water at the cloud top, with most of the ice being found near the cloud base (Carey et al., 2008). Thus, cloud phase identification from satellite radiances is greatly influenced by the penetration depth of the radiation into the cloud, which is wavelength dependent (e.g. does the radiometer sense both the liquid water and ice?). The ABI cloud type/phase algorithm utilizes infrared radiation, which has a small penetration depth relative to near-infrared and visible radiation. In addition, the goal of the algorithm is to identify the cloud **top** phase. Given the observational evidence and the small penetration depth of infrared radiation, most clouds that fall into the middle cloud-top temperature bins should be classified as supercooled liquid water or mixed phase, depending on the penetration depth. Further, Korolev et al. (2003) found that at temperatures below 238.0 K, the ice phase is dominant. As such, most clouds that fall into the cold mid-level category should be composed primarily of ice. These physical concepts were taken into account when choosing thresholds.

The cumulative distribution function (CDF) of $\beta_{sopaque}(8.5/11\mu m)$ for the 5 CALIOP-derived cloud top temperature bins is shown for 5 different bins of 7.4 μm opaque cloud temperature in Figure 9. The 7.4 μm opaque cloud temperature ($T_{opaque}(7.4\mu m)$) provides an additional piece of information. The smaller the 7.4 μm opaque cloud temperature, the greater the likelihood of ice. As can be seen, clouds that fall into the warm liquid water category (warmer than melting point of water) can be differentiated from definite ice clouds (colder than homogeneous freezing point) with a high degree of skill. Clouds

in the warm mid-level category also generally have very little overlap with definite ice clouds. In the two lowest (coldest) $T_{opaque}(7.4\mu m)$ bins (see Figure 9), the $\beta_{sopaque}(8.5/11\mu m)$ thresholds were chosen such that most of the observations would be classified as ice. This decision was largely based on the analysis of independent near-infrared reflectance data. For the final three $T_{opaque}(7.4\mu m)$ bins, $\beta_{sopaque}(8.5/11\mu m)$ thresholds were chosen such that intermediate mid-level clouds would be classified as ice about 50% of the time.

In order to make this test more robust, a few additional constraints are applied. As discussed earlier, the $\beta_{sopaque}(8.5/11\mu m)$ value near cloud edges may be suspect, so the $\beta_{sopaque}(8.5/11\mu m)$ value at the pixel Local Radiative Center (LRC) is also checked for conformance to the $\beta_{sopaque}(8.5/11\mu m)$ threshold values. In addition, a gross check on the $\beta_{stropo}(12/11\mu m)$ value is performed when the 7.4 μm opaque cloud temperature is undefined, like in Panel E of Figure 9. All of the thresholds used in this test can be found in Table 13 through Table 18. Given that the $\beta_{sopaque}(8.5/11\mu m)$ threshold is dependent on sensor and $T_{opaque}(7.4\mu m)$, each threshold "function" is stored in it's own table.

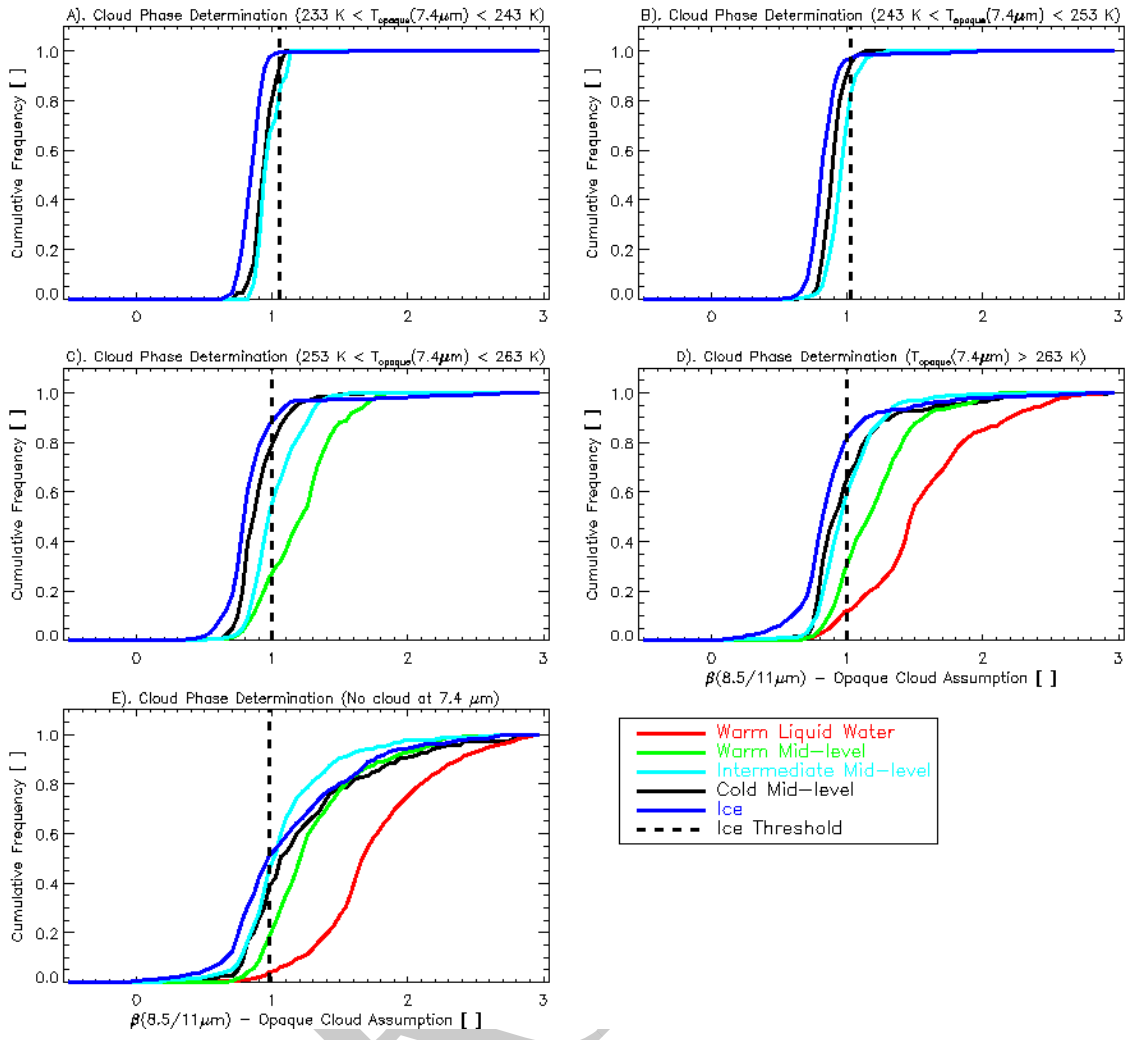

Figure 9: The cumulative distribution function (CDF) of $\beta_{sopaque}(8.5/11\mu m)$ for 5 CALIOP-derived cloud top temperature bins is shown for 5 different bins of 7.4 μm opaque cloud temperature ($T_{opaque}(7.4\mu m)$). In panel A, 233 K < $T_{opaque}(7.4\mu m)$ < 243 K. In panel B, 243 K < $T_{opaque}(7.4\mu m)$ < 253 K. In panel C, 253 K < $T_{opaque}(7.4\mu m)$ < 263 K. In panel D, $T_{opaque}(7.4\mu m)$ > 263 K. Finally in panel E, $T_{opaque}(7.4\mu m)$ is undefined because the cloud is well below the peak of the 7.4 μm weighting function or the cloud is too optically thin to be differentiated from the 7.4 μm clear sky signal.

Table 13: "BOWVIC_Thresh1" threshold values used in the $\beta_{sopaque}(8.5/11\mu m)$ and Water Vapor Ice Cloud (BOWVIC) Test as a function of sensor and 7.4 μm opaque cloud temperature ($T_{opaque}(7.4\mu m)$).

Sensor	$T_{opaque}(7.4\mu m)$ is invalid	180 K ≤ $T_{opaque}(7.4\mu m)$ < 233 K	233 K ≤ $T_{opaque}(7.4\mu m)$ < 243 K	243 K ≤ $T_{opaque}(7.4\mu m)$ < 253 K	253 K ≤ $T_{opaque}(7.4\mu m)$ < 263 K	$T_{opaque}(7.4\mu m)$ ≥ 263 K
NPP VIIRS	N/A	N/A	N/A	N/A	N/A	N/A

GOES-R ABI	0.10	0.10	0.10	0.10	0.10	0.10
Met-8 SEVIRI	0.10	0.10	0.10	0.10	0.10	0.10
Met-9 SEVIRI	0.10	0.10	0.10	0.10	0.10	0.10
Terra MODIS	0.10	0.10	0.10	0.10	0.10	0.10
Aqua MODIS	0.10	0.10	0.10	0.10	0.10	0.10

Table 14: "BOWVIC_Thresh2" threshold values used in the $\beta_{sopaque}$(8.5/11μm) and Water Vapor Ice Cloud (BOWVIC) Test as a function of sensor and 7.4 μm opaque cloud temperature (T_{opaque}(7.4μm)).

Sensor	T_{opaque}(7.4μm) is invalid	180 K ≤ T_{opaque}(7.4μm) < 233 K	233 K ≤ T_{opaque}(7.4μm) < 243 K	243 K ≤ T_{opaque}(7.4μm) < 253 K	253 K ≤ T_{opaque}(7.4μm) < 263 K	T_{opaque}(7.4μm) ≥ 263 K
NPP VIIRS	N/A	N/A	N/A	N/A	N/A	N/A
GOES-R ABI	0.98	1.10	1.05	1.02	1.00	1.00
Met-8 SEVIRI	0.98	1.10	1.05	1.02	1.00	1.00
Met-9 SEVIRI	0.98	1.10	1.05	1.02	1.00	1.00
Terra MODIS	0.75	1.10	1.05	0.87	0.85	0.80
Aqua MODIS	0.75	1.10	1.05	0.87	0.85	0.80

Table 15: "BOWVIC_Thresh3" threshold values used in the $\beta_{sopaque}$(8.5/11μm) and Water Vapor Ice Cloud (BOWVIC) Test as a function of sensor and 7.4 μm opaque cloud temperature (T_{opaque}(7.4μm)).

Sensor	T_{opaque}(7.4μm) is invalid	180 K ≤ T_{opaque}(7.4μm) < 233 K	233 K ≤ T_{opaque}(7.4μm) < 243 K	243 K ≤ T_{opaque}(7.4μm) < 253 K	253 K ≤ T_{opaque}(7.4μm) < 263 K	T_{opaque}(7.4μm) ≥ 263 K
NPP VIIRS	N/A	N/A	N/A	N/A	N/A	N/A
GOES-R ABI	0.10	-10000.0	-10000.0	-10000.0	0.10	0.10
Met-8 SEVIRI	0.10	-10000.0	-10000.0	-10000.0	0.10	0.10
Met-9 SEVIRI	0.10	-10000.0	-10000.0	-10000.0	0.10	0.10
Terra MODIS	0.10	-10000.0	-10000.0	-10000.0	0.10	0.10
Aqua MODIS	0.10	-10000.0	-10000.0	-10000.0	0.10	0.10

Table 16: "BOWVIC_Thresh4" threshold values used in the $\beta_{sopaque}$(8.5/11μm) and Water Vapor Ice Cloud (BOWVIC) Test as a function of sensor and 7.4 μm opaque cloud temperature (T_{opaque}(7.4μm)).

Sensor	$T_{opaque}(7.4\mu m)$ is invalid	180 K ≤ $T_{opaque}(7.4\mu m)$ < 233 K	233 K ≤ $T_{opaque}(7.4\mu m)$ < 243 K	243 K ≤ $T_{opaque}(7.4\mu m)$ < 253 K	253 K ≤ $T_{opaque}(7.4\mu m)$ < 263 K	$T_{opaque}(7.4\mu m)$ ≥ 263 K
NPP VIIRS	N/A	N/A	N/A	N/A	N/A	N/A
GOES-R ABI	0.98	10000.0	10000.0	10000.0	1.00	1.00
Met-8 SEVIRI	0.98	10000.0	10000.0	10000.0	1.00	1.00
Met-9 SEVIRI	0.98	10000.0	10000.0	10000.0	1.00	1.00
Terra MODIS	0.75	10000.0	10000.0	10000.0	0.85	0.80
Aqua MODIS	0.75	10000.0	10000.0	10000.0	0.85	0.80

Table 17: "BOWVIC_Thresh5" threshold values used in the $\beta_{sopaque}(8.5/11\mu m)$ and Water Vapor Ice Cloud (BOWVIC) Test as a function of sensor and 7.4 μm opaque cloud temperature ($T_{opaque}(7.4\mu m)$).

Sensor	$T_{opaque}(7.4\mu m)$ is invalid	180 K ≤ $T_{opaque}(7.4\mu m)$ < 233 K	233 K ≤ $T_{opaque}(7.4\mu m)$ < 243 K	243 K ≤ $T_{opaque}(7.4\mu m)$ < 253 K	253 K ≤ $T_{opaque}(7.4\mu m)$ < 263 K	$T_{opaque}(7.4\mu m)$ ≥ 263 K
NPP VIIRS	N/A	N/A	N/A	N/A	N/A	N/A
GOES-R ABI	0.99	-10000.0	-10000.0	-10000.0	-10000.0	-10000.0
Met-8 SEVIRI	0.99	-10000.0	-10000.0	-10000.0	-10000.0	-10000.0
Met-9 SEVIRI	0.99	-10000.0	-10000.0	-10000.0	-10000.0	-10000.0
Terra MODIS	0.95	-10000.0	-10000.0	-10000.0	-10000.0	-10000.0
Aqua MODIS	0.95	-10000.0	-10000.0	-10000.0	-10000.0	-10000.0

Table 18: "BOWVIC_Thresh6" threshold values used in the $\beta_{sopaque}(8.5/11\mu m)$ and Water Vapor Ice Cloud (BOWVIC) Test as a function of sensor and 7.4 μm opaque cloud temperature ($T_{opaque}(7.4\mu m)$).

Sensor	$T_{opaque}(7.4\mu m)$ is invalid	180 K ≤ $T_{opaque}(7.4\mu m)$ < 233 K	233 K ≤ $T_{opaque}(7.4\mu m)$ < 243 K	243 K ≤ $T_{opaque}(7.4\mu m)$ < 253 K	253 K ≤ $T_{opaque}(7.4\mu m)$ < 263 K	$T_{opaque}(7.4\mu m)$ ≥ 263 K
NPP VIIRS	N/A	N/A	N/A	N/A	N/A	N/A
GOES-R ABI	0.99	10000.0	10000.0	10000.0	10000.0	10000.0
Met-8 SEVIRI	0.99	10000.0	10000.0	10000.0	10000.0	10000.0
Met-9 SEVIRI	0.99	10000.0	10000.0	10000.0	10000.0	10000.0
Terra MODIS	0.95	10000.0	10000.0	10000.0	10000.0	10000.0
Aqua MODIS	0.95	10000.0	10000.0	10000.0	10000.0	10000.0

3.4.2.6.10 $\beta_{sopaque}$(8.5/11μm) and Water Vapor Ice Cloud LRC-only (BOWVIC-LRC) Test

Purpose: Utilize the cloud phase information offered by β(8.5/11μm) (see Figure 3), with the "opaque cloud assumption" (see Section 3.4.2.1.3), and the Local Radiative Center (LRC) concept to identify optically thin ice clouds.

Inputs:

- T_{opaque}(7.4μm) at the pixel Local Radiative Center (LRC) [T_{opaque}(7.4μm)_LRC]
- $\beta_{sopaque}$(8.5/11μm) at the pixel LRC [$\beta_{sopaque}$(8.5/11μm)_LRC]
- β_{stropo}(12/11μm)

Logic:

It is important to note that the first two thresholds symbolized in the logic below are a function of T_{opaque}(7.4μm)_LRC.

If $\beta_{sopaque}$(8.5/11μm)_LRC > BOWVIC_Thresh1(T_{opaque}(7.4μm)_LRC) **AND**
$\beta_{sopaque}$(8.5/11μm)_LRC < BOWVIC_Thresh2(T_{opaque}(7.4μm)_LRC) **AND**
β_{stropo}(12/11μm) > BOWVIC-LRC_Thresh3 **AND**
β_{stropo}(12/11μm) < BOWVIC-LRC_Thresh4)

Output = TRUE (an ice cloud was detected)

Else

Output = FALSE

Thresholds and rational:
This test relies on the 7.4 μm channel, which is not available from VIIRS, so this test is not used in the current JRRCT algorithm and only used in the ACT algorithm. Future improvements to the JRRCT algorithm code will remove this dependency and make this test relevant. This test is a slight variant on the $\beta_{sopaque}$(8.5/11μm) and Water Vapor Ice Cloud (BOWVIC) Test (see Section 3.4.2.6.9). In this version of the test, only the value of $\beta_{sopaque}$(8.5/11μm) at the pixel Local Radiative Center (LRC) is examined, and different β_{stropo}(12/11μm) thresholds are applied. The $\beta_{sopaque}$(8.5/11μm) thresholds can be found in Table 13 and Table 14. The β_{stropo}(12/11μm) thresholds can be found in Table 19. This test is motivated by the desire to detect as many thin cirrus clouds as possible.

Table 19: The third and fourth thresholds used by the $\beta_{sopaque}$(8.5/11μm) and Water Vapor Ice Cloud LRC-only (BOWVIC-LRC) Test as a function of sensor.

Sensor	BOWVIC-LRC_Thresh3	BOWVIC-LRC_Thresh4
NPP VIIRS	N/A	N/A
GOES-R ABI	0.95	1.50

Met-8 SEVIRI	0.95	1.50
Met-9 SEVIRI	0.95	1.50
Terra-MODIS	0.92	1.45
Aqua-MODIS	0.92	1.45

3.4.2.6.11 $\beta_{sopaque}$(8.5/11μm) Opaque Ice Cloud (BOIC) Test

Purpose: Utilize the cloud phase information offered by β(8.5/11μm) (see Figure 3), with the "opaque cloud assumption" (see Section 3.4.2.1.3) to identify opaque mid-level glaciated clouds.

Inputs:

- Results from the OCTD Test (see Section 3.4.2.6.3) (Not used with NPP VIIRS currently)
- $\varepsilon_{stropo}(11\mu m)$
- $T_{opaque}(11\mu m)$
- $\beta_{opaque}(8.5/11\mu m)$
- $\beta_{opaque}(8.5/11\mu m)$ at the pixel Local Radiative Center (LRC) [$\beta_{opaque}(8.5/11\mu m)$_LRC]

Logic:

If (OCTD Test = TRUE **AND**
$\varepsilon_{stropo}(11\mu m)$ > BOIC_Thresh1 AND
$T_{opaque}(11\mu m)$ < 273.16 K **AND**
$\beta_{opaque}(8.5/11\mu m)$ > BOIC_Thresh2 **AND**
$\beta_{opaque}(8.5/11\mu m)$ < BOIC_Thresh3 **AND**
$\beta_{opaque}(8.5/11\mu m)$_LRC > BOIC_Thresh4 **AND**
$\beta_{opaque}(8.5/11\mu m)$_LRC < BOIC_Thresh5)

Output = TRUE (an ice cloud was detected)

Else

Output = FALSE

Thresholds and rational:
This test relies on the OCTD test (7.4 μm channel needed), which is not available from VIIRS, so this test is not used in the current JRRCT algorithm and only used in the ACT algorithm. Future improvements to the JRRCT algorithm code will remove this dependency and make this test relevant. This test is a simple complement to the $\beta_{sopaque}(8.5/11\mu m)$ and Water Vapor Ice Cloud (BOWVIC) Test designed to make sure that opaque mid-level glaciated clouds do not get missed. Since this test is designed to detect mid-level opaque glaciated clouds, the 11 μm opaque cloud temperature must be

less than the melting point of water (273.16 K). The $\beta_{sopaque}(8.5/11\mu m)$ thresholds were chosen based on the manual analysis of independent near-infrared reflectance data. The thresholds are listed in Table 20.

Table 20: The thresholds used by the $\beta_{sopaque}(8.5/11\mu m)$ Opaque Ice Cloud (BOIC) Test as a function of sensor.

Sensor	BOIC_ Thresh1	BOIC_ Thresh2	BOIC_ Thresh3	BOIC_ Thresh4	BOIC_ Thresh5
NPP VIIRS	0.08	0.10	0.98	0.10	0.98
GOES-R ABI	0.08	0.40	1.10	0.40	1.12
Met-8 SEVIRI	0.08	0.40	1.10	0.40	1.12
Met-9 SEVIRI	0.08	0.40	1.10	0.40	1.12
Terra MODIS	0.08	0.40	0.95	0.40	0.97
Aqua MODIS	0.08	0.40	0.95	0.40	0.97

3.4.2.6.12 $\beta_{stropo}(8.5/11\mu m)$ and Water Vapor Ice Cloud (BTWVIC) Test

Purpose: Utilize the cloud phase information offered by $\beta(8.5/11\mu m)$ (see Figure 3), with the "top of troposphere assumption" (see Section 3.4.2.1.1), to identify optically thin ice clouds over low emissivity surfaces.

Inputs:

- Result of Low Surface Emissivity (LSE) Test
- $T_{opaque}(7.4\mu m)$
- $\beta_{stropo}(8.5/11\mu m)$
- $\beta_{sopaque}(12/11\mu m)$

Logic:

It is important to note that the first two thresholds symbolized in the logic below are a function of $T_{opaque}(7.4\mu m)$.

If (LSE Test = TRUE **AND**
$\beta_{stropo}(8.5/11\mu m) > BTWVIC\_Thresh1(T_{opaque}(7.4\mu m))$ **AND**
$\beta_{stropo}(8.5/11\mu m) < BTWVIC\_Thresh2(T_{opaque}(7.4\mu m))$ **AND**
$\beta_{sopaque}(12/11\mu m) > BTWVIC\_Thresh3$ **AND**
$\beta_{sopaque}(12/11\mu m) < BTWVIC\_Thresh4$)

Output = TRUE (an ice cloud was detected)

Else

Output = FALSE

Thresholds and rational:

This test relies on the 7.4 μm channel, which is not available from VIIRS, so this test is not used in the current JRRCT algorithm and only used in the ACT algorithm. Future improvements to the JRRCT algorithm code will remove this dependency and make this test relevant. Comparisons to CALIOP have shown that $\beta_{sopaque}(8.5/11\mu m)$ is a more robust cloud phase metric than $\beta_{stropo}(8.5/11\mu m)$, except over low emissivity surfaces. That is why this test is only applied over low emissivity surfaces. Over very low emissivity surfaces, the effective cloud level needs to be reasonably accurate; otherwise the cloud microphysical information offered by $\beta(8.5/11\mu m)$ will be minimal (Pavolonis, 2010a). For optically thin ice clouds in the upper troposphere, the "opaque cloud assumption" generally results in an effective cloud level that is much lower than the actual cloud level. In order to accurately identify thin cirrus clouds over low emissivity surfaces like the Sahara Desert, the "top of troposphere assumption" is needed. Table 21 through Table 23 list the thresholds required by this test. The thresholds were determined through analysis of CALIOP data and manual analysis of multi-spectral imagery. The cumulative distribution function (CDF) of $\beta_{stropo}(8.5/11\mu m)$ for the 5 CALIOP-derived cloud top temperature bins is shown for 3 different bins of 7.4 μm opaque cloud temperature in Figure 10. Figure 10 is analogous to Figure 9. As Figure 10 shows, very conservative $\beta_{stropo}(8.5/11\mu m)$ thresholds were chosen to prevent false ice cloud detects. In addition, we found that the value $\beta_{stropo}(8.5/11\mu m)$ tend to be lower over low emissivity surfaces, which influenced our choice of threshold values.

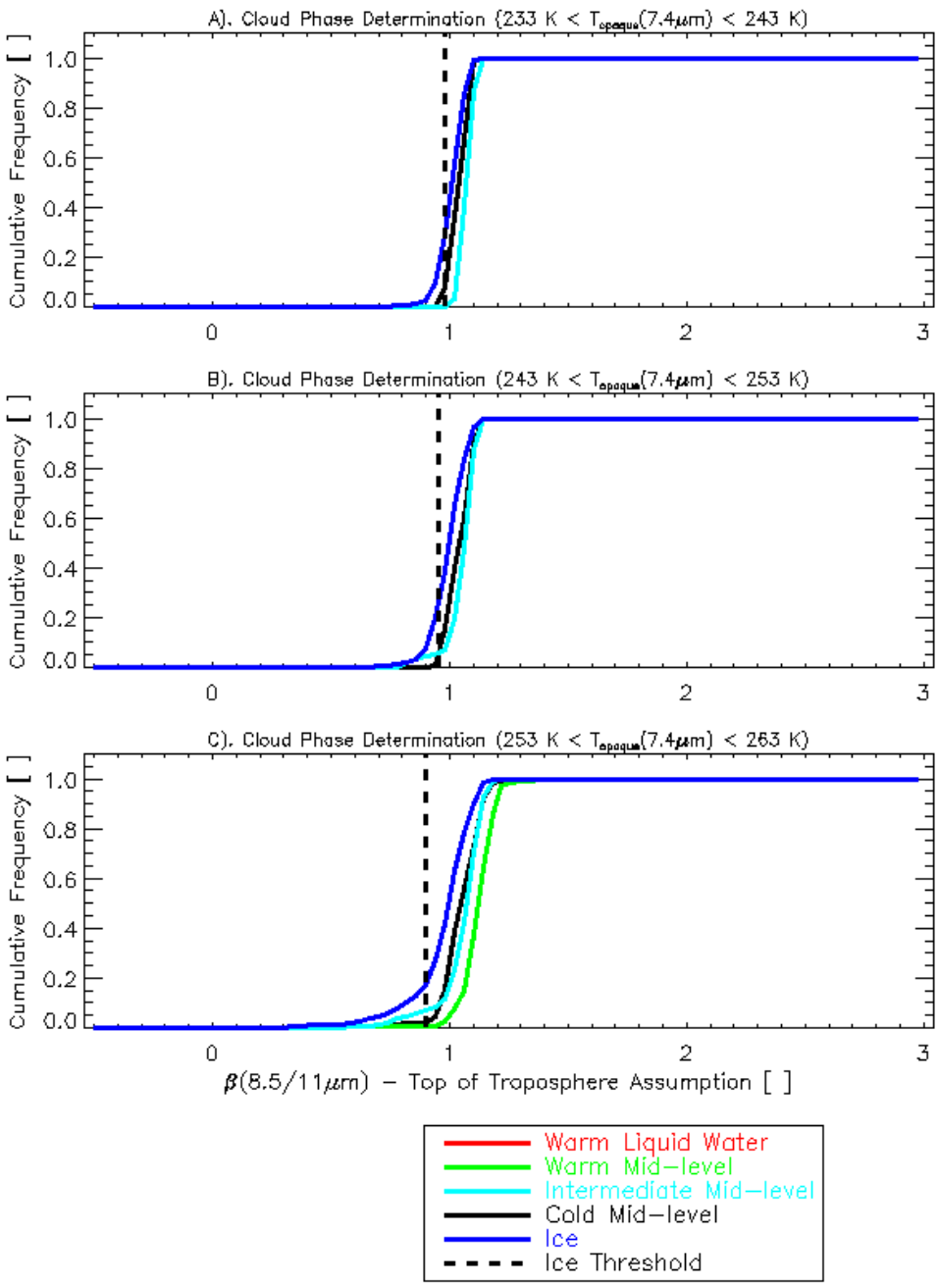

Figure 10: The cumulative distribution function (CDF) of β_{stropo}(8.5/11μm) for 5 CALIOP-derived cloud top temperature bins is shown for 3 different bins of 7.4 μm opaque cloud temperature (T_{opaque}(7.4μm)). In panel A, 233 K < T_{opaque}(7.4μm) < 243 K. In panel B, 243 K < T_{opaque}(7.4μm) < 253 K. In panel C, 253 K < T_{opaque}(7.4μm) < 263 K.

Table 21: "BTWVIC_Thresh1" threshold values used in the β_{stropo}(8.5/11μm) and Water Vapor Ice Cloud (BTWVIC) Test as a function of sensor and 7.4 μm opaque cloud temperature (T_{opaque}(7.4μm)).

Sensor	T_{opaque}(7.4μm) is < 233 K or is invalid	233 K ≤ T_{opaque}(7.4μm) < 243 K	243 K ≤ T_{opaque}(7.4μm) < 253 K	253 K ≤ T_{opaque}(7.4μm) < 263 K	T_{opaque}(7.4μm) ≥ 263 K
NPP VIIRS	N/A	N/A	N/A	N/A	N/A
GOES-R ABI	10000.0	0.40	0.40	0.40	10000.0
Met-8 SEVIRI	10000.0	0.40	0.40	0.40	10000.0
Met-9 SEVIRI	10000.0	0.40	0.40	0.40	10000.0
Terra MODIS	10000.0	0.40	0.40	0.40	10000.0
Aqua MODIS	10000.0	0.40	0.40	0.40	10000.0

Table 22: "BTWVIC_Thresh2" threshold values used in the β_{stropo}(8.5/11μm) and Water Vapor Ice Cloud (BTWVIC) Test as a function of sensor and 7.4 μm opaque cloud temperature (T_{opaque}(7.4μm)).

Sensor	T_{opaque}(7.4μm) is < 233 K or is invalid	233 K ≤ T_{opaque}(7.4μm) < 243 K	243 K ≤ T_{opaque}(7.4μm) < 253 K	253 K ≤ T_{opaque}(7.4μm) < 263 K	T_{opaque}(7.4μm) ≥ 263 K
NPP VIIRS	N/A	N/A	N/A	N/A	N/A
GOES-R ABI	-10000.0	0.98	0.95	0.90	-10000.0
Met-8 SEVIRI	-10000.0	0.98	0.95	0.90	-10000.0
Met-9 SEVIRI	-10000.0	0.98	0.95	0.90	-10000.0
Terra MODIS	-10000.0	0.93	0.90	0.85	-10000.0
Aqua MODIS	-10000.0	0.93	0.90	0.85	-10000.0

Table 23: The "BTWVIC_Thresh3" and " BTWVIC_Thresh4" thresholds used by the β_{stropo}(8.5/11μm) Water Vapor Ice Cloud (BTWVIC) Test as a function of sensor.

Sensor	BTWVIC_Thresh3	BTWVIC_Thresh4
NPP VIIRS	N/A	N/A

GOES-R ABI	1.00	2.00
Met-8 SEVIRI	1.00	2.00
Met-9 SEVIRI	1.00	2.00
Terra MODIS	0.98	2.00
Aqua MODIS	0.98	2.00

3.4.2.6.13 Overall Ice Cloud (OIC) Test

Purpose: To combine the results from the Homogeneous Freezing (HF), $\beta_{sopaque}(8.5/11\mu m)$ and Water Vapor Ice Cloud (BOWVIC), $\beta_{sopaque}(8.5/11\mu m)$ and Water Vapor Ice Cloud LRC-only (BOWVIC-LRC), $\beta_{sopaque}(8.5/11\mu m)$ Opaque Ice Cloud (BOIC), and $\beta_{stropo}(8.5/11\mu m)$ and Water Vapor Ice Cloud (BTWVIC) Tests to determine if an ice phase or glaciated cloud is present.

Input:

- HF Test Results (see Section 3.4.2.6.8)
- BOWVIC Test Results (see Section 3.4.2.6.9) (Not used with NPP VIIRS currently)
- BOWVIC-LRC Test Results (see Section 3.4.2.6.10) (Not used with NPP VIIRS currently)
- BOIC Test Results (see Section 3.4.2.6.11) (Not used with NPP VIIRS currently)
- BTWVIC Test Results (see Section 3.4.2.6.12) (Not used with NPP VIIRS currently)

Logic:

If (HF Test = TRUE **OR**
BOWVIC Test = TRUE **OR**
BOWVIC-LRC = TRUE **OR**
BOIC = TRUE **OR**
BTWVIC = TRUE)

Output = TRUE (an ice cloud was detected)

Else

Output = FALSE

Thresholds and rational:
If any of the previous ice cloud tests were positive (TRUE), then an ice cloud is assumed to be present.

3.4.2.6.14 Sub-classify Ice Cloud (SCIC) Test

Purpose: Given an ice cloud, determine if it belongs in the semi-transparent cloud type category or the opaque cloud category.

Input:

- Results of Overall Opaque Cloud (OOC) Test (see Section 3.4.2.6.4)
- $\varepsilon_{stropo}(11\mu m)$

Logic:

If ($\varepsilon_{stropo}(11\mu m)$ < SCIC_Thresh1 **OR**
(OOC Test = FALSE **AND** $\varepsilon_{stropo}(11\mu m)$ < SCIC_Thresh2))

Output = TRUE (the cloud is semi-transparent)

Else

Output = FALSE

Thresholds and rational:
This test simply utilizes previously established information on whether or not an ice cloud has an 11-μm optical depth of approximately 2.0 or less. Loose $\varepsilon_{stropo}(11\mu m)$ thresholds are also included to decrease the odds of misclassification. The $\varepsilon_{stropo}(11\mu m)$ thresholds can be found in Table 24.

Table 24: The thresholds used by the Sub-classify Ice Cloud (SCIC) Test as a function of sensor.

Sensor	SCIC_Thresh1	SCIC_Thresh2
NPP VIIRS	0.35	0.85
GOES-R ABI	0.40	0.85
Met-8 SEVIRI	0.40	0.85
Met-9 SEVIRI	0.40	0.85
Terra-MODIS	0.40	0.85
Aqua-MODIS	0.40	0.85

3.4.2.6.15 Mixed Phase (MP) Test

Purpose: Utilize the cloud phase information offered by $\beta(8.5/11\mu m)$ (see Figure 3), with the "opaque cloud assumption" (see Section 3.4.2.1.3) to identify optically thick clouds that are potentially mixed phase near cloud top.

Inputs:

- $T_{opaque}(11\mu m)$
- $T_{opaque}(11\mu m)$ at the pixel Local Radiative Center (LRC) [$T_{opaque}(11\mu m)\_LRC$]
- $\beta_{sopaque}(8.5/11\mu m)$
- $\beta_{sopaque}(8.5/11\mu m)$ at the pixel LRC [$\beta_{sopaque}(8.5/11\mu m)\_LRC$]

Logic:

It is important to note that the thresholds symbolized in the logic below are a function of $T_{opaque}(11\mu m)$ or $T_{opaque}(11\mu m)\_LRC$.

If ($\beta_{sopaque}(8.5/11\mu m) > MP\_Thresh1(T_{opaque}(11\mu m))$ **AND**
$\beta_{sopaque}(8.5/11\mu m) < MP\_Thresh2(T_{opaque}(11\mu m))$ **AND**
$\beta_{sopaque}(8.5/11\mu m)\_LRC > MP\_Thresh3(T_{opaque}(11\mu m)\_LRC)$ **AND**
$\beta_{sopaque}(8.5/11\mu m)\_LRC < MP\_Thresh4(T_{opaque}(11\mu m)\_LRC)$

Output = TRUE (the cloud is potentially mixed phase)

Else

Output = FALSE

Thresholds and rational:

Other than a small number of aircraft data sets, very few of which can be co-located with proxy GOES-R ABI data, unambiguous information on the phase of hydrometeors that are colder than the melting point of water or warmer than the homogeneous freezing temperature of water is unavailable. As such, $\beta_{sopaque}(8.5/11\mu m)$ CDF's, like those constructed to determine the thresholds used in the $\beta_{sopaque}(8.5/11\mu m)$ and Water Vapor Ice Cloud (BOWVIC) Test (see Section 3.4.2.6.9), were used to develop thresholds to identify mixed phase clouds. Since mixed phase clouds may be present at altitudes that are below the 7.4 μm weighting function, the $\beta_{sopaque}(8.5/11\mu m)$ thresholds are expressed as a function of the 11 μm opaque cloud temperature instead of the 7.4 μm opaque cloud temperature. The CDF of $\beta_{sopaque}(8.5/11\mu m)$ for the 5 CALIOP-derived cloud top temperature bins is shown for 4 different bins of 11 μm opaque cloud temperature ($T_{opaque}(11\mu m)$) in Figure 11. The thresholds were chosen such that about 50% of the warm mid-level clouds in the 263 K < $T_{opaque}(11\mu m)$ < 273 K bin are classified as mixed phase (see Figure 11, Panel D) and the $\beta_{sopaque}(8.5/11\mu m)$ threshold is increased by 0.05 increments moving to lower $T_{opaque}(11\mu m)$ bins. This choice is primarily based on limited aircraft measurements (Cober et al., 2001). The actual threshold values are listed in Table 25 –

Table 28.

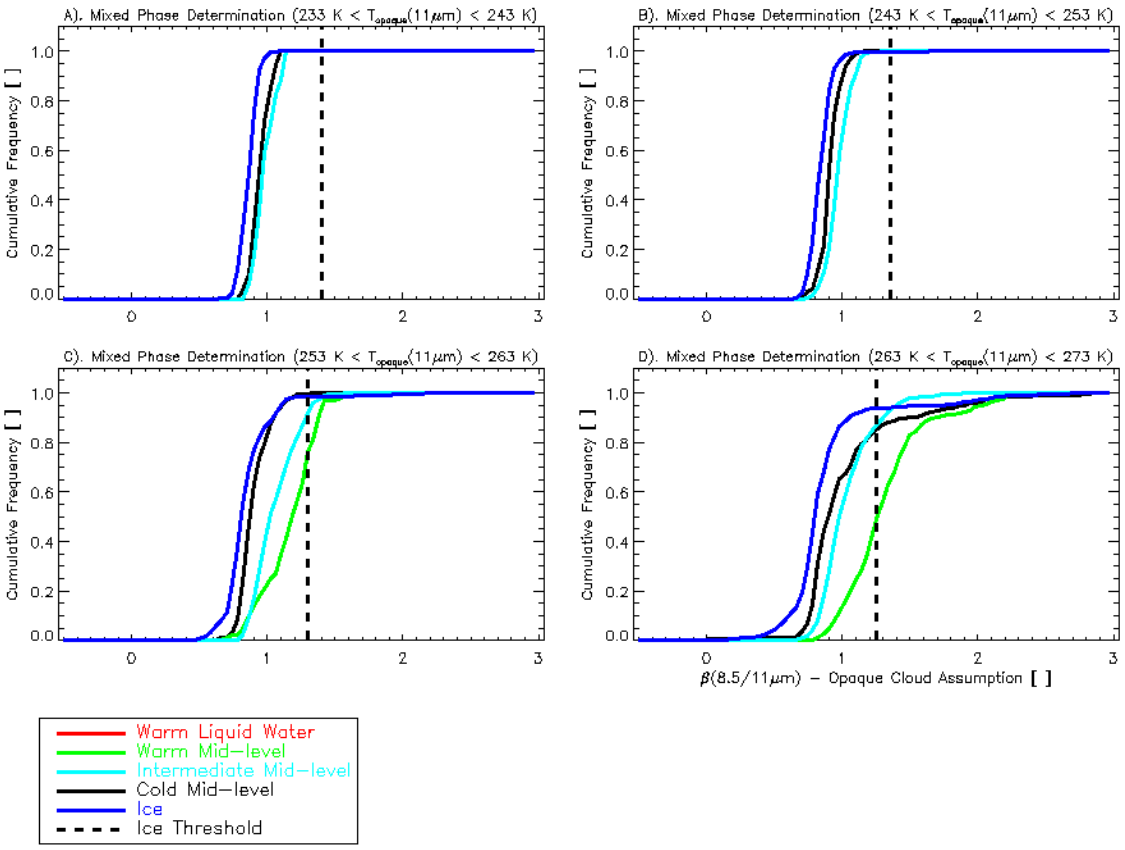

Figure 11: The cumulative distribution function (CDF) of $\beta_{sopaque}$(8.5/11μm) for 5 CALIOP-derived cloud top temperature bins is shown for 4 different bins of 11 μm opaque cloud temperature (T_{opaque}(11μm)). In panel A, 233 K < T_{opaque}(11μm) < 243 K. In panel B, 243 K < T_{opaque}(11μm) < 253 K. In panel C, 253 K < T_{opaque}(11μm) < 263 K. In panel D, 263 K < T_{opaque}(11μm) < 273 K.

Table 25: "MP_Thresh1" threshold values used in the Mixed Phase (MP) Test as a function of sensor and 11 μm opaque cloud temperature (T_{opaque}(11μm)).

Sensor	233 K ≤ T_{opaque}(11μm) < 243 K	243 K ≤ T_{opaque}(11μm) < 253 K	253 K ≤ T_{opaque}(11μm) < 263 K	263 K ≤ T_{opaque}(11μm) < 273 K
NPP VIIRS	0.40	0.40	0.40	0.40
GOES-R ABI	0.40	0.40	0.40	0.40
Met-8 SEVIRI	0.40	0.40	0.40	0.40
Met-9	0.40	0.40	0.40	0.40

SEVIRI				
Terra MODIS	0.40	0.40	0.40	0.40
Aqua MODIS	0.40	0.40	0.40	0.40

Table 26: "MP_Thresh2" threshold values used in the Mixed Phase (MP) Test as a function of sensor and 11 μm opaque cloud temperature ($T_{opaque}(11\mu m)$).

Sensor	**233 K ≤ $T_{opaque}(11\mu m)$ < 243 K**	**243 K ≤ $T_{opaque}(11\mu m)$ < 253 K**	**253 K ≤ $T_{opaque}(11\mu m)$ < 263 K**	**263 K ≤ $T_{opaque}(11\mu m)$ < 273 K**
NPP VIIRS	1.40	1.35	1.30	1.25
GOES-R ABI	1.40	1.35	1.30	1.25
Met-8 SEVIRI	1.40	1.35	1.30	1.25
Met-9 SEVIRI	1.40	1.35	1.30	1.25
Terra MODIS	1.25	1.20	1.15	1.10
Aqua MODIS	1.25	1.20	1.15	1.10

Table 27: "MP_Thresh3" threshold values used in the Mixed Phase (MP) Test as a function of sensor and 11 μm opaque cloud temperature ($T_{opaque}(11\mu m)$).

Sensor	**233 K ≤ $T_{opaque}(11\mu m)$ < 243 K**	**243 K ≤ $T_{opaque}(11\mu m)$ < 253 K**	**253 K ≤ $T_{opaque}(11\mu m)$ < 263 K**	**263 K ≤ $T_{opaque}(11\mu m)$ < 273 K**
NPP VIIRS	0.40	0.40	0.40	0.40
GOES-R ABI	0.40	0.40	0.40	0.40
Met-8 SEVIRI	0.40	0.40	0.40	0.40
Met-9 SEVIRI	0.40	0.40	0.40	0.40
Terra MODIS	0.40	0.40	0.40	0.40
Aqua MODIS	0.40	0.40	0.40	0.40

Table 28: "MP_Thresh4" threshold values used in the Mixed Phase (MP) Test as a function of sensor and 11 μm opaque cloud temperature ($T_{opaque}(11\mu m)$).

Sensor	233 K ≤ $T_{opaque}(11\mu m)$ < 243 K	243 K ≤ $T_{opaque}(11\mu m)$ < 253 K	253 K ≤ $T_{opaque}(11\mu m)$ < 263 K	263 K ≤ $T_{opaque}(11\mu m)$ < 273 K
NPP VIIRS	1.40	1.35	1.30	1.25
GOES-R ABI	1.40	1.35	1.30	1.25
Met-8 SEVIRI	1.40	1.35	1.30	1.25
Met-9 SEVIRI	1.40	1.35	1.30	1.25
Terra MODIS	1.25	1.20	1.15	1.10
Aqua MODIS	1.25	1.20	1.15	1.10

3.4.2.6.16 Supercooled Liquid Water (SLW) Test

Purpose: Determine if a cloud is potentially composed of supercooled liquid water.

Inputs:

- $T_{opaque}(11\mu m)$

Logic:

If ($T_{opaque}(11\mu m)$ < 273.16 K **AND** $T_{opaque}(11\mu m)$ > 170.0 K)

Output = TRUE (the cloud is potentially composed of supercooled liquid water)

Else

Output = FALSE

Thresholds and rational:
The 11-μm opaque cloud temperature ($T_{opaque}(11\mu m)$) is used to determine if a liquid water phase cloud is at a temperature lower than the melting point of water (273.16 K).

3.4.2.6.17 Determining Cloud Type from Test Results

Once the results from all of the individual tests described in Section 3.4.2.6.1 through Section 3.4.2.6.16 have been compiled, the cloud type is determined using a simple

decision tree, which is shown in Figure 12. The decision tree requires the results from the Overall Multilayered Cloud (OMC) Test (Section 3.4.2.6.7), the Overall Ice Cloud (OIC) Test (Section 3.4.2.6.13), the Sub-classify Ice Cloud (SCIC) Test (Section 3.4.2.6.14), the Mixed Phase (MP) Test (Section 3.4.2.6.15), and the Supercooled Liquid Water (SLW) Test (Section 3.4.2.6.16).

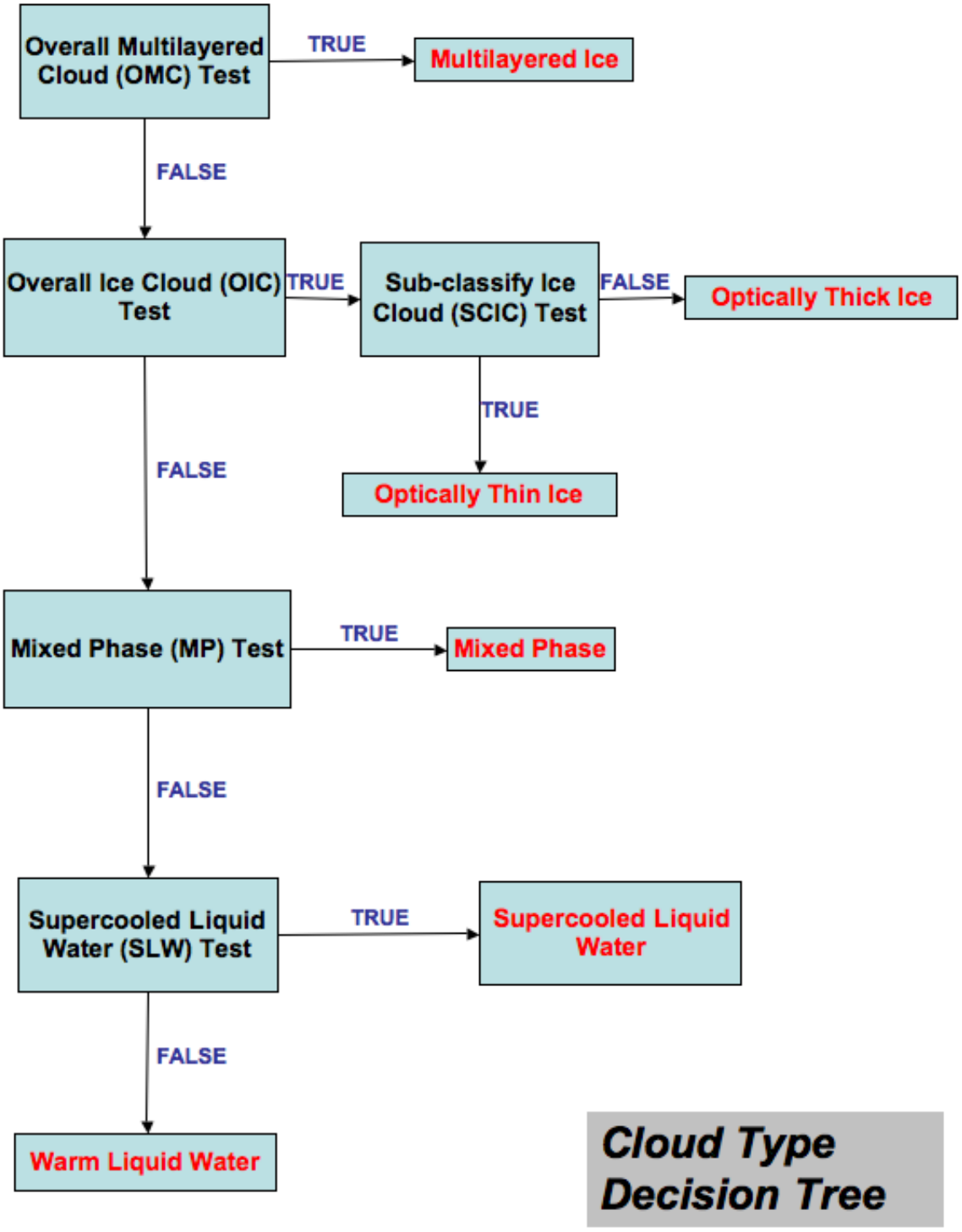

Figure 12: A flow chart of the decision tree used to determine cloud type using the results of several logical tests described in Section 3.4.2.6.1 through Section 3.4.2.6.16 is shown.

3.4.2.7 Noise Filtering

In order to remove any visual artifacts associated with the use of the LRC technique described in Section 3.4.2.4, the cloud type product is run through a standard median filter. The median filter simply replaces the value at each pixel with the median value of a 3 x 3 pixel array centered on that pixel. Figure 13 shows that the median filter is effective at removing spatial artifacts without impacting the scientific integrity of the product. Care is exercised so that pixels that were flagged as cloudy before the median filter retain a valid cloud type after the filtering, while pre-median filter clear pixels remained tagged as such after the filtering. In other words, the finished cloud type and cloud phase product are always consistent with the cloud mask. The generic median filter procedure is described in detail in the AIADD Document.

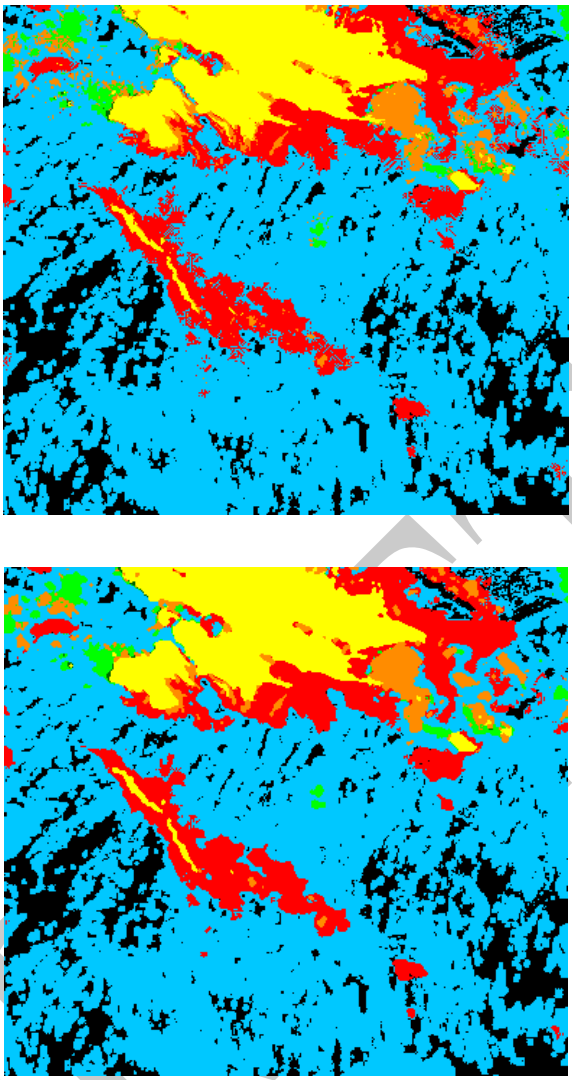

Figure 13: The impacts of the median filter are shown. Unfiltered cloud type output is shown on the top and filtered cloud type output on the bottom. Note how the median filter removes artifacts near the edge of the different cloud categories indicated by different colors.

3.4.2.8 Determining Cloud Phase from Cloud Type

The cloud phase categories are derived directly from the cloud type categories. The category conversion rules are shown in Table 29.

Table 29: Correspondence between cloud phase and cloud type categories.

Cloud Phase Category	Corresponding Cloud Type Categories
Clear	Clear
Liquid Water Phase	Liquid Water

Supercooled Water Phase	Supercooled Water
Mixed Phase	Mixed
Ice Phase	Thick Ice, Thin Ice, and Multilayered Ice

3.4.3 Algorithm Output

3.4.3.1 Product Output

The final output of this algorithm is an 8-category cloud typing and a 5-category cloud phase. The output values and description of their meaning is provided in Table 30 and Table 31.

Table 30: A description of the cloud type output.

Category	Description	Value
Clear	Confidently clear according to cloud mask	0
Spare	Spare	1
Liquid Water	Liquid water cloud with an opaque cloud temperature greater than 273 K	2
Supercooled Liquid Water	Liquid water topped cloud with an opaque cloud temperature less than 273 K	3
Mixed Phase	High probability of containing liquid water and ice near cloud top	4
Optically Thick Ice	High emissivity ice topped clouds with an infrared optical depth greater than 2.0	5
Optically Thin Ice	Ice clouds which have an infrared optical depth of about 2.0 or less	6
Multilayered Ice	Semi-transparent ice cloud overlapping a lower, opaque cloud layer	7
Cloud type could not be determined	Unable to determine cloud phase due to bad input data	8

Table 31: A description of the cloud phase output.

Category	Description	Value
Clear	Confidently clear according to cloud mask	0
Liquid Water	Liquid water cloud with an opaque cloud temperature greater than 273 K	1
Supercooled Liquid Water	Liquid water topped cloud with an opaque cloud temperature less than 273 K	2
Mixed Phase	High probability of containing liquid water and ice near cloud top	3

Ice	All ice topped clouds	4
Cloud phase could not be determined	Unable to determine cloud phase due to bad input data	5

3.4.3.2 Quality Flags (QF)

A complete and self-contained description of the GOES-R ACT and JRRCT quality flag output is listed in Table 32.

Table 32: A complete description of the cloud type/phase quality flag output is shown.

Bit(s)	QF Description	Bit Interpretation
1	**Overall cloud phase/type product quality flag** - the overall quality will be set to "low quality" if any of the more specific quality flags listed below are set to "low quality"	0 = high quality 1 = low quality
2	**L1b quality flag** – this will be set to "low quality" if any of the spectral data used in the algorithm is of low quality, based on L1b calibration flags	0 = high quality spectral data 1 = low quality spectral data
3	**Beta quality flag** – this will be set to "low quality" if $\beta_{stropo}(12/11\mu m)$, $\beta_{sopaque}(12/11\mu m)$, $\beta_{stropo}(8.5/11\mu m)$, **or** $\beta_{sopaque}(8.5/11\mu m)$ fall outside of the 0.1 – 10.0 range	0 = high quality beta calculation 1 = low quality beta calculation
4	**Ice cloud quality flag** – this will be set to "low quality" if the cloud phase was determined to be ice and the $\varepsilon_{stropo}(11\mu m) < 0.05$	0 = ice cloud determination based on strong radiative signal 1 = ice cloud determination based on weak radiative signal (low quality)
5	**Surface emissivity quality flag** – this will be set to "low quality" if the result of the Low Surface Emissivity (LSE) Test is TRUE and the result of the Overall Opaque Cloud (OOC) Test is FALSE	0 = surface emissivity does NOT significantly impact product quality 1 = surface emissivity significantly impacts product quality (low quality)
6	**Satellite zenith angle quality flag** – this will be set to "low quality" if the cosine of the satellite zenith angle is less than 0.15 (~82 degrees)	0 = satellite zenith angle does NOT significantly impact product quality 1 = satellite zenith angle significantly impacts product quality (low quality)

3.4.3.3 Product Quality Information (PQI)

A complete and self-contained description of the GOES-R ACT and JRRCT Product Quality Information (PQI) output is listed in Table 33.

Table 33: A complete description of the cloud type/phase Product Quality Information (PQI) output is shown.

Bit(s)	PQI Description	Bit Interpretation
1	Pixel is earth geolocated, has valid spectral data, and is cloudy	0 = FALSE 1 = TRUE
2	Pixel has a valid Local Radiative Center (LRC) (e.g. valid LRC array indices are available for the current pixel)	0 = FALSE 1 = TRUE
3	Result of Low Surface Emissivity (LSE) Test (see Section 3.4.2.6.1)	0 = FALSE 1 = TRUE
4	Result of $\beta_{sopaque}$(12/11μm) Opaque Cloud (BOC) Test (see Section 3.4.2.6.2)	0 = FALSE 1 = TRUE
5	Result of Opaque Cloud Temperature Difference (OCTD) Test (see Section 3.4.2.6.3)	0 = FALSE 1 = TRUE
6	Result of Overall Opaque Cloud (OOC) Test (see Section 3.4.2.6.4)	0 = FALSE 1 = TRUE
7	Result of Water Vapor Multilayered Detection (WVMD) Test (see Section 3.4.2.6.5)	0 = FALSE 1 = TRUE
8	Result of Infrared Window Multilayered Detection (IWMD) Tests (see Section 3.4.2.6.6)	0 = FALSE 1 = TRUE
9	Result of Overall Multilayered Cloud (OMC) Test (see Section 3.4.2.6.7)	0 = FALSE 1 = TRUE
10	Result of Homogeneous Freezing (HF) Test (see Section 3.4.2.6.8)	0 = FALSE 1 = TRUE
11	Result of $\beta_{sopaque}$(8.5/11μm) and Water Vapor Ice Cloud (BOWVIC) Test (see Section 3.4.2.6.9)	0 = FALSE 1 = TRUE
12	Result of $\beta_{sopaque}$(8.5/11μm) and Water Vapor Ice Cloud LRC-only (BOWVIC-LRC) Test (see Section 3.4.2.6.10)	0 = FALSE 1 = TRUE
13	Result of $\beta_{sopaque}$(8.5/11μm) Opaque Ice Cloud (BOIC) Test (see Section 3.4.2.6.11)	0 = FALSE 1 = TRUE
14	Result of β_{stropo}(8.5/11μm) and Water Vapor Ice Cloud (BTWVIC) Test (see Section 3.4.2.6.12)	0 = FALSE 1 = TRUE
15	Result of Overall Ice Cloud (OIC) Test (see Section 3.4.2.6.13)	0 = FALSE 1 = TRUE
16	Result of Sub-classify Ice Cloud (SCIC) Test (see Section 3.4.2.6.14)	0 = FALSE 1 = TRUE

17	Result of Mixed Phase (MP) Test (see Section 3.4.2.6.15)	0 = FALSE 1 = TRUE
18	Result of Supercooled Liquid Water (SLW) Test (see Section 3.4.2.6.16)	0 = FALSE 1 = TRUE
19-22	Pixel cloud type result prior to applying the median filter (see Section 3.4.2.7)	See Table 30
23	Same as Bit 4 (BOC Test) substituting: $\beta_{sopaque}(8.5/11\mu m)$ for $\beta_{sopaque}(12/11\mu m)$	0 = FALSE 1 = TRUE
24	Same as Bit 4 (BOC Test) substituting: $\beta_{sopaque}(13/11\mu m)$ for $\beta_{sopaque}(12/11\mu m)$	0 = FALSE 1 = TRUE
25	Same as Bit 5 (OCTD Test) substituting: $T_{opaque}(6.7\mu m)$ for $T_{opaque}(7.4\mu m)$	0 = FALSE 1 = TRUE
26	Same as Bit 7 (WVMD Test) substituting: $\beta_{stropo}(13/11\mu m)$ for $\beta_{stropo}(12/11\mu m)$ $\beta_{mtropo}(13/11\mu m)$ for $\beta_{mtropo}(12/11\mu m)$ $\beta_{mopaque}(13/11\mu m)$ for $\beta_{mopaque}(12/11\mu m)$	0 = FALSE 1 = TRUE
27	Same as Bit 7 (WVMD Test) substituting: $\varepsilon_{stropo}(6.7\mu m)$ for $\varepsilon_{stropo}(7.4\mu m)$ $\beta_{mtropo}(6.7/11\mu m)$ for $\beta_{mtropo}(7.4/11\mu m)$	0 = FALSE 1 = TRUE
28	Same as Bit 7 (WVMD Test) substituting: $\varepsilon_{stropo}(6.7\mu m)$ for $\varepsilon_{stropo}(7.4\mu m)$ $\beta_{mtropo}(6.7/11\mu m)$ for $\beta_{mtropo}(7.4/11\mu m)$ $\beta_{stropo}(13/11\mu m)$ for $\beta_{stropo}(12/11\mu m)$ $\beta_{mtropo}(13/11\mu m)$ for $\beta_{mtropo}(12/11\mu m)$ $\beta_{mopaque}(13/11\mu m)$ for $\beta_{mopaque}(12/11\mu m)$	0 = FALSE 1 = TRUE
29	Same as Bit 8 (IWMD Test) substituting: $\beta_{stropo}(13/11\mu m)$ for $\beta_{stropo}(12/11\mu m)$ $\beta_{mtropo}(13/11\mu m)$ for $\beta_{mtropo}(12/11\mu m)$ $\beta_{mopaque}(13/11\mu m)$ for $\beta_{mopaque}(12/11\mu m)$	0 = FALSE 1 = TRUE
30	Same as Bit 11 (BOWVIC Test) substituting: $\beta_{stropo}(13/11\mu m)$ for $\beta_{stropo}(12/11\mu m)$	0 = FALSE 1 = TRUE
31	Same as Bit 14 (BTWVIC Test) substituting: $\beta_{sopaque}(13/11\mu m)$ for $\beta_{sopaque}(12/11\mu m)$	0 = FALSE 1 = TRUE
32	Same as Bit 12 (BOWVIC-LRC test) substituting: $\beta_{stropo}(13/11\mu m)$ for $\beta_{stropo}(12/11\mu m)$	0 = FALSE 1 = TRUE
33	Used in place of Bit 13 (BOIC Test) if 8.5 μm channel is not available	0 = FALSE 1 = TRUE
34	Used in place of Bit 13 (BOIC Test) if 8.5 μm and 12 μm channels are not available	0 = FALSE 1 = TRUE

3.4.3.4 Product Metadata

A complete and self-contained description of the GOES-R ACT and JRRCT metadata output is listed in Table 34.

Table 34: A complete description of the cloud type/phase metadata output is shown.

Metadata Description
Number of cloud phase categories (5 categories)
Definition of clear cloud phase category
Definition of warm liquid water cloud phase category
Definition of supercooled liquid water cloud phase category
Definition of mixed cloud phase category
Definition of ice cloud phase category
Percent of clear pixels
Percent of warm liquid water cloud pixels
Percent of supercooled liquid water cloud pixels
Percent of mixed phase cloud pixels
Percent of ice phase cloud pixels
Total number of cloudy pixels
Percent of pixels with each QF flag value

3.5 GOES-17 Loop Heat Pipe Anomaly Mitigation

Post-launch testing of GOES-17 revealed an issue with the loop heat pipe (LHP) subsystem responsible for cooling the ABI detectors. The issue results in inadequate cooling of the infrared channel detectors, leading to increased thermal noise and the occasional loss of imagery data. Calibration work has been performed to reduce the impacts created by the cooling issue, but once the focal plane temperature (FPT) exceeds certain channel-specific thresholds the increased striping and noise degrades the data to a point it can no longer be accurately used for product generation (see Figure 14).

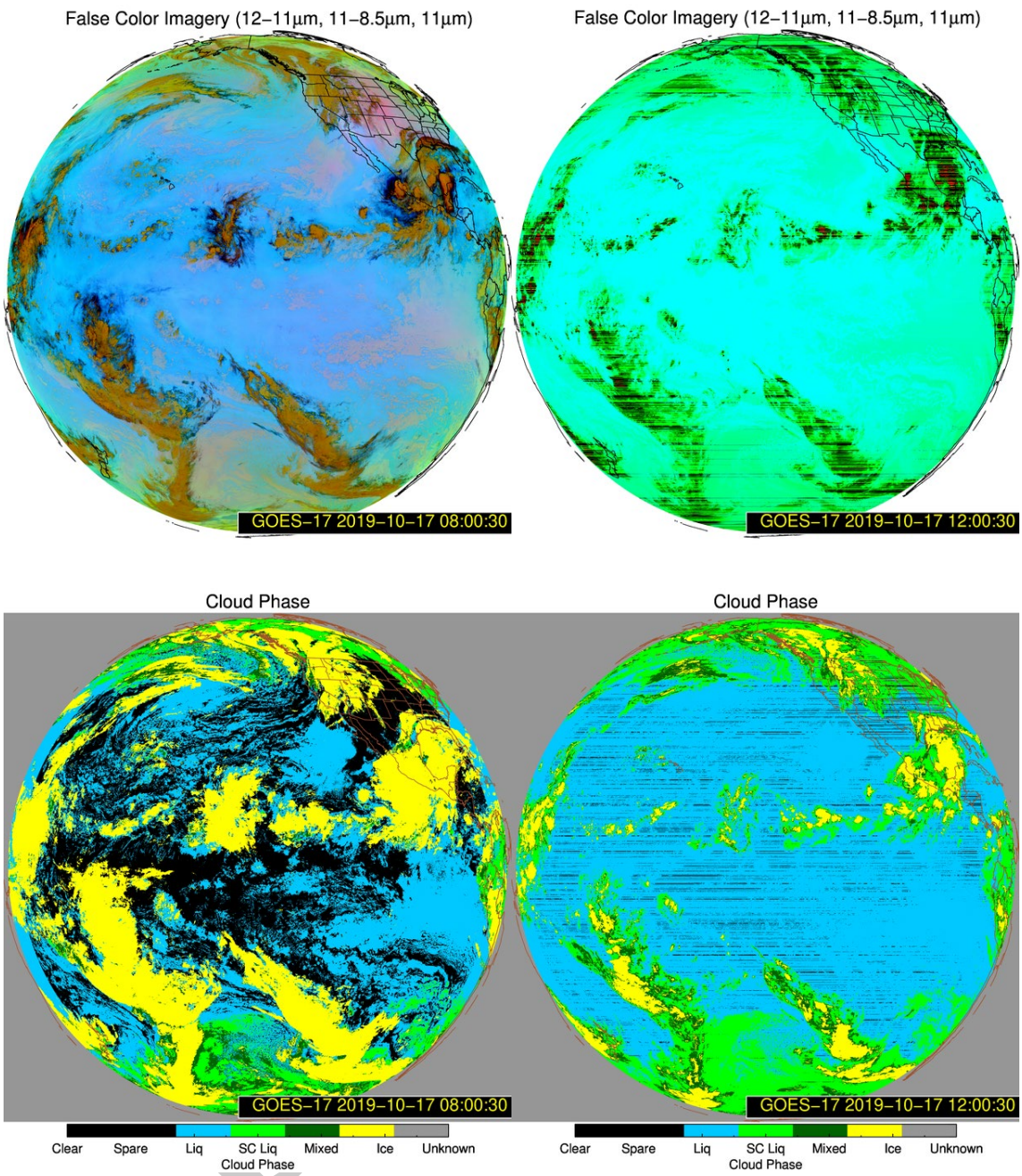

Figure 14 - False color images for GOES-17 on October 17, 2019 at 8:00/12:00 UTC (top left/right respectively) and the corresponding GOES-17 cloud phase products (bottom left/right respectively). The GOES-17 data was not impacted by the LHP anomaly at 8:00 UTC, but severely impacted at 12:00 UTC.

3.5.1 GOES-17 Mitigated Cloud Type/Phase Determination Logic

The ACT algorithm is designed to run using a variety of channel combinations (e.g., ABI channels 10, 11, 14, 15 or VIIRS channels M14, M15, M16). While additional channels

provide useful information, the core channels utilizing the 8.4 μm, 11.2 μm, and 12.3 μm channels are paramount for cloud type/phase determination. When these channels are all available the ACT products are produced using the threshold-based logic described above. If the FPT threshold is exceeded for any of these channels the products will be severely degraded. For this reason, additional channels and logic were incorporated into the ACT algorithm to mitigate product quality issues during periods when the FPT is elevated. Rather than using threshold-based tests, a "naïve" Bayes probabilistic model and classifier approach is used to determine cloud type/phase during the mitigation period and is described in detail below.

3.5.1.1 Channel Checking using Focal Plane Temperature Thresholds

Temperature thresholds for each IR channel were provided by the GOES-R program office as an initial guideline. The complete list of channel-specific FPT thresholds used for the ACT is shown in Table 35.

Table 35: The GOES-17 IR channel focal plane temperature thresholds used for the ACT algorithm.

Band #	Approx. Central Wavelength (μm)	Focal Plane Temperature Threshold (K)
7	3.9	150.0
8	6.2	94.0
9	7.0	94.5
10	7.3	92.0
11	8.4	97.0
12	9.6	90.0
13	10.3	150.0
14	11.2	150.0
15	12.3	92.0
16	13.3	91.0

When the FPT exceeds the threshold for a given channel/channels, those channels, and any cloud type test associated with them, are turned off and not used in the final ACT product determination.

If either the 8.4 μm or 12.3 μm channels are unavailable, the ACT product quality may become severely degraded and undependable. For this reason a naïve Bayesian mitigation logic is used in lieu of the threshold-based approach. The naïve Bayesian mitigation logic utilizes ABI channels 7 (3.9 μm), 13 (10.3 μm) and 14 (11.2 μm) and is meant to reduce product degradation when the 8.4 μm or 12.3 μm channels are unreliable. All of the IR channels are impacted by the LHP issue, however, ABI channels 13 (10.3 μm) and 14 (11.2 μm) are important components to the mitigation logic explained below. To ensure

these channels are available throughout the mitigation period the FPT thresholds defined in the ACT algorithm for these channels were increased to 150K, a temperature the FPT should never exceed.

3.5.1.2 Naïve Bayes Probabilistic Model

Wilks (2006) and Kossin and Sitkowski (2008) provide detailed descriptions of Bayes' theorem along with examples of how it can be used for meteorological applications. The discussion herein summarizes the description of the naïve Bayesian probabilistic model from Kossin and Sitkowski (2008).

The Bayes' model returns a conditional probability that an "event" will occur given a set of measureable features (classifiers), and can be described by the following equation.

$$P(C_{yes} \mid F) = \frac{P(C_{yes})P(F \mid C_{yes})}{P(F)} \qquad \text{(Eq. 15)}$$

The term $P(C_{yes})$ is the probability that the event will occur given no measured features. For a meteorological application this can be represented by a climatological probability that the event occurs. $P(F \mid C_{yes})$ represents the conditional probability that the set of features are observed given the event occurs and $P(F)$ is the probability that the set of features are observed independent of event occurrence. The conditional probabilities $P(F \mid C_{yes})$, and its counterpart $P(F \mid C_{no})$, are obtained by training the model using known data. A problem that arises with this method is that even with a relatively small number of features the calculations can become very computationally expensive, growing exponentially with respect to the number of features used. A way around this issue is to make a reasonable assumption that all the features are independent of one another. This assumption produces the "naïve" aspect of the Bayes' classifier (Kossin and Sitkowski 2008). With this assumption the term $P(F \mid C_{yes})$ can be represented by $\prod_{i=1}^{N} P(F_i \mid C_{yes})$ where F_i is a single feature of the set F and equation 15 can be written as

$$P(C_{yes} \mid F) = \frac{P(C_{yes})\prod_{i=1}^{N} P(F_i \mid C_{yes})}{P(F)} \qquad \text{(Eq. 16)}$$

Due to the relationship $P(C_{yes} \mid F) + P(C_{no} \mid F) = 1$ the denominator in equation 16 can be rewritten as

$$P(F) = P(C_{yes})\prod_{i=1}^{N} P(F_i \mid C_{yes}) + P(C_{no})\prod_{i=1}^{N} P(F_i \mid C_{no}) \qquad \text{(Eq. 17)}$$

These equations now represent a more computationally friendly model initially described by equation 15.

For the ACT algorithm the "event" in the naïve Bayesian model is that ice cloud is present at a given satellite pixel determined using the following features:

- 10.3 μm and 11.2 μm single layer troposphere emissivity ($\varepsilon_{stropo}(10\mu m)$, $\varepsilon_{stropo}(11\mu m)$)
- 3.9 μm pseudo-emissivity calculated with the 10.3 μm and 11.2 μm BT ($\varepsilon_{pseudo}(3.9{,}10\mu m)$, $\varepsilon_{pseudo}(3.9{,}11\mu m)$)
- 10.3/11.2 μm beta ratios ($\beta_{stropo}(10/11\mu m)$, $\beta_{mtropo}(10/11\mu m)$, $\beta_{sopaque}(10/11\mu m)$, $\beta_{mopaque}(10/11\mu m)$)

Additional details of how these features are trained and used in the naïve Bayesian model are described in the next few sections.

3.5.1.3 Training the Naïve Bayesian Features

The data set used to train the Bayesian model was created by manually analyzing 12 GOES-16 full disk scenes from August 18, 2018 and separately labeling pixels determined, with high confidence, as "ice" or "liquid" cloud. Approximately 50 million pixels were labeled over land and water covering all solar viewing angles. Using this "truth" data set the conditional probabilities were calculated for a unique set of features and stored in easily accessible look-up tables (LUTs).

The climatological probability was not calculated using this training data. Due to the nature of the manual training, only pixels that were confidently determined to be ice or liquid phase were labeled. A large number of pixels containing clear sky or unknown cloud phase were not labeled. For this reason, along with the fact that only a single day was manually trained, it is not accurate to calculate a climatological probability using this data set. The climatological probability of ice clouds was instead estimated by tracking the distribution of the full-disk GOES-16 cloud phase product over a 6-month period from June 1, 2017 to November 24, 2017 (see Figure 15).

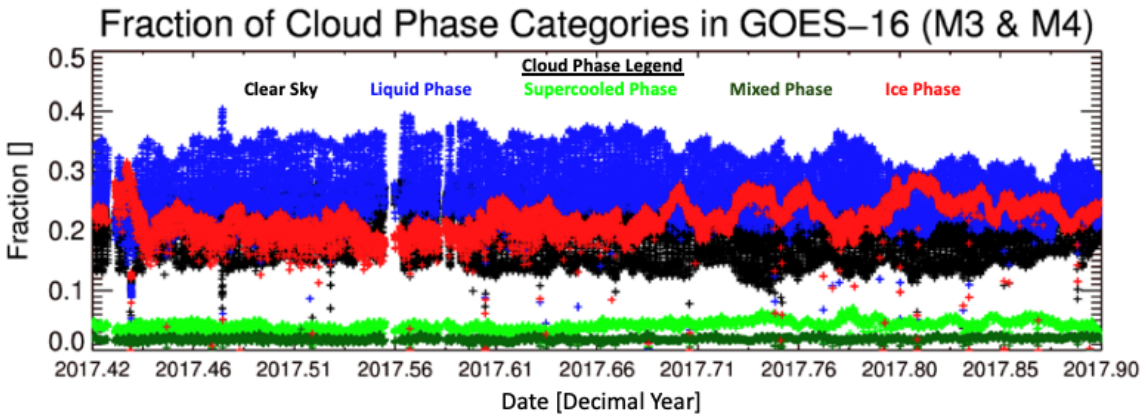

Figure 15 – Time series of the ACT cloud phase fraction from GOES-16 full-disk data from June 1, 2017 – November 24, 2017. The red data points represent the fraction of ice clouds

Analysis of the GOES-16 cloud phase time series shows ice clouds were detected for ~25% of full-disk pixels throughout the 6-month period. This time series is a better representation of the climatological record than the limited manually-labeled training data set so the climatological probability of ice clouds used for Bayesian model was set to 25%. This value may require future tuning.

3.5.1.3.1 10.3/11.2 μm Single Layer Troposphere Emissivity

The calculation of the 10.3 μm and 11.2 μm single layer tropopause emissivity is described in detail in section 3.4.2.1.1. This is primarily used to provide information on the cloud optical depth. Figure 16 shows an example distribution of each emissivity determined using the manually-labeled GOES-16 training data set for pixels over water. This parameter is used in combination with each of the 3.9μm pseudo-emissivity and 10/11μm Beta ratio parameters to create 2-dimensional conditional probabilities of the presence of ice clouds for a given satellite pixel.

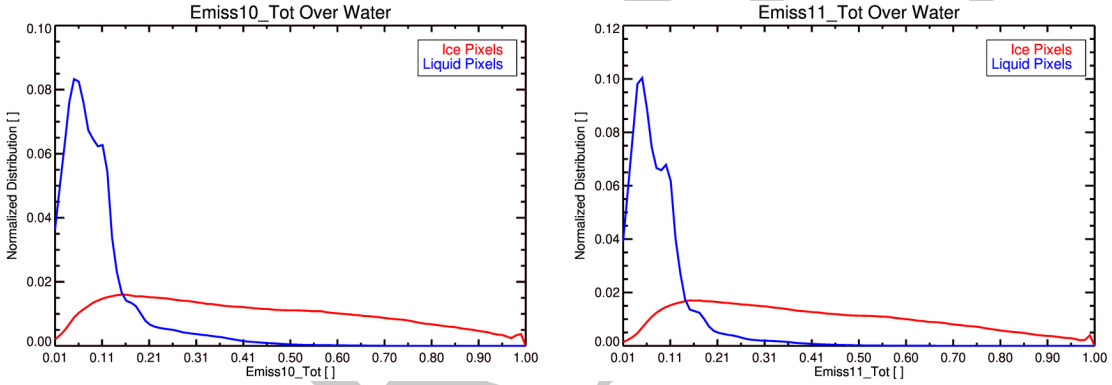

Figure 16 - Distribution of the 10.3 μm (left) and 11.2 μm (right) single layer tropopause emissivity for liquid and ice pixels determined by a manually-labeled GOES-16 training data set.

3.5.1.3.2 3.9 μm Pseudo-Emissivity

The 3.9 μm pseudo-emissivity is calculated as the ratio of the observed 3.9 μm radiance and the 3.9 μm blackbody radiance calculated using the 10 μm (ABI channel 13) or 11 μm (ABI channel 14) brightness temperature. This parameter has previously been used by Pavolonis and Heidinger (2004) to determine cloud phase at night. The 3.9 μm pseudo-emissivity is not used for daytime pixels due to the influence of reflected solar radiation. Figure 17 shows an example distribution of each pseudo-emissivity determined using the manually-labeled GOES-16 training data set for pixels over water. Ice clouds generally have higher 3.9 μm pseudo-emissivity values than clouds composed of liquid water so this relationship is used to help differentiate cloud phase.

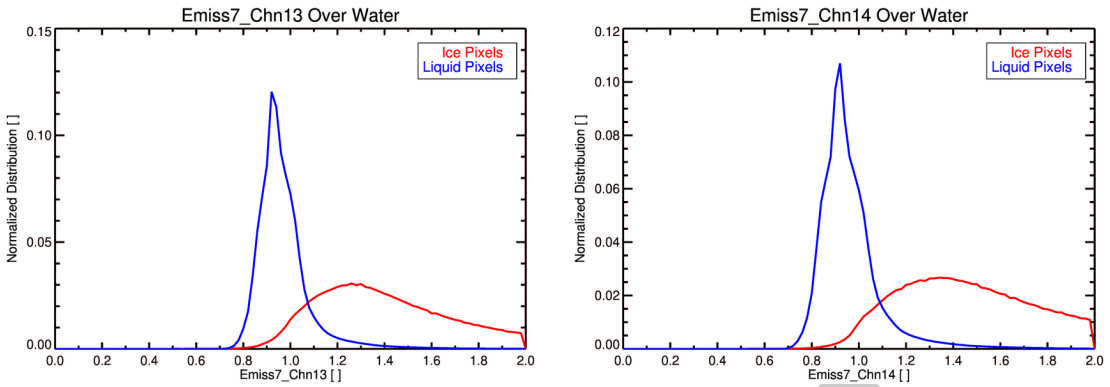

Figure 17 - Distribution of the 3.9 µm pseudo-emissivity calculated using the 10.3 µm (left) and 11.2 µm (right) BT for liquid and ice pixels determined by a manually-labeled GOES-16 training data set.

3.5.1.3.3 10.3/11.2 µm Beta Ratios

The relationship between the 8.4/11 µm channels provides the best information about cloud phase. However, the 8.4 µm channel is also highly susceptible to contamination due to the LHP anomaly. The goal of the mitigation work is to improve the cloud phase discrimination using channels that are less-severely impacted by the LHP anomaly. For this reason, the 10.3 µm channel is substituted in place of the 8.4 µm channel. While not as robust as the $\beta(8.4/11\mu m)$, the $\beta(10/11\mu m)$ still provides useful information to help determine cloud phase. The calculations of the 10.3/11.2 µm Beta ratios using the single/multi-layer tropopause/opaque assumptions are described in detail in section 3.4.2.1. Figure 18 shows an example distribution of each $\beta(10/11\mu m)$ determined using the manually-labeled GOES-16 training data set for pixels over water. The distributions show that ice clouds tend to have higher $\beta(10/11\mu m)$ values than liquid water clouds. This relationship is used to help determine cloud phase.

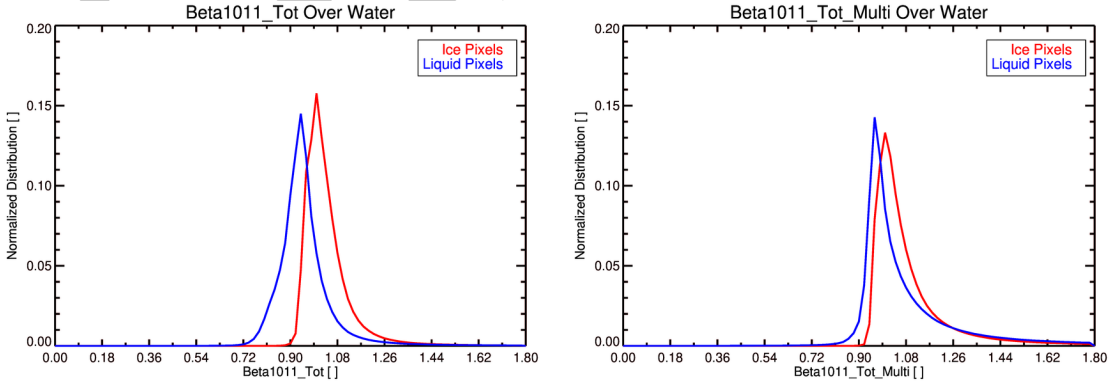

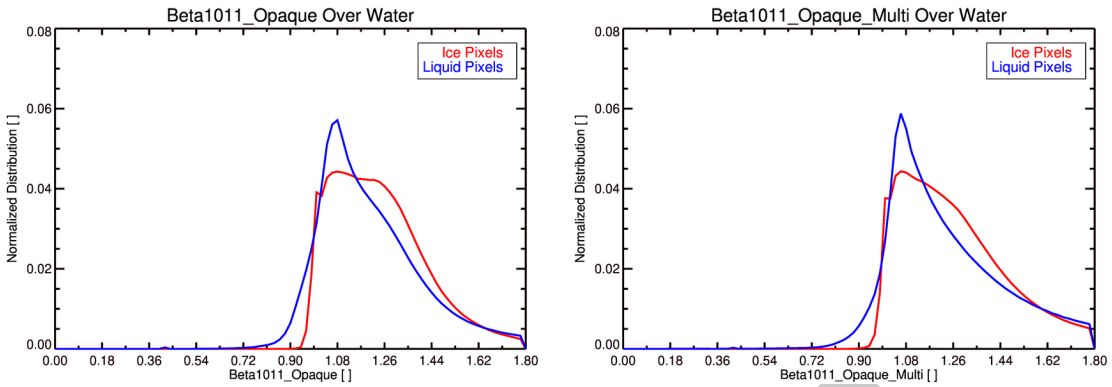

Figure 18 - Distribution of the 10.3/11.2 μm Beta ratios calculated using the single-layer tropopause (top left), multi-layer tropopause (top right), single-layer opaque (bottom left) and multi-layer opaque (bottom right) assumptions for liquid and ice pixels determined by a manually-labeled GOES-16 training data set.

3.5.1.4 Calculating the Bayesian Probability of Ice Clouds

To calculate the Bayesian ice cloud probability, LUTs are trained by computing the conditional probabilities that a unique set of features are observed when either ice or liquid cloud pixels are present (determined using the manually-labeled GOES-16 training data). The following 6 unique sets of features are used for the GOES-17 Bayesian mitigation logic:

1. $\varepsilon_{stropo}(10\mu m)$ and $\varepsilon_{pseudo}(3.9{,}10\mu m)$ - *night pixels only*
2. $\varepsilon_{stropo}(11\mu m)$ and $\varepsilon_{pseudo}(3.9{,}11\mu m)$ - *night pixels only*
3. $\varepsilon_{stropo}(10\mu m)$ and $\beta_{stropo}(10/11\mu m)$
4. $\varepsilon_{stropo}(10\mu m)$ and $\beta_{mtropo}(10/11\mu m)$
5. $\varepsilon_{stropo}(10\mu m)$ and $\beta_{sopaque}(10/11\mu m)$
6. $\varepsilon_{stropo}(10\mu m)$ and $\beta_{mopaque}(10/11\mu m)$

The first two LUTs listed above containing the $\varepsilon_{pseudo}(3.9{,}10\mu m)$ and $\varepsilon_{pseudo}(3.9{,}11\mu m)$ were trained using night pixels only. The other 4 feature sets are independent of solar orientation and were trained using both day and night pixels. The conditional probabilities for each set are also calculated and stored for land and water pixels separately. It is difficult to comprehend the influences by visualizing the conditional probabilities alone as their impacts only become sensible when combined by the Bayesian model. However, due to the nature of the naïve Bayesian equation, the ratio of the ice/no ice conditional probabilities will generally provide insight to regions of the LUTs that are associated with higher probabilities. The conditional probability ratios for the 2-dimensional LUTs created using the single layer tropopause emissivity along with the 3.9 μm pseudo-emissivity and 10/11 μm beta ratio parameters, over water, are shown in Figure 19 and Figure 20 respectively.

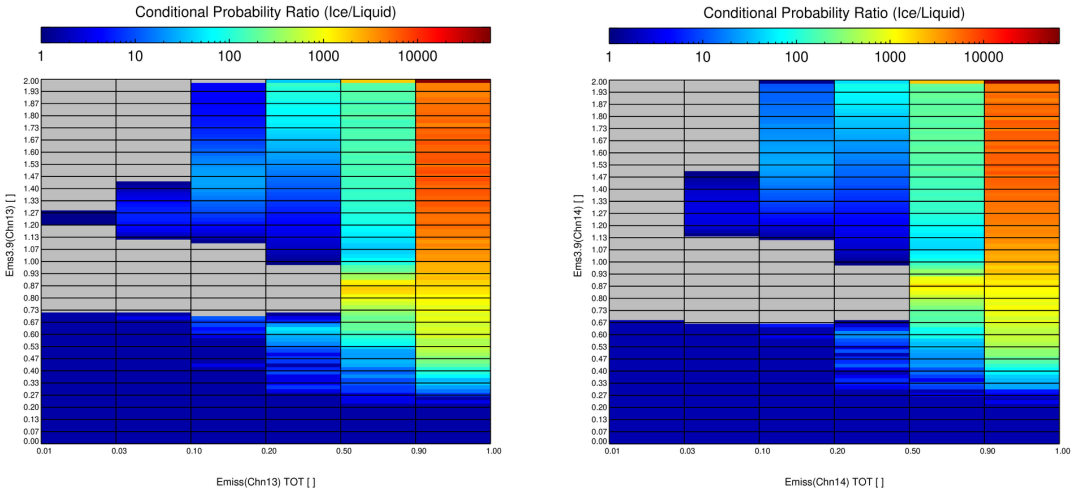

Figure 19 – Ratio of the ice/liquid conditional probabilities pertaining to the $[\varepsilon_{stropo}(10\mu m), \varepsilon_{pseudo}(3.9, 10\mu m)]$ (left) and $[\varepsilon_{stropo}(11\mu m), \varepsilon_{pseudo}(3.9, 11\mu m)]$ (right) LUTs for pixels over water. All bins contain ratio values greater than 0.0 with bin values less than 1.0 shaded gray.

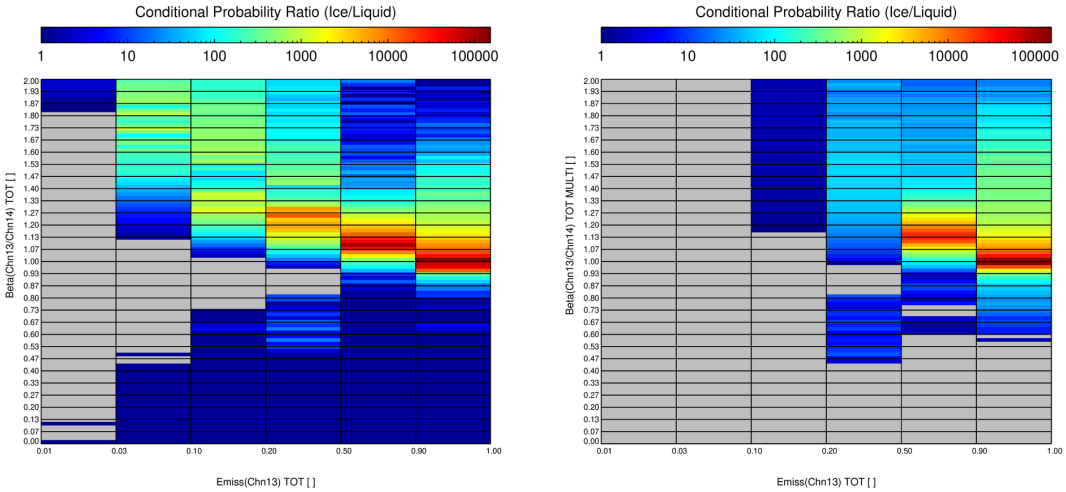

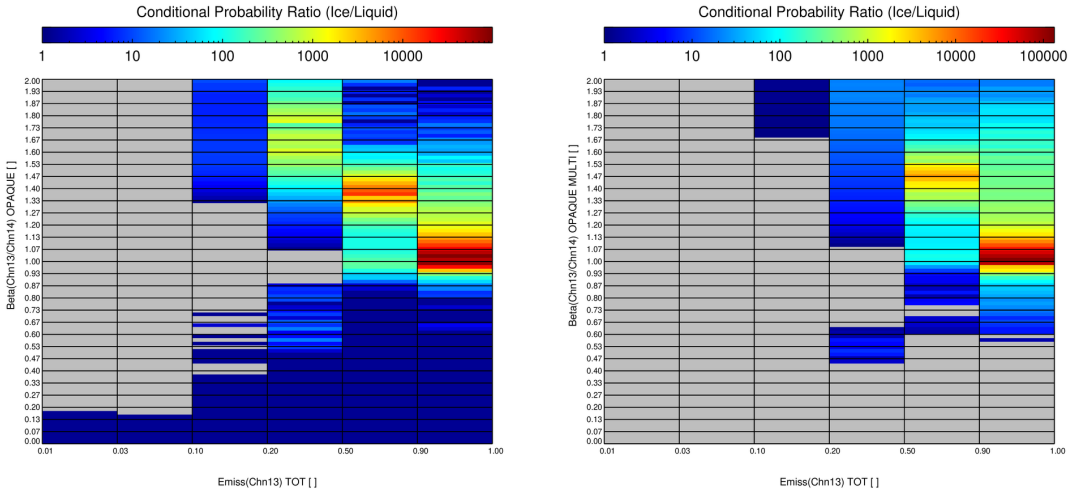

Figure 20 - Ratio of the ice/liquid conditional probabilities pertaining to the $[\varepsilon_{stropo}(10\mu m), \beta_{stropo}(10/11\mu m)]$ (top left), $[\varepsilon_{stropo}(10\mu m), \beta_{mtropo}(10/11\mu m)]$ (top right), $[\varepsilon_{stropo}(10\mu m), \beta_{sopaque}(10/11\mu m)]$ (bottom left) and $[\varepsilon_{stropo}(10\mu m), \beta_{mopaque}(10/11\mu m)]$ (bottom right) LUTs for pixels over water. All bins contain ratio values greater than 0.0 with bin values less than 1.0 shaded gray.

The colors in the conditional probability ratio images above relate to areas in the LUTs that are generally associated with higher or lower overall Bayesian ice probability. Bins shaded toward the dark red spectrum contain higher ratio values and are usually indicative of higher probabilities. Bins shaded toward the dark blue spectrum contain ratios ~1.0 and are more neutral. Gray-shaded bins contain ratios less than 1.0 and are usually associated with lower overall probability of ice.

The conditional probability LUTs and climatological probabilities are stored in a NetCDF file. The ACT algorithm reads this information into memory on the first scanline segment to produce the Bayesian probability that an ice cloud is present when the GOES-17 mitigation logic is necessary.

The Bayesian ice cloud probability is calculated using the naïve Bayesian model and LUTs described above. For daytime pixels, only the 4 sets of LUTs that include the 10.3/11.2 μm Beta ratio parameters are used. For nighttime pixels, the LUT containing the $\varepsilon_{stropo}(10\mu m)$ and $\varepsilon_{pseudo}(3.9,10\mu m)$ is also included. An example of the Bayesian ice cloud probability output for a nighttime GOES-17 CONUS scene is shown in Figure 21.

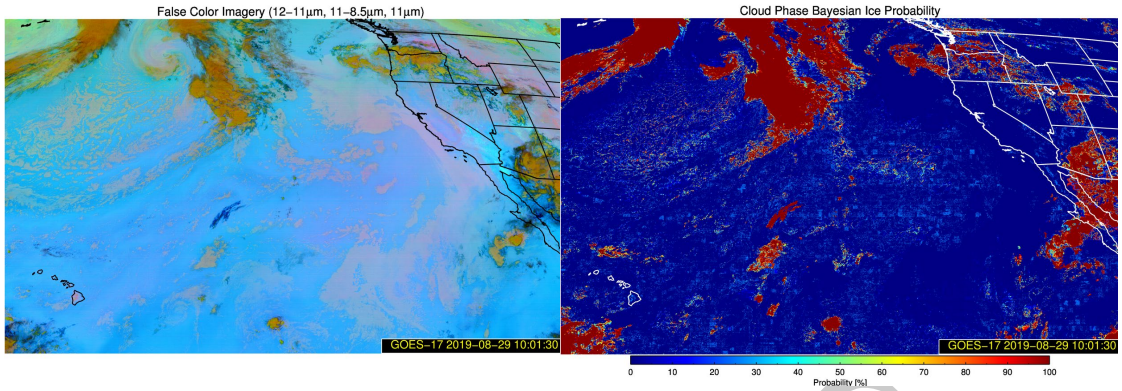

Figure 21 – False color image (left) and Bayesian ice cloud probability (right) for the GOES-17 CONUS domain on August 29, 2019 at 10:01 UTC.

In the false color image above, ice clouds appear dark blue or gold in color, liquid water clouds appear light yellow or pink and clear sky appears light blue. The higher Bayesian ice cloud probabilities in Figure 21 correspond well to where ice clouds are present in the false color image. The probabilities are significantly lower where liquid clouds or clear sky are present.

If for any reason the 10.3 μm channel (ABI channel 13) is missing (e.g., channel data outage), the LUT containing the $\varepsilon_{stropo}(11\mu m)$ and $\varepsilon_{pseudo}(3.9{,}11\mu m)$ can be substituted. In this case, the four $\beta(10/11\mu m)$ ratio parameters would also be unavailable so the Bayesian ice cloud probability would be calculated using the single LUT for nighttime pixels only.

3.5.1.5 Determining Cloud Type from Bayesian Ice Probability

Once the Bayesian probability of ice is calculated the Bayes cloud type is determined using a simple decision tree shown in Figure 22.

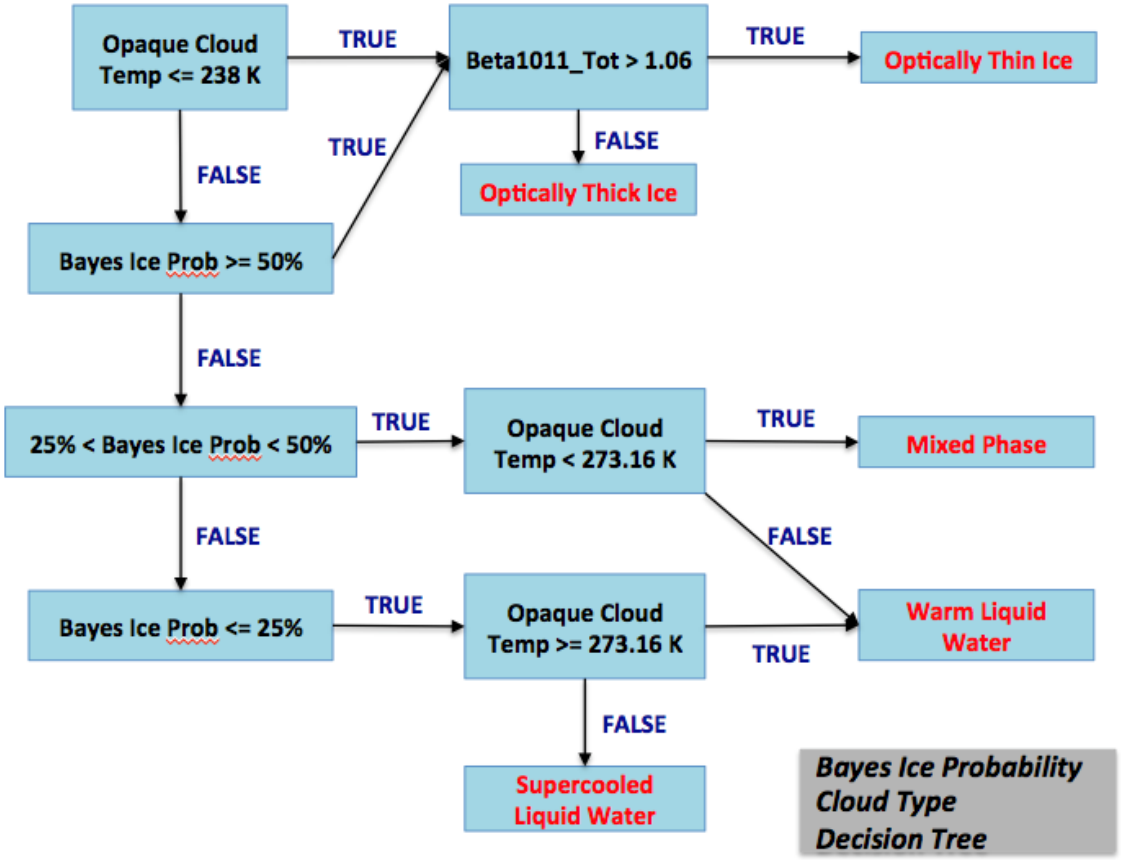

Figure 22: A flow chart of the decision tree used to determine cloud type during the GOES-17 FPT mitigation period using the calculated Bayesian ice probability.

The Bayes cloud phase categories are derived directly from the Bayes cloud type categories as described in section 3.4.2.8. The Bayesian ice cloud probability thresholds used in the decision tree were determined using manual analysis and may require future tuning. An example of the cloud type and cloud phase products produced from the Bayesian ice probabilities is shown in Figure 23.

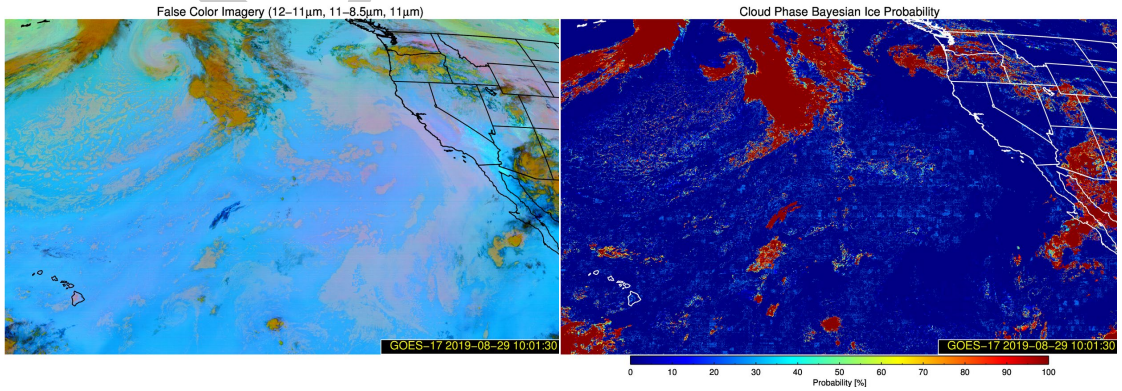

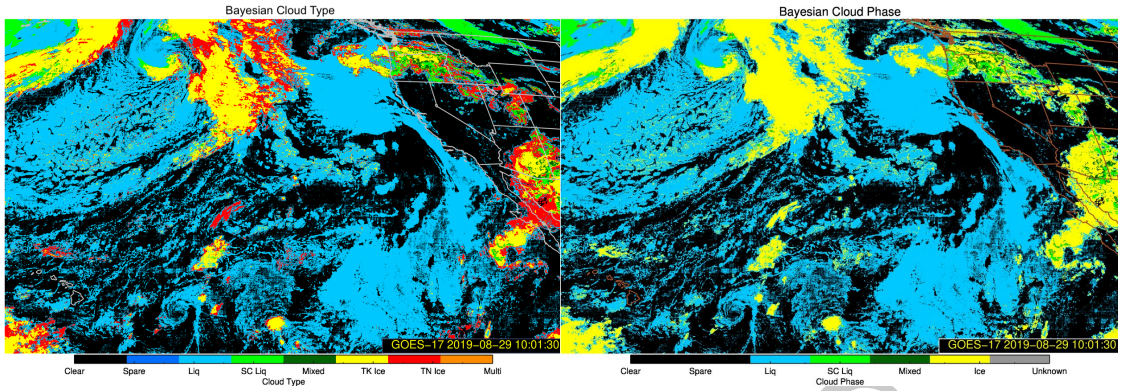

Figure 23 - False color image (top left), Bayesian ice cloud probability (top right), cloud type (bottom left) and cloud phase (bottom right) for the GOES-17 CONUS domain on August 29, 2019 at 10:01 UTC. The cloud type and cloud phase products were both generated using the Bayesian ice cloud probability.

3.5.2 GOES-17 Mitigated Cloud Phase Comparison to GOES-16

GOES-16 is not impacted by the same LHP anomaly on GOES-17 and can therefore be used as a baseline to compare the ACT products. To assess the impact of the GOES-17 LHP mitigation, the cloud phase products produced for GOES-17, both with and without the mitigation logic, were compared to the GOES-16 cloud phase product. There is a small region off the west coast of Central America where both the GOES-16 and GOES-17 full-disk domains overlap where the products can be directly compared (see Figure 24).

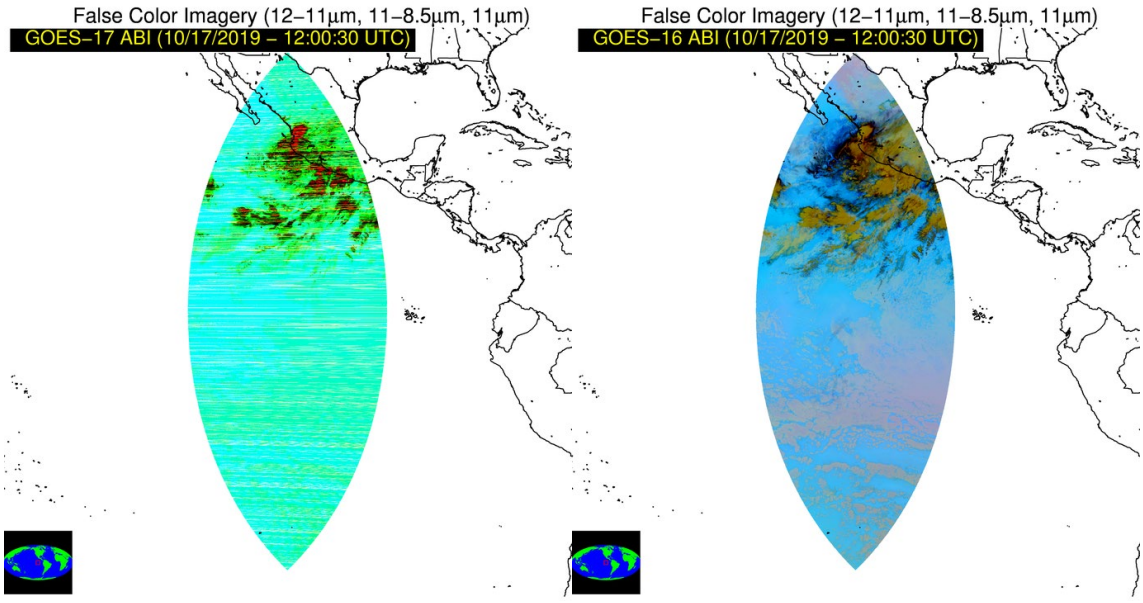

Figure 24 – False color images for GOES-17 (left) and GOES-16 (right) on October 17, 2019 at 12:00 UTC where the full-disk domains overlap and satellite viewing angles are less than 50º. The GOES-17 image is severely degraded due to the LHP anomaly.

A combination of ABI channels 11 (8.5 μm), 14 (11.2 μm) and 15 (13.3 μm) were used to create the false color images in Figure 24. These same channels are vital for the ACT products. When the impacts of the LHP anomaly are nominal, the false color images, and ACT products, created using GOES-17 and GOES-16 data are comparable. However, increased striping and noise caused by the LHP anomaly severely degrades the GOES-17 data and, in turn, the quality of the GOES-17 cloud type/phase products. The GOES-16 and GOES-17 (both with and without mitigation logic) cloud phase products were produced for this scene for qualitative comparison (see Figure 25).

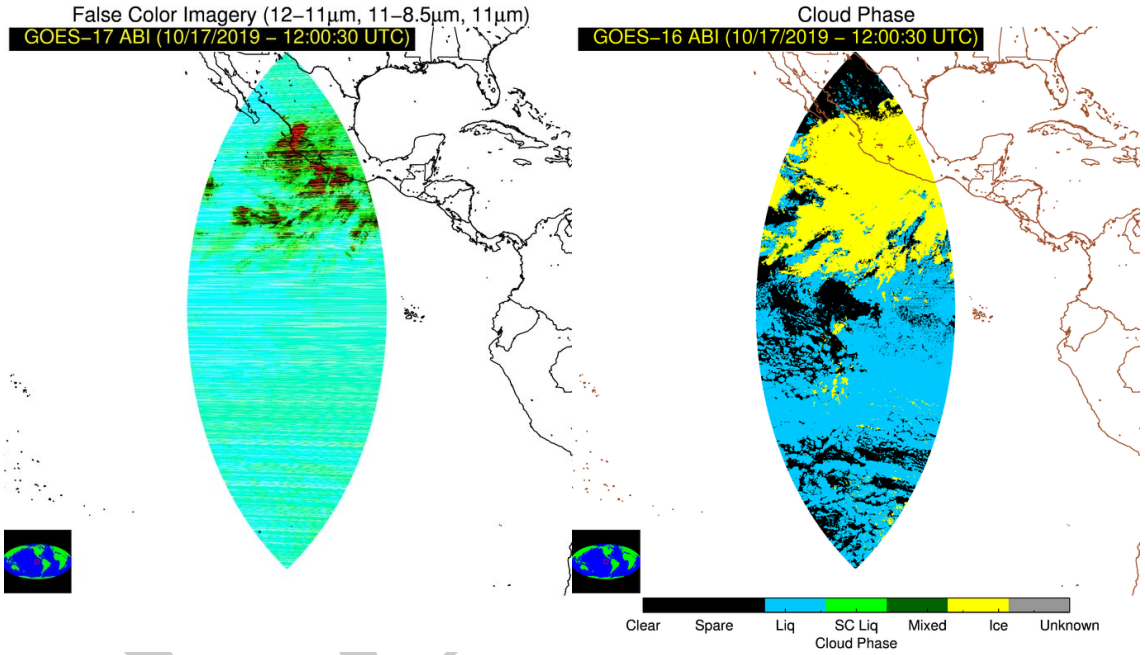

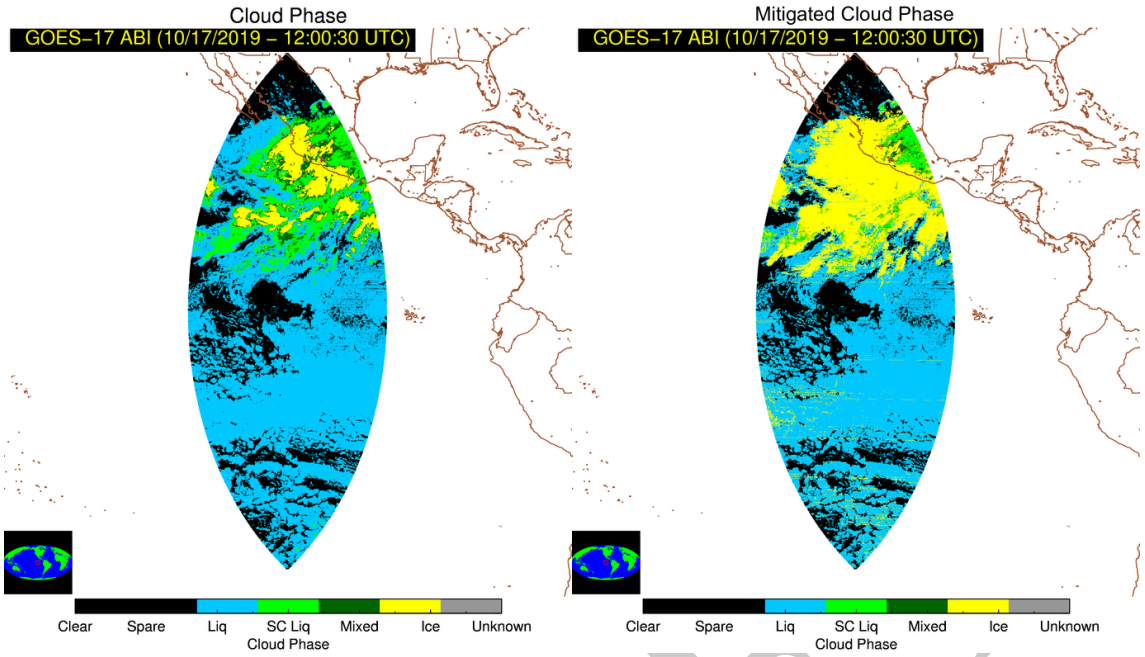

Figure 25 - False color image for GOES-17 (top left), GOES-16 cloud phase (top right), GOES-17 cloud phase produced without mitigation logic (bottom left) and GOES-17 cloud phase produced with mitigation logic (bottom right) on October 17, 2019 at 12:00 UTC where the full-disk domains overlap and satellite viewing angles are less than 50º.

The GOES-17 cloud phase product produced without the mitigation logic is noticeably degraded compared to the GOES-16 cloud phase result. Although liquid clouds appear to be well-determined, ice clouds are significantly under detected. Including the mitigation logic for the GOES-17 cloud phase considerably increases the number of pixels detected as ice clouds, comparing more favorably to the GOES-16 product. The GOES-17 LHP mitigation logic will not perfectly correct all the issues caused by degraded data, however, it will improve the ACT product quality when the level-1 IR data quality is negatively impacted due to the LHP anomaly.

Qualitatively the LHP mitigation logic appears to improve the performance of the GOES-17 cloud phase product. To quantitatively assess the impact, the GOES-16 and GOES-17 cloud phase products were compared to an independent "truth" data set created for a single day on October 17, 2019. The "truth" data was compiled by manually-labeling ice and liquid clouds from GOES-16 imagery (same as the Bayesian classifier training data set) over the GOES-16/17 overlap region. The GOES-16, GOES-17 (unmitigated) and GOES-17 (mitigated) cloud phase products were then each compared to the "truth" data to determine the distribution of detected phase categories where pixels were manually-labeled ice and liquid clouds. To remove impacts of cloud masking the comparison was only performed for pixels where all three cloud phase products indicated clouds and a valid "truth" label of ice or liquid existed. The analysis was split into 2 groups determined by time. The first group compared pixels from times when the GOES-17 data were unaffected by the LHP anomaly (0:00 – 9:00 UTC and 18:00 – 23:00 UTC). The

second group compared pixels from times when the GOES-17 data were degraded (9:00 – 18:00 UTC. The results of these analyses are shown in Table 36 and Table 37.

Table 36 - Collocated GOES-16, GOES-17 (unmitigated) and GOES-17 (mitigated) cloud phase product categories compared to "truth" data composed of manually-labeled ice/liquid cloud pixels from October 17, 2019 between 0-9 UTC and 18-23 UTC, when the GOES-17 data is not impacted by the LHP anomaly.

	Liquid # of pixels (%)	Supercooled # of pixels (%)	Mixed # of pixels (%)	Ice # of pixels (%)	Product Version
"Truth" Ice	1281 (~0%)	73 (~0%)	324 (~0%)	1561067 (99.9%)	GOES-16
	25975 (1.7%)	620 (~0%)	4448 (0.3%)	1531702 (98.0%)	GOES-17
	25975 (1.7%)	620 (~0%)	4448 (0.3%)	1531702 (98.0%)	GOES-17 Mitigated
"Truth" Liquid	2994734 (96.4%)	819 (~0%)	6536 (0.2%)	104346 (3.4%)	GOES-16
	3050347 (98.2%)	2360 (~0%)	6622 (0.2%)	47106 (1.5%)	GOES-17
	3050347 (98.2%)	2360 (~0%)	6622 (0.2%)	47106 (1.5%)	GOES-17 Mitigated

Both the GOES-16 and GOES-17 cloud phase products compared well to the "truth" when the GOES-17 data were not degraded due to the LHP anomaly (see Table 36). The results of the unmitigated and mitigated GOES-17 cloud phase are identical because the mitigation logic is not employed. The GOES-16 cloud phase accurately detected 99.9% and 96.4% of ice and liquid cloud pixels respectively. The GOES-17 cloud phase accurately detected 98.0% and 98.2% of ice and liquid cloud pixels respectively. Small differences between the GOES-16 and GOES-17 cloud phase products are expected, even when the GOES-17 cloud phase products are unimpacted by the LHP anomaly, due to differences in instrument calibration and because parallax error is unaccounted for.

Table 37 – Collocated GOES-16, GOES-17 (unmitigated) and GOES-17 (mitigated) cloud phase product categories compared to "truth" data composed of manually-labeled ice/liquid cloud pixels from October 17, 2019 between 9-18 UTC when the GOES-17 data is degraded by the LHP anomaly.

	Liquid # of pixels (%)	Supercooled # of pixels (%)	Mixed # of pixels (%)	Ice # of pixels (%)	Product Version
"Truth" Ice	1862 (0.2%)	49 (~0%)	139 (~0%)	851694 (99.8%)	GOES-16
	75455 (8.8%)	88700 (10.4%)	88189 (10.3%)	601400 (70.4%)	GOES-17
	24420 (2.9%)	5136 (0.6%)	12039 (1.4%)	811989 (95.1%)	GOES-17 Mitigated
"Truth" Liquid	2303224 (96.9%)	513 (~0%)	4463 (0.2%)	69661 (2.9%)	GOES-16
	2300932 (96.8%)	7433 (0.3%)	4387 (0.2%)	65109 (2.7%)	GOES-17
	2243819 (94.4%)	3860 (0.2%)	3108 (0.1%)	126728 (5.3%)	GOES-17 Mitigated

When the GOES-17 data were degraded by the LHP anomaly the GOES-16 cloud phase performed better than the unmitigated GOES-17 cloud phase product (see Table 37). The GOES-16 cloud phase again compared well to the "truth" data accurately detecting 99.8% of ice pixels and 96.9% of liquid pixels correctly. These results are expectedly consistent with those from Table 36 since GOES-16 is never impacted by the LHP anomaly. The GOES-17 (unmitigated) cloud phase accurately detected 96.8% of liquid pixels, but detected significantly fewer (70.4%) ice pixels. Compared to the unmitigated

phase product, the GOES-17 mitigated cloud phase correctly detected a slightly lower 94.4% of liquid pixels, but was noticeably improved detecting 95.1% of ice pixels.

The qualitative comparison and quantitative assessment above prove the GOES-17 cloud phase product, generated using the Bayesian mitigation logic, compares noticeably better to the GOES-16 cloud phase. Using the GOES-17 LHP mitigation logic when the data is corrupted by the LHP anomaly will not eliminate all negative impacts, however, it will reduce the severity of product quality degradation for the ACT products generated for GOES-17.

4 TEST DATA SETS AND OUTPUTS

4.1 Simulated/Proxy Input Data Sets

The data used to test the ACT algorithm consists of Spinning Enhanced Visible and Infrared Imager (SEVIRI) observations and the data used to test the JRRCT algorithm consists of Suomi NPP VIIRS observations. The cloud phase/type is validated using the CALIOP on-board the CALIPSO satellite. Both of these data sets are briefly described below

4.1.1 SEVIRI and VIIRS Data

SEVIRI provides 11 spectral channels with a spatial resolution of 3 km and provides spatial coverage of the full disk with a temporal resolution of 15 minutes. SEVIRI provides the best source of data currently for testing and developing the ACT. The SEVIRI to ABI channel mapping is shown in Table 38. Figure 26, shown below, is a full-disk SEVIRI image from 12 UTC on November 24, 2006. SEVIRI data are readily available from the University of Wisconsin Space Science and Engineering Center (SSEC) Data Center.

Table 38: The SEVIRI bands used to test the ACT algorithm is shown relative to the corresponding ABI bands.

SEVIRI Band Number	SEVIRI Wavelength Range (μm)	SEVIRI Central Wavelength (μm)	ABI Band Number	ABI Wavelength Range (μm)	ABI Central Wavelength (μm)
6	6.85 – 7.85	7.30	10	7.30 – 7.50	7.40
7	8.30 – 9.10	8.70	11	8.30 – 8.70	8.50
9	9.80 – 11.80	10.80	14	10.80 – 11.60	11.20
10	11.00 – 13.00	12.00	15	11.80 – 12.80	12.30

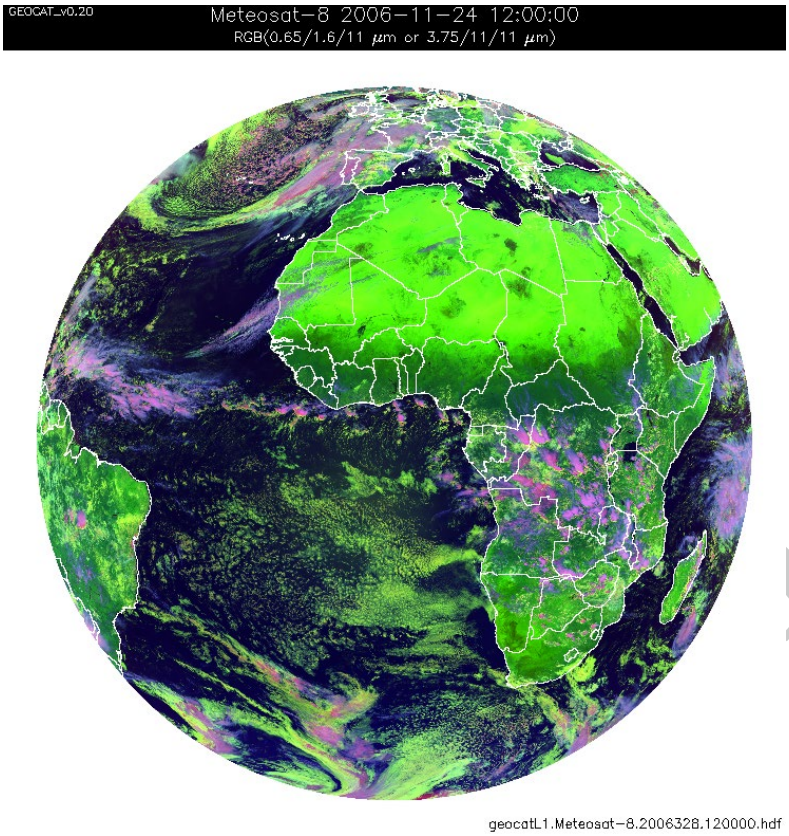

Figure 26: SEVIRI RGB image from 12 UTC on November 24, 2006.

VIIRS provides 16 spectral channels with a moderate spatial resolution of 750 meters and provides daily global spatial coverage of Earth. In addition, there are 5 spectral channels with an imagery spatial resolution of 375 meters and a day-night band. The VIIRS bands used to test the JRRCT algorithm are shown in Table 39.

Table 39: The VIIRS bands used to test the JRRCT algorithm.

VIIRS Band	VIIRS Wavelength Range (μm)	VIIRS Central Wavelength (μm)
M14	8.4 – 8.7	8.55
M15	10.26 – 11.26	10.763
M16	11.54 – 12.49	12.013

4.1.1.1 CALIOP Data

With the launch of the CALIPSO into the Earth Observing System (EOS) A-train in April 2006, the ability to validate satellite-based cloud and aerosol products increased significantly. The CALIOP on-board the CALIPSO satellite is a dual wavelength depolarization lidar. CALIPSO is in an afternoon sun-synchronous low earth orbit. Thus, it can be closely co-located in space and time with the SEVIRI and Suomi NPP

VIIRS at certain times of the day. We primarily use the CALIOP cloud layer product to validate the ACT product and the CALIOP cloud layer and phase products to validate the JRRCT product. The CALIOP vertical cloud boundaries can be combined with co-located NWP temperature profiles to provide a good estimate of cloud top temperature, which can be used to infer cloud top phase for certain temperature ranges. The CALIOP cloud boundaries can also be used to calculate a quality estimate of the true cloud emissivity, as in Heidinger and Pavolonis (2009). The horizontal resolution of the CALIOP cloud layer data used in the validation is 1-km. An example 1-km CALIOP cross section is shown in Figure 27. All of the validation data sources and procedures, including CALIOP, are described in detail the ABI Cloud Products Validation Plan Document.

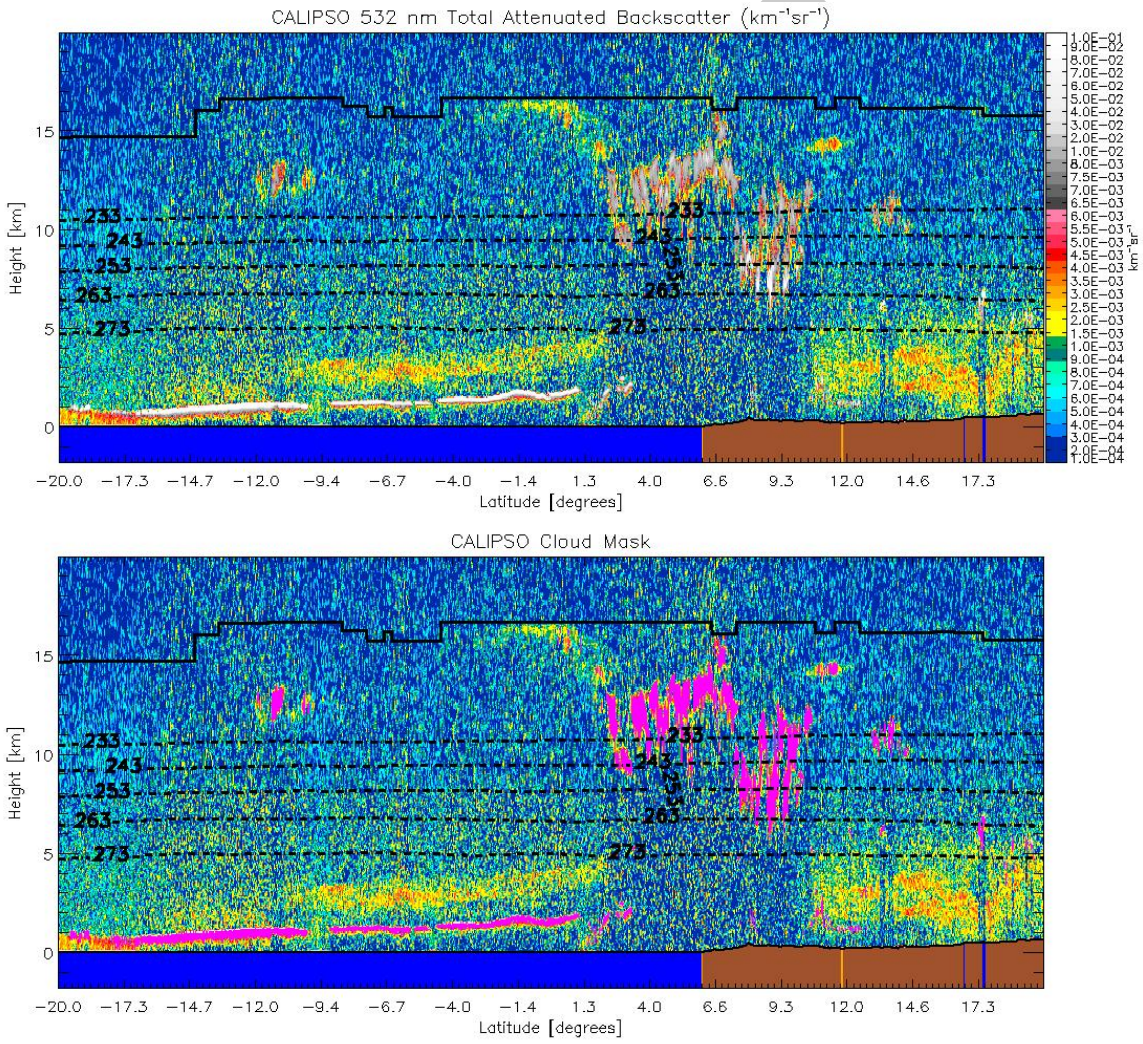

Figure 27: Illustration of the CALIPSO data used in this study. Top image shows a 2d backscatter profile. Bottom image shows the detected cloud layers overlaid onto the backscatter image. Cloud layers are color magenta.

4.2 Output from Simulated/Proxy Inputs Data Sets

The ACT was tested on many SEVIRI full disks. As an example, results from November 25, 2005 at 12 UTC are shown below. A more detailed zoomed in view of a smaller region is also shown. Note that the results match the phase indicated by the false color images well (magenta=ice and yellow=water in the false color imagery). A more quantitative validation is shown in the next section.

As shown at the Test Readiness Review (TRR), the cloud phase and type output from the online (Framework) and offline (Cloud Algorithm Working Group) processing systems match exactly. These tests were conducted under different conditions using the same input for both the online and offline tests.

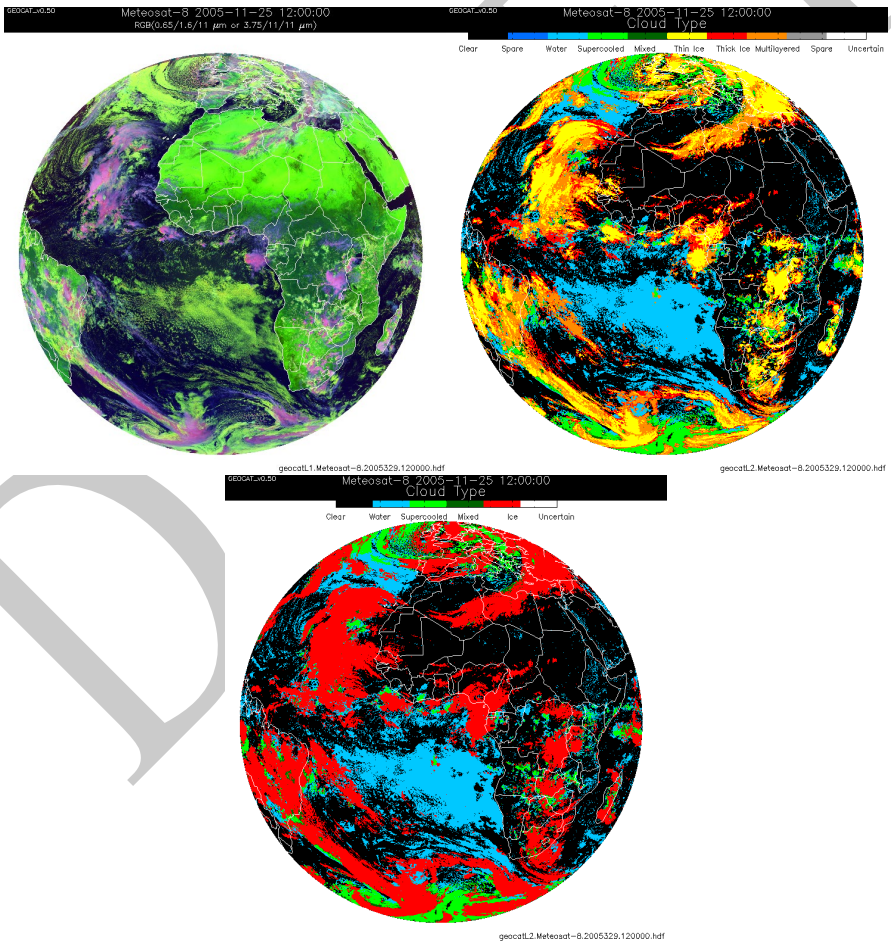

Figure 28: Example results (using SEVIRI) from the ACT algorithm for November 25, 2005. The top, left panel is a RGB false color image and the top, right and bottom, left panels show the cloud type and cloud phase results, respectively.

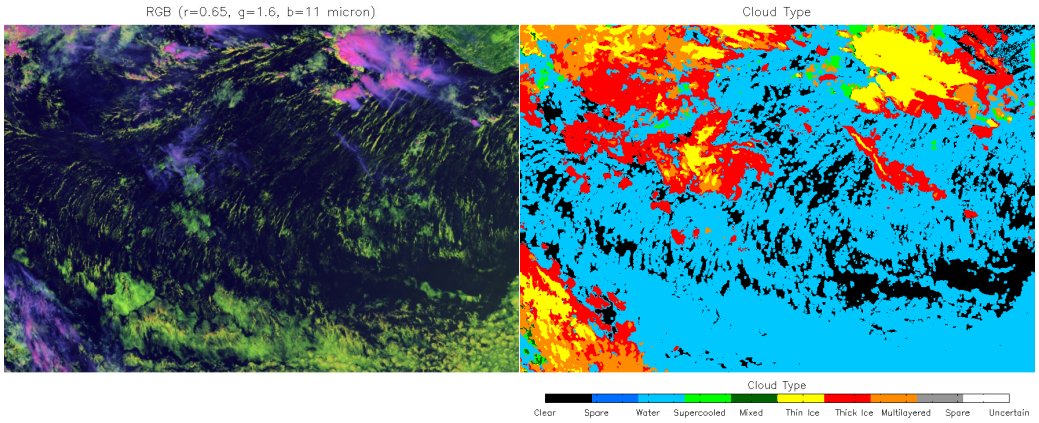

Figure 29: A more detailed look at the cloud type results shown in Figure 28 for a small region near the Ivory Coast of Africa.

Figure 30 shows output from the JRRCT algorithm (bottom panel) from 03:39 UTC on November 10, 2012. The results match the phase indicated by the false color images well (top two panels).

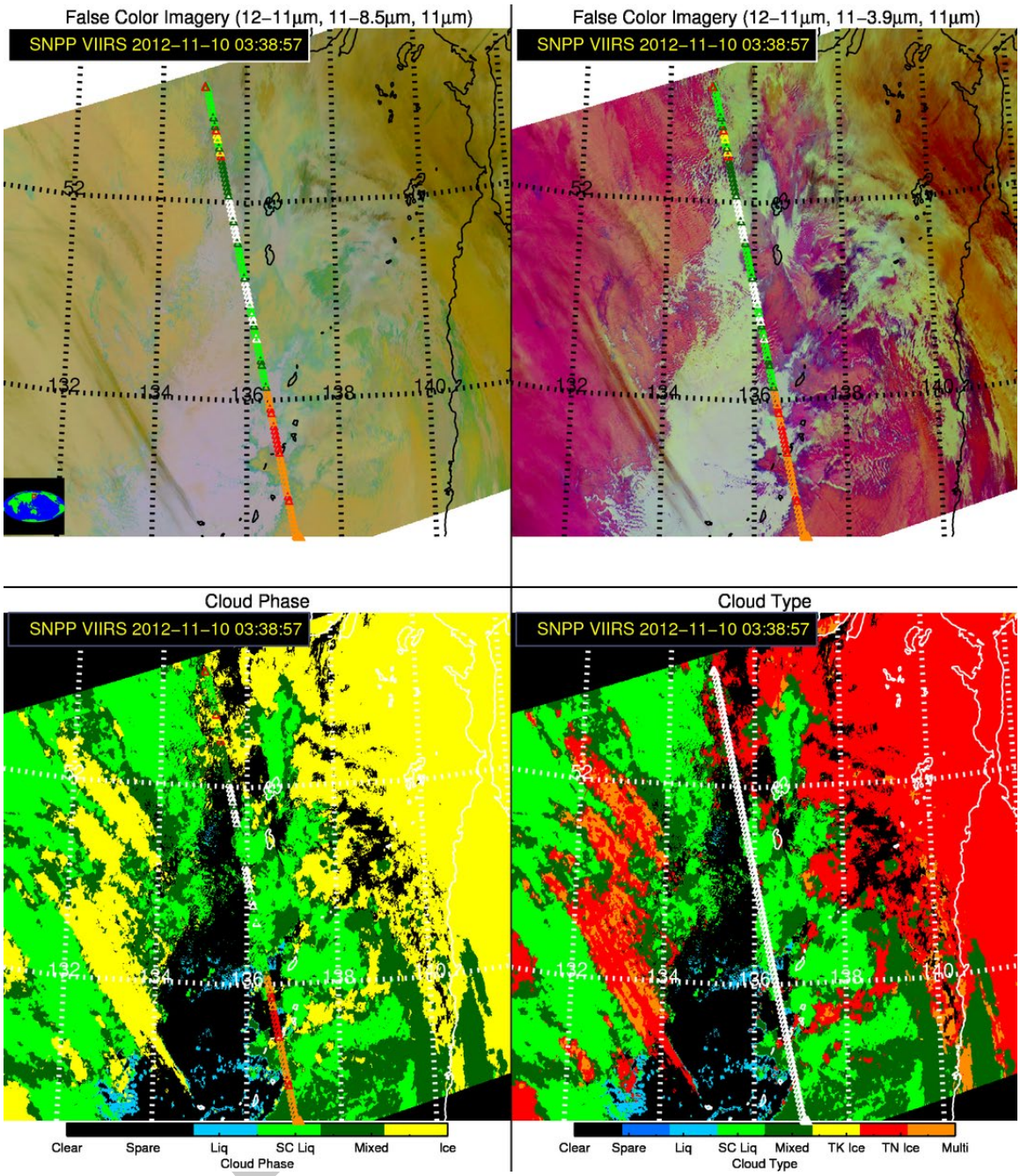

Figure 30: Example cloud top phase and cloud type output are shown for a VIIRS granule over Asia on November 10, 2012 at 03:39 UTC. False color images are shown in the top two panels and the cloud phase (left) and type (right) are shown in the bottom two panels. The CALIPSO ground track is overlaid on each panel.

4.2.1 Precisions and Accuracy Estimates

To estimate the precision and accuracy of the ACT and the JRRCT, comparisons to CALIOP data from the National Aeronautics and Space Agency (NASA) EOS A-train were performed. CALIOP provides unprecedented information on cloud and aerosol

vertical structure and horizontal location on a global scale. While CALIOP provides an unprecedented view of clouds, especially in regards to cloud location (both in the vertical and horizontal), it does not provide a direct measurement of cloud phase. Cloud phase must be retrieved. As discussed in Section 3.4.2.5, the CALIOP cloud phase product at the time of validating the ACT algorithm was not considered to be accurate (Hu et al, 2009). Thus, we decided to mainly focus on using the CALIOP cloud boundaries along with NWP temperature profiles to identify clouds with a cloud top temperature less than 233 K (definite ice clouds) and clouds with a cloud top temperature (T_{cld}) greater than 273 K (definite liquid water clouds). Fundamental thermodynamic and cloud physics theory dictates that liquid water is exceedingly unlikely at temperatures less than 233 K and ice is not possible at temperatures greater than 273 K. In addition, Korolev et al. (2003) sampled a large number of mid-level clouds with aircraft probes and found that for in-cloud temperatures in the 268 – 273 K range, liquid water dominated. Conversely, Korolev et al. (2003) also found that for in-cloud temperatures in the 233 – 238 K range, ice is by far the dominant phase. Given these in-situ observations, the "definite" liquid water phase and "definite" ice phase categories derived from CALIOP are expanded to $T_{cld} \geq 268$ K and $T_{cld} \leq 238$ K, respectively. At the present, potentially mixed phase clouds ($268 \text{ K} < T_{cld} < 238 \text{ K}$) cannot be validated, mainly because of a lack of truth data. As will be shown, potentially mixed phase clouds (when the mixed phase cloud is the highest cloud layer) are not as common as liquid water or ice clouds. As such, even if large errors are assumed, the cloud phase algorithm will meet the accuracy specifications. Nevertheless, future "deep dive" validation efforts will focus on validating potentially mixed phase clouds as CALIOP retrievals improve and as combined CALIOP and CloudSat (spaceborne cloud radar) data products mature.

4.2.2 Error Budget

The ACT was applied to SEVIRI then compared to CALIOP using the cloud top temperature classification discussed in the previous section. The JRRCT was applied to S-NPP VIIRS.

4.2.2.1 Cloud Phase Error Budget

ABI cloud phase validation results are shown in Table 40 and Table 41. Note that the liquid water and supercooled water categories are combined, since differences between the two categories are solely a function of the measured 11-μm brightness temperature. The validation data set consists of 95,000 SEVIRI/CALIOP cloudy match-ups, covering all seasons. Potentially mixed phase clouds are not included in the total error estimate shown in these tables. The impact of errors in the classification of potentially mixed phase clouds will be discussed shortly. The statistics shown in Table 40 includes all clouds detected by the ABI cloud mask, many of which have an optical depth (at visible wavelengths) < 1.0. According to the F&PS, the accuracy specifications (20% error for cloud phase and 40% error for cloud type) only apply to clouds with an optical greater

than 1.0. As the cloud phase validation results show, when potentially mixed phase clouds are not considered, the ABI Cloud Phase comfortably meets the accuracy specification (cloud phase specification: 20% error) without invoking the optical depth qualifier. Note how the liquid water and ice phase categories each meet the accuracy specification when considered alone. Table 41 shows the validation statistics when clouds with an optical depth > 1.0 are filtered out (based on the cloud emissivity calculated using the CALIOP cloud boundaries) per the product accuracy qualifier.

Table 40: ABI cloud phase validation statistics *without* invoking minimum cloud optical depth qualifier are shown. The liquid water and supercooled water categories are combined since differences between the two categories are solely a function of the measured 11-μm brightness temperature. Potentially mixed phase clouds (268 K < T_{cld} < 238 K) are counted in the total statistics.

Category	CALIOP Count	ABI Phase Count	Percent Agree	Percent Disagree
Liquid Water/ Supercooled Water	49,642	44,915	90.48%	9.52%
Potentially Mixed Phase	21,434 (not counted in total)	TBD	TBD	TBD
Ice Phase	45,607	38,693	84.84%	15.16%
Total	**95,249**	**83,608**	**87.78%**	**12.22%**

Table 41: Same as Table 40, except the minimum cloud optical depth qualifier *is* invoked.

Category	CALIOP Count	ABI Phase Count	Percent Agree	Percent Disagree
Liquid Water/ Supercooled Water	34,446	31,105	90.30%	9.70%
Potentially Mixed Phase	13,087 (not counted in total)	TBD	TBD	TBD
Ice Phase	17,597	17,322	98.44%	1.56%
Total	**52,043**	**48,427**	**93.05%**	**6.95%**

The cloud phase errors shown in Table 40 and Table 41 do not include clouds that have a cloud top temperature (T_{cld}) that is 268 K < T_{cld} < 238 K because accurate validation of potentially mixed phase clouds using CALIOP is not possible at this time. In lieu of validating these clouds, we calculated the maximum error in classifying potentially mixed phase clouds that can be tolerated while still meeting the accuracy specification overall. Figure 31 shows the total cloud phase error as a function of the assumed error in classifying potentially mixed phase clouds with and without the minimum cloud optical

depth qualifier. Note in Table 40 and Table 41 that the potentially mixed phase category is the least populated category. Because of this, very large errors in the classification of potentially mixed phase clouds can be tolerated. Figure 31 indicates that errors as large as 54% and 72% can be tolerated **without** and **with** the minimum cloud optical depth qualifier, respectively. While we will strive to validate this category and achieve as much skill as possible, this type of cloud does not pose a serious overall risk.

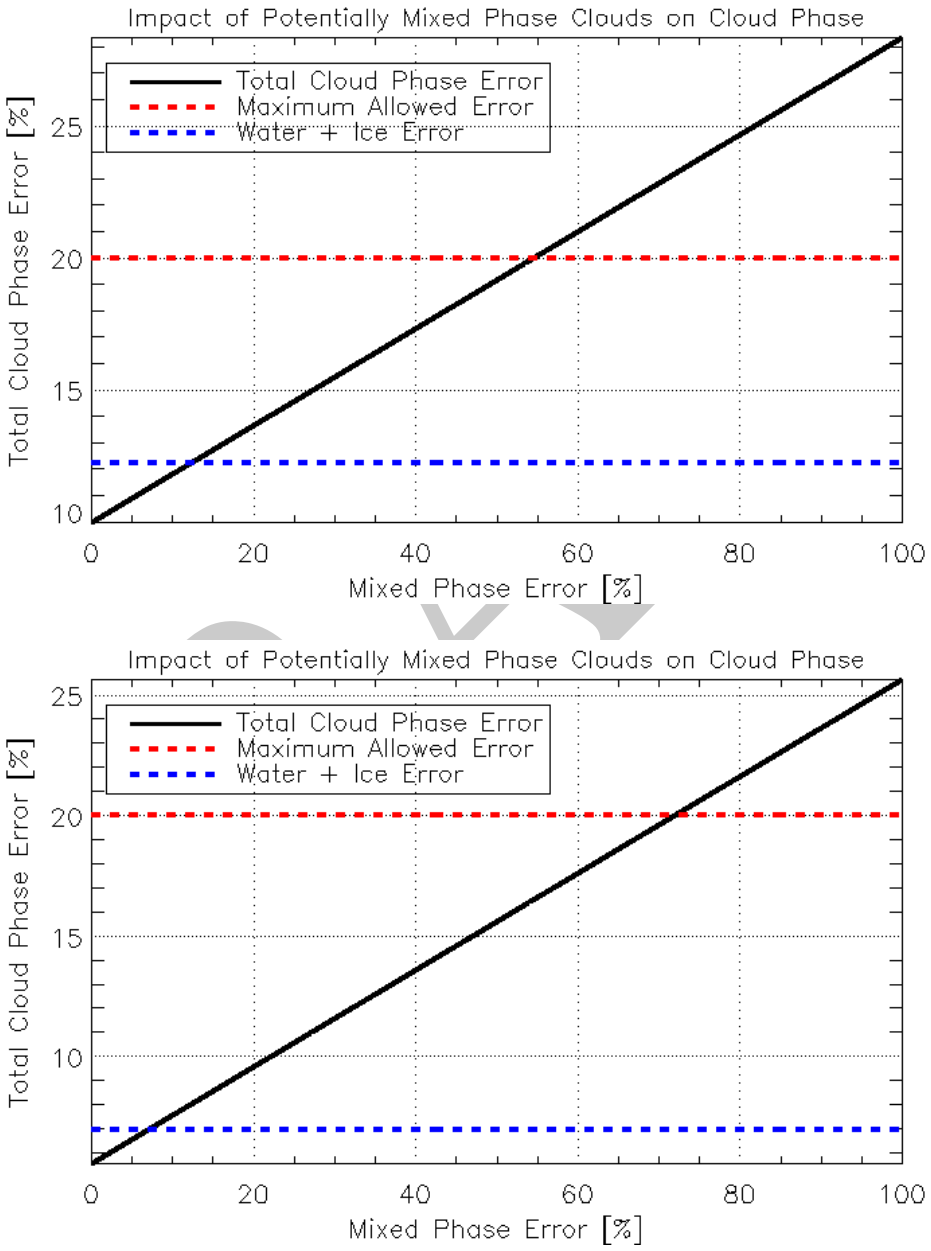

Figure 31: The total cloud phase error as a function of the assumed error in classifying potentially mixed phase clouds is shown when the minimum cloud optical depth qualifier is *ignored* (top) and when it *is* applied (bottom) with the solid black line. The dashed red line is the allowed error from the F&PS. The dashed blue line

is the actual accuracy achieved without including potentially mixed phase clouds in the validation analysis.

The accuracy of the JRRCT was assessed as a function of the CALIOP cloud optical depth and geographic region (including a global assessment). Table 42 below shows that the cloud top phase from the JRRCT comfortably meets the 0.80 accuracy specification.

Table 42: The accuracy of the JRRCT cloud phase product is shown as a function the minimum CALIOP cloud optical depth considered and the geographic region. The numbers in parenthesis indicates the number of data points where the JRRCT and CALIOP agree compared to the total number of VIIRS/CALIOP matchups.

OD	>0.0	>0.1	>0.2	>0.3	>0.4	>0.5	>2.0
All data	0.826 (101144/ 122402)	0.876 (86632/ 98945)	0.882 (78632/ 89122)	0.885 (73889/ 83528)	0.885 (70792/ 79971)	0.885 (68246/ 77090)	0.849 (33375/ 39317)
Day time	0.822 (46123/ 56133)	0.875 (37517/ 42874)	0.881 (33982/ 38585)	0.880 (31653/ 35966)	0.880 (30307/ 34431)	0.880 (29267/ 33240)	0.822 (13703/ 16671)
Night time	0.830 (55021/ 66269)	0.876 (49115/ 56071)	0.884 (44650/ 50537)	0.888 (42236/ 47562)	0.889 (40485/ 45540)	0.889 (38979/ 43850)	0.869 (19672/ 22646)
Over land	0.862 (26242/ 30446)	0.897 (21655/ 24153)	0.904 (19429/ 21487)	0.907 (17766/ 19581)	0.909 (16888/ 18584)	0.910 (16193/ 17796)	0.868 (5999/ 6913)
Over water	0.815 (74902/ 91956)	0.869 (64977/ 74792)	0.875 (59203/ 67635)	0.878 (56123/ 63947)	0.878 (53904/ 61387)	0.878 (52053/ 59294)	0.845 (27376/ 32404)
Lat > 60 deg	0.860 (23218/ 26983)	0.870 (18754/ 21561)	0.873 (17127/ 19612)	0.873 (16046/ 18387)	0.873 (15407/ 17642)	0.872 (14772/ 16949)	0.782 (6264/ 8007)
Lat < 60 deg	0.817 (77926/ 95419)	0.877 (67878/ 77384)	0.885 (61505/ 69510)	0.888 (57843/ 65141)	0.889 (55385/ 62329)	0.889 (53474/ 60141)	0.866 (27111/ 31310)

4.2.2.2 Cloud Type Error Budget

The error budget analysis performed on the cloud phase product was modified slightly and applied to the cloud type product. The only changes made were to break the ice phase category into 3 separate categories, optically thick ice, optically thin ice, and multilayered ice. Single layered ice clouds with an 11-μm (0.65-μm) optical depth of 1.0 (2.0) or less are defined as optically thin clouds. Other single layer ice clouds are classified as optically thick ice clouds. The true 11-μm cloud optical depth is calculated using CALIOP cloud boundaries as explained previously in Section 3.4.2.5. Multilayered ice cloud is defined as a semi-transparent ice cloud that overlaps a lower cloud layer such that a clear sky layer separates the multiple cloud layers. Given these definitions, the cloud type validation statistics are shown in Table 43 and Table 44, **without** and **with** the minimum cloud optical depth qualifier, respectively. The cloud type product comfortably meets the F&PS accuracy specification (cloud type specification: 40% error) when potentially mixed phase clouds are excluded. The maximum error in classifying potentially mixed phase clouds that can be tolerated while

still meeting the cloud type accuracy specification overall is shown in Figure 32 **without** and **with** applying the minimum cloud optical depth qualifier. As was determined for the cloud phase product, errors in classifying potentially mixed phase clouds do not pose a risk to the cloud type product, as the cloud type product will still meet the F&PS accuracy specification even if the error in classifying potentially mixed phase clouds is 100% (when the minimum cloud optical depth qualifier **is** applied).

Table 43: ABI cloud type validation statistics *without* invoking minimum cloud optical depth qualifier are shown. The liquid water and supercooled water categories are combined since differences between the two categories are solely a function of the measured 11-μm brightness temperature. Potentially mixed phase clouds (268 K < T_{cld} < 238 K) are counted in the total statistics.

Category	CALIOP Count	ABI Phase Count	Percent Agree	Percent Disagree
Liquid Water/ Supercooled Water	49,642	44,915	90.48%	9.52%
Potentially Mixed Phase	21,434 (not counted in total)	TBD	TBD	TBD
Optically Thick Ice	5763	4975	86.33%	13.67%
Optically Thin Ice	15,689	9183	58.53%	41.47%
Multilayered Ice	24,155	9570	39.62%	60.38%
Total	**95,249**	**68,643**	**72.07%**	**27.93%**

Table 44: Same as Table 43, except the minimum cloud optical depth qualifier *is* invoked.

Category	CALIOP Count	ABI Phase Count	Percent Agree	Percent Disagree
Liquid Water/ Supercooled Water	34,446	31,105	90.30%	9.70%
Potentially Mixed Phase	13,087 (not counted in total)	TBD	TBD	TBD
Optically Thick Ice	5752	4965	86.32%	13.68%
Optically Thin Ice	5482	2716	49.54%	50.46%
Multilayered Ice	6363	3612	56.77%	43.23%
Total	**52,043**	**42,398**	**81.47%**	**18.53%**

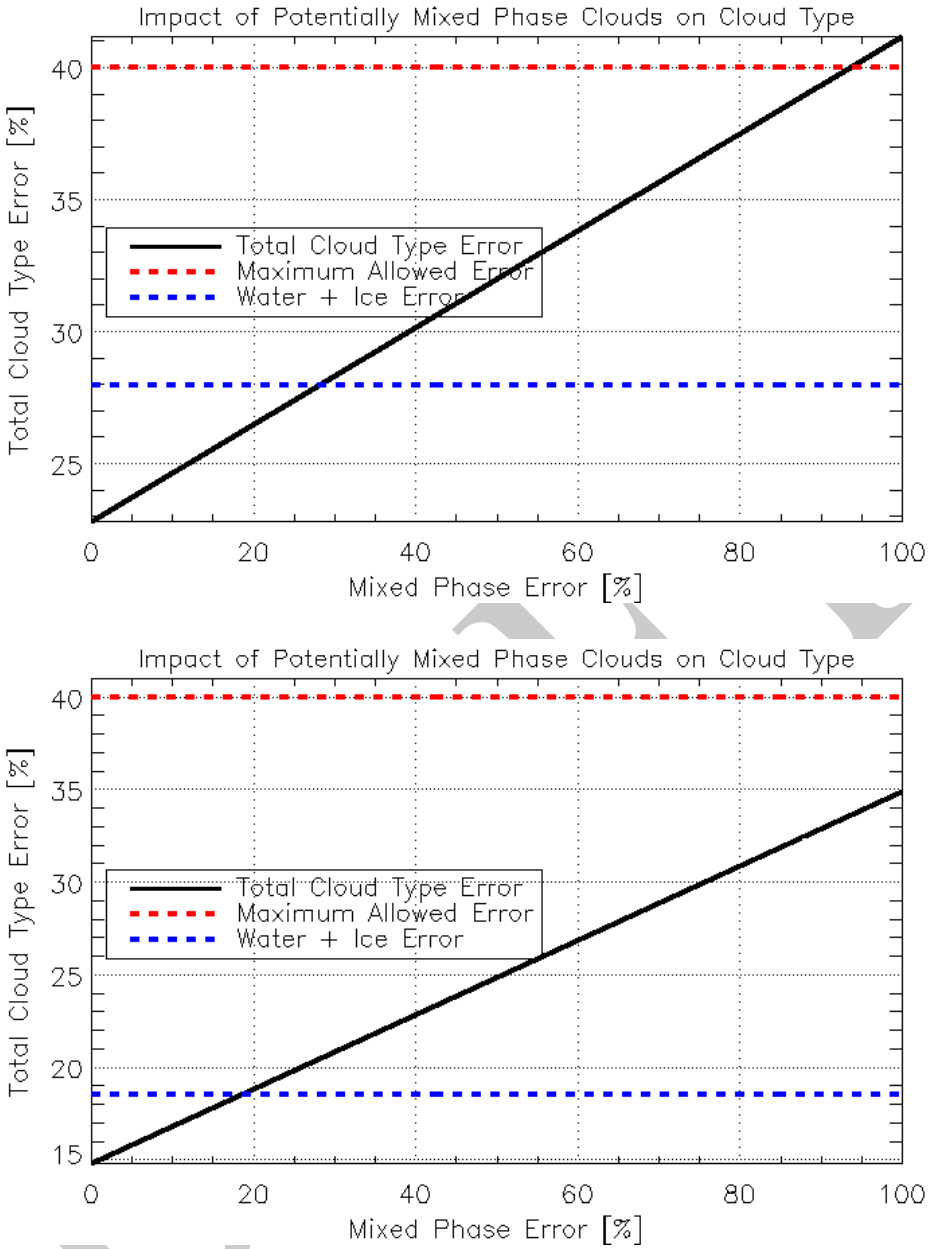

Figure 32: Same as Figure 31, except for cloud type.

The accuracy of the JRRCT was assessed as a function of the CALIOP cloud optical depth and geographic region (including a global assessment). Table 45 below shows that the cloud type from the JRRCT comfortably meets the 0.60 accuracy specification.

Table 45: The accuracy of the JRRCT cloud type product is shown as a function the minimum CALIOP cloud optical depth considered and the geographic region. The numbers in parenthesis indicates the number of data points where the JRRCT and CALIOP agree compared to the total number of VIIRS/CALIOP matchups.

OD	> 0.0	>0.1	>0.2	>0.3	>0.4	>0.5	>2.0
All data	0.726 (82679/ 113807)	0.778 (71968/ 92555)	0.791 (65841/ 83244)	0.799 (62265/ 77943)	0.802 (59771/ 74539)	0.805 (57802/ 71847)	0.775 (28372/ 36601)
Day time	0.712 (35328/ 49614)	0.775 (29527/ 38104)	0.790 (27015/ 34180)	0.797 (25307/ 31770)	0.799 (24247/ 30357)	0.803 (23514/ 29293)	0.754 (11044/ 14642)
Night time	0.738 (47351/ 64193)	0.779 (42441/ 54451)	0.791 (38826/ 49064)	0.800 (36958/ 46173)	0.804 (35524/ 44182)	0.806 (34288/ 42554)	0.789 (17328/ 21959)
Over land	0.719 (19737/ 27445)	0.753 (16429/ 21819)	0.760 (14670/ 19315)	0.763 (13393/ 17547)	0.766 (12755/ 16656)	0.768 (12261/ 15965)	0.676 (4118/ 6095)
Over water	0.729 (62942/ 86362)	0.785 (55539/ 70736)	0.800 (51171/ 63929)	0.809 (48872/ 60396)	0.812 (47016/ 57883)	0.815 (45541/ 55882)	0.795 (24254/ 30506)
Lat > 60 deg	0.803 (15903/ 19805)	0.844 (13560/ 16063)	0.865 (12557/ 14514)	0.876 (11874/ 13556)	0.881 (11399/ 12945)	0.884 (10980/ 12426)	0.837 (4846/ 5789)
Lat < 60 deg	0.710 (66776/ 94002)	0.764 (58408/ 76492)	0.775 (53284/ 68730)	0.783 (50391/ 64387)	0.785 (48372/ 61594)	0.788 (46822/ 59421)	0.764 (23526/ 30812)

4.2.3 Validation Summary

The following points summarize the results of the cloud phase and type validation.

- According to the F&PS, the cloud phase product must correctly classify 80% of clouds with an optical depth (visible wavelength optical depth) greater than 1.0.
- According to the F&PS, the cloud type product must correctly classify 60% of clouds with an optical depth (visible wavelength optical depth) greater than 1.0.
- A small subset (relative to all other cloud classes) of mid-level clouds termed, "potentially mixed phase clouds," was excluded from the validation analysis due to the lack of quality validation data.
- The validation analysis was performed **with** and **without** invoking the greater than 1.0 cloud optical depth qualifier.
- The cloud phase product derived from SEVIRI correctly classifies 93% of clouds **with** the cloud optical depth qualifier and 88% of clouds **without** the cloud optical depth qualifier, both of which are well within the F&PS accuracy specification.
- The cloud type product derived from SEVIRI correctly classifies 82% of clouds **with** the cloud optical depth qualifier and 72% of clouds **without** the cloud

optical depth qualifier, both of which are well within the F&PS accuracy specification.

- The cloud phase product derived from VIIRS correctly classifies 89% of clouds **with** the cloud optical depth qualifier and 83% of clouds **without** the cloud optical depth qualifier, both of which are well within the F&PS accuracy specification.

- The cloud type product derived from VIIRS correctly classifies 81% of clouds **with** the cloud optical depth qualifier and 73% of clouds **without** the cloud optical depth qualifier, both of which are well within the F&PS accuracy specification.

- The analysis also indicates that the exclusion of "potentially mixed phase clouds" from the analysis will not prevent the cloud phase and type products from meeting the F&PS accuracy specifications, as very large errors in classifying "potentially mixed phase clouds" can be tolerated.

- Remaining validation efforts will focus on performing a detailed analysis of "potentially mixed phase clouds" through the development of multi-sensor "deep dive" tools. Regardless of the results of this "deep dive" analysis, the cloud phase and type products meet the F&PS accuracy specifications.

5 PRACTICAL CONSIDERATIONS

5.1 Numerical Computation Considerations

Prior to converting cloud emissivity to optical depth, the cloud emissivity must be checked to ensure that it is greater than 0.0 and less than 1.0 to prevent an illegal natural logarithm operation.

5.2 Programming and Procedural Considerations

The ACT and JRRCT makes heavy use of clear-sky radiative transfer calculations. Our current system computes the clear-sky atmospheric transmittances at low spatial resolution and with enough angular resolution to capture sub-grid variation path-length changes. This step is critical, as performing clear-sky atmospheric transmittance calculations for each pixel requires extensive memory and CPU time, but does not produce significantly better scientific results. The AIADD Document describes this procedure in detail.

NWP data is heavily utilized in the ACT and JRRCT algorithm. The algorithm can tolerate the use NWP data for forecasts ranging from 0 to 24 hours.

The ACT algorithm can provide usable results out to a viewing angle of 80 degrees (the F&PS minimum requirement is 65 degrees). The cloud phase/type algorithm is not applied to pixels that have a viewing angle greater than 80 degrees (the cloud phase and cloud type are set to zero in this case).

5.3 Quality Assessment and Diagnostics

It is recommended that clear sky radiance biases are regularly monitored and that the validation exercises described earlier are applied routinely. Further, algorithm performance issues are best diagnosed by examining the β-ratios used to make cloud type decisions.

5.4 Exception Handling

Prior to use, the ACT and JRRCT checks to make sure that each channel falls within the expected measurement range and that valid clear sky radiance and transmittance profiles are available for each channel. The ACT and JRRCT are only applied to a given pixel if all channels used in the algorithm contain valid data (according to the L1b calibration flags); otherwise the algorithm output is flagged as missing. The science of the cloud phase/type algorithm does not allow for a graceful degradation of the products at this time. The algorithm, however, can tolerate the use NWP data for forecasts ranging from 0 to 24 hours.

5.5 Algorithm Validation

Cloud phase/type products derived from spaceborne lidar or ground-based lidar and cloud radar will serve as the main source of validation data. During the GOES-R pre-launch period, CALIOP will serve as the main source of validation, as described earlier. During the post-launch period, spaceborne lidar data from the European Space Agency (ESA) EarthCARE mission will be used in validation (pending a successful and on-time mission). In the absence of EarthCARE, the combination of ground-based lidar and millimeter cloud radar, such as those deployed by the Atmospheric Radiation Measurement (ARM) program, will be used for validation. Please refer to the ABI Cloud Products Validation Plan Document for extensive information on pre and post launch validation plans.

6 ASSUMPTIONS AND LIMITATIONS

The following sections describe the current limitations and assumptions in the current version of the ACT and JRRCT Algorithm.

6.1 Performance

The following assumptions have been made in developing and estimating the performance of the ACT and JRRCT. The following lists contain the current assumptions and proposed mitigation strategies.

1. NWP data of comparable or superior quality to the current 6 hourly Global Forecast System (GFS) forecasts are available. (Mitigation: Use longer-range GFS forecasts or switch to another NWP source – e.g. ECMWF).

2. TOA clear sky radiances are available for each pixel and 101 level profiles of clear sky atmospheric transmittance and radiance are available at the NWP data horizontal resolution. (Mitigation: Use reduced spatial resolution TOA clear sky radiances. The profiles of transmittance and radiance must be present at, at least, the NWP spatial resolution and 101 vertical levels).

3. All of the static ancillary data are available at the pixel level. (Mitigation: Reduce the spatial resolution of the surface type, land mask and or coast mask).

4. The processing system allows for processing of multiple scan lines at once for application of important spatial analysis techniques. (Mitigation: No mitigation is possible).

5. All ABI or NPP VIIRS channels required by the algorithm must be available. (Mitigation: Develop a modified version of the algorithm. Graceful degradation is not possible because there are too many possible channel permutations.).

In addition, the clear sky radiance calculations are prone to large errors, especially near coastlines, in mountainous regions, snow/ice field edges, and atmospheric frontal zones, where the NWP surface temperature and atmospheric profiles are less accurate. The impact of these errors on the cloud phase/type depends on the cloud optical depth. For optically thick clouds (infrared optical depth of about 1.0 or greater), these errors have a small impact on the calculation of the effective absorption optical depth ratios since the difference between the observed and black cloud radiance approaches zero as the cloud optical depth increases. This is not the case for optically thin clouds, where inaccurate NWP data can have serious impacts. The ACT and JRRCT algorithm utilizes the Local Radiative Center (LRC) (see 3.4.2.4 for details) concept to minimize these impacts, but improvements in NWP fields should lead to additional improvements in the ACT and JRRCT products.

6.2 Assumed Sensor Performance

We assume the sensor will meet its current specifications. However, the ACT and JRRCT will be dependent on the following instrumental characteristics.

- Unknown spectral shifts in some channels will cause biases in the clear-sky Radiative Transfer Model (RTM) calculations that may impact the performance of the ACT and JRRCT. Clear sky radiance biases need to be monitored throughout ABI's lifetime and NPP VIIRS lifetime, respectively.

6.3 Pre-Planned Product Improvements

We expect in the coming years to focus on the following improvements.

6.3.1 Incorporation of solar channels

Channels that are sensitive to reflected solar radiation are very useful for providing additional information on cloud phase. Future version of the ACT and JRRCT may include an enhanced daytime version that utilizes these channels.

6.3.2 Use of 10.4-μm channel

The 10.4 μm channel is new to the world of satellite imagers. Large variations in cloud emissivity occur in the 10 – 13 μm spectral range. With the 10.4 μm channel additional cloud emissivity relationships can be exploited in determining cloud phase and type. We expect to incorporate this channel into the ACT to improve our cloud phase determination. We expect the GOES-R Risk Reduction projects to demonstrate its use before implementation into the operational algorithm.

6.3.3 Use of additional water vapor channels

Stronger absorbing water vapor channels (ABI channels 8 and 9) can be used to improve the multilayered cloud detection. Future versions of the algorithm may incorporate these channels.

7 REFERENCES

Carey, L. D., J. Niu, P. Yang, J. A. Kankiewicz, V. E. Larson, and T. H. Vonder Haar, 2008: The vertical profile of liquid and ice water content in midlatitude mixed-phase altocumulus clouds. *J. Appl. Meteorol. And Climatology*, **47**, 2487-2495.

Cober, S. G., G. A. Isaac, A. V. Korolev, and J. W. Strapp, 2001: Assessing Cloud-Phase Conditions. *J.Appl.Meteorol.,* **40**, 1967-1983.

Cox, S. K., 1976: Observations of Cloud Infrared Effective Emissivity. *J.Atmos.Sci.,* **33**, 287-289.

Downing, H. D., D. Williams, 1975: Optical-Constants of Water in Infrared. *Journal of Geophysical Research,* **80**, 1656-1661.

Giraud, V., J. C. Buriez, Y. Fouquart, F. Parol, and G. Seze, 1997: Large-scale analysis of cirrus clouds from AVHRR data: Assessment of both a microphysical index and the cloud-top temperature. *J.Appl.Meteorol.,* **36**, 664-675.

Heidinger, A. K. and M. J. Pavolonis, 2005: Global daytime distribution of overlapping cirrus cloud from NOAA's Advanced Very High Resolution Radiometer. *J. Climate*, **18 (22)**, 4772-4784.

Heidinger, A. K. and M. J. Pavolonis, 2009: Nearly 30 years of gazing at cirrus clouds through a split-window. Part I: Methodology. *J.Appl.Meteorol. and Climatology*, **48(6)**, 110-1116.

Hu, Y. and Co-authors, 2009: CALIPSO/CALIOP cloud phase discrimination algorithm. *J. Atmos. and Oceanic Technol.*, In Press (early online release).

Inoue, T., 1987: A Cloud Type Classification with Noaa 7 Split-Window Measurements. *J.Geophys.Res.-Atmos.,* **92**, 3991-4000.

Korolev, A. V., G. A. Isaac, S. G. Cober, J. W. Strapp, and J. Hallett, 2003: Microphysical characterization of mixed-phase clouds. *Q. J. R. Meteorol. Soc.*, **129**, 39-65.

Kossin, J.P. and M. Sitkowski, 2008: An Objective Model for Identifying Secondary Eyewall Formation in Hurricanes. *Mon. Wea. Rev.,* **137,** 876-892.

Mitchell, D. L., 2000: Parameterization of the Mie extinction and absorption coefficients for water clouds. *J.Atmos.Sci.,* **57**, 1311-1326.

Parol, F., J. C. Buriez, G. Brogniez, and Y. Fouquart, 1991: Information-Content of Avhrr Channels 4 and 5 with Respect to the Effective Radius of Cirrus Cloud Particles. *J.Appl.Meteorol.,* **30**, 973-984.

Pavolonis, M. J. and Heidinger, A. K., 2004: Advances in identifying cirrus and multilayered cloud systems from operational satellite imagers at night. Applications with Weather Satellites II, Honolulu, Hawaii, 9-11 November 2004. Proceedings. SPIE-International Society for Optical Engineering, Bellingham, WA, 2005, pp. 225-234.

Pavolonis, M. J., A. K. Heidinger, 2004: Daytime cloud overlap detection from AVHRR and VIIRS. *J.Appl.Meteorol.,* **43**, 762-778.

Pavolonis, M. J., A. K. Heidinger, and T. Uttal, 2005: Daytime global cloud typing from AVHRR and VIIRS: Algorithm description, validation, and comparisons. *J.Appl.Meteorol.,* **44**, 804-826.

Pavolonis, M. J., 2010a: Advances in extracting cloud composition information from spaceborne infrared radiances: A robust alternative to brightness temperatures. Part I: Theory. *J. Applied Meteorology and Climatology*, In Press (available online).

Pavolonis, M. J., 2010b: Advances in extracting cloud composition information from spaceborne infrared radiances: A robust alternative to brightness temperatures. Part II: Proof of concept. To be submitted to the *J. Applied Meteorology and Climatology.*

Rogers, R. R. and M. K. Yau, 1989: A short course in cloud physics. Third Edition. Butterworth-Heinemann. 290 pp.

Seemann, S. W., E. E. Borbas, R. O. Knuteson, G. R. Stephenson, and H. Huang, 2008: Development of a global infrared land surface emissivity database for application to clear sky sounding retrievals from multispectral satellite radiance measurements. *J.Appl.Meteorol.Climatol.,* **47**, 108-123, doi:10.1175/2007JAMC1590.1.

Turner, D. D., 2005: Arctic mixed-phase cloud properties from AERI lidar observations: Algorithm and results from SHEBA. *J.Appl.Meteorol.,* **44**, 427-444.

Van de Hulst, H. C., 1980: *Multiple Light Scattering, Tables, Formulas, and Applications.* Vol. 2. Academic Press, 739 pp.

Warren, S. G., R. E. Brandt, 2008: Optical constants of ice from the ultraviolet to the microwave: A revised compilation. *J.Geophys.Res.-Atmos.,* **113**, D14220, doi:10.1029/2007JD009744.

Wilks, D. S., 2006. Statistical Methods in the Atmospheric Sciences. 2nd ed. International Geophysics Series, Vol. 91, Academic Press, 627

Yang, P., H. L. Wei, H. L. Huang, B. A. Baum, Y. X. Hu, G. W. Kattawar, M. I. Mishchenko, and Q. Fu, 2005: Scattering and absorption property database for nonspherical ice particles in the near- through far-infrared spectral region. *Appl.Opt.,* **44**, 5512-5523.

Zhang, H., W. P. Menzel, 2002: Improvement in thin cirrus retrievals using an emissivity-adjusted CO2 slicing algorithm. *J.Geophys.Res.-Atmos.,* **107**, 4327, doi:10.1029/2001JD001037.